Supplementary Information

The locust genome provides insight into swarm formation and long-distance flight

Xianhui Wang[1], Xiaodong Fang[2], Pengcheng Yang[1,3], Xuanting Jiang[2], Feng Jiang[1,3], Dejian Zhao[1], Bolei Li[1], Feng Cui[1], Jianing Wei[1], Chuan Ma[1,3], Yundan Wang[1,3], Jing He[1], Yuan Luo[1], Zhifeng Wang[1], Xiaojiao Guo[1], Wei Guo[1], Xuesong Wang[1,3], Yi Zhang[1], Meiling Yang[1], Shuguang Hao[1], Bing Chen[1], Zongyuan Ma[1,3], Dan Yu[1], Zhiqiang Xiong[2], Yabing Zhu[2], Dingding Fan[2], Lijuan Han[2], Bo Wang[2], Yuanxin Chen[2], Junwen Wang[2], Lan Yang[2], Wei Zhao[2], Yue Feng[2], Guanxing Chen[2], Jinmin Lian[2], Qiye Li[2], Zhiyong Huang[2], Xiaoming Yao[2], Na Lv[4], Guojie Zhang[2], Yingrui Li[2], Jian Wang[2], Jun Wang[2], Baoli Zhu[4], Le Kang[1,3#]

1 State Key Laboratory of Integrated Management of Pest Insects and Rodents, Institute of Zoology, Chinese Academy of Sciences, 1 Beichen West Road, Chaoyang District, Beijing 100101, China

2 BGI-Shenzhen, Beishan Industrial Zone, Yantian District, Shenzhen 518083, China

3 Beijing Institutes of Life Science, Chinese Academy of Sciences, 1 Beichen West Road, Chaoyang District, Beijing 100101, China

4 CAS Key Laboratory of Pathogenic Microbiology and Immunology, Institute of Microbiology, Chinese Academy of Sciences, 1 Beichen West Road, Chaoyang District, Beijing 100101, China

#Send correspondence to:

Dr. Le Kang,

Institute of Zoology, Chinese Academy of Sciences, Beijing 100101, China

Tel: 86-10-64807219; Fax: 86-10-84379559; E-mail: lkang@ioz.ac.cn

Supplementary Figures

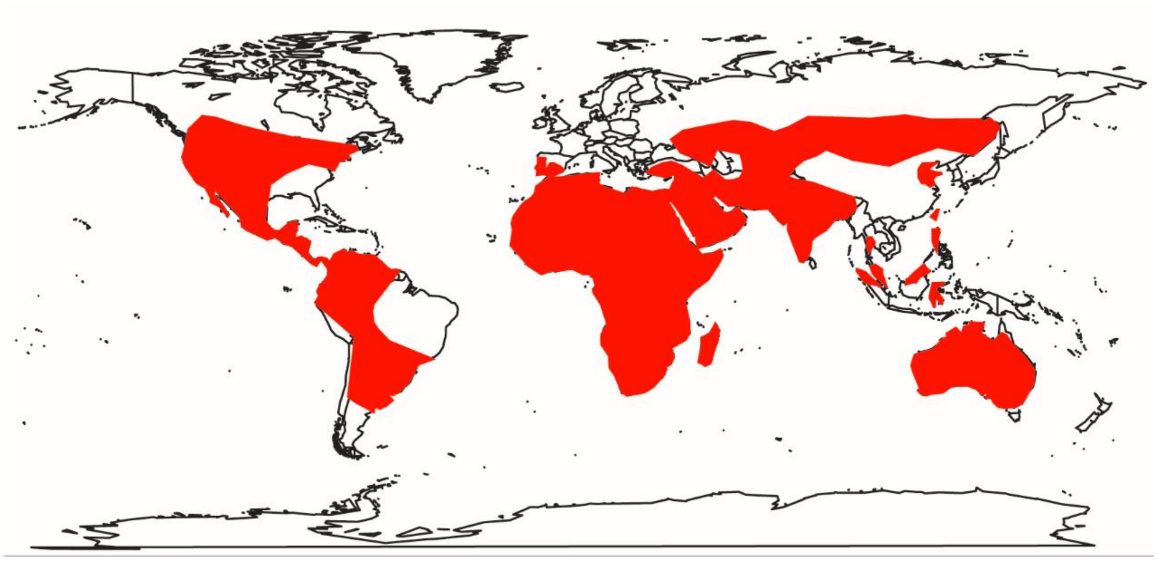

Supplementary Figure S1 Worldwide distribution of locust plagues.

Locust plague occurs in most continents of the world except Antarctic Continent. This figure was reproduced according to the reviews by Hemming[71]. Major locust species include *Locusta migratoria*, *Schistocerca gregaria*, *Calliptamus italicu*, *Chortoicetes terminifera*, *Schistocerca americana* and so on.

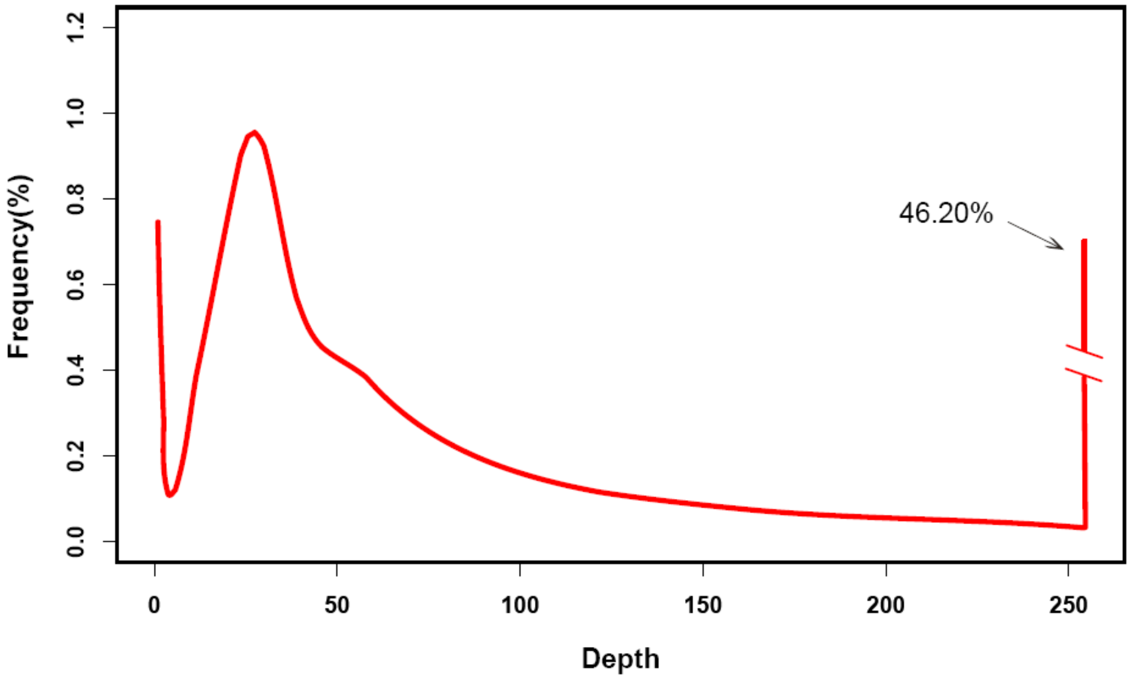

Supplementary Figure S2 The distribution of 17-mer frequency in *L. migratoria* genome sequencing reads.

Fifteen lanes of short (< 1 kb) paired-end genome sequencing reads that passed quality control were used to generate the 17-mer sequences. The 17-mer frequencies proportion to total 17-mer number was plotted against the 17-mer depth. The peak depth was 23X. The genome size of *L. migratoria* was estimated to be 6.3 Gb based on the formula: #Total 17-mer number / 17-mer depth (Supplementary Table S2).

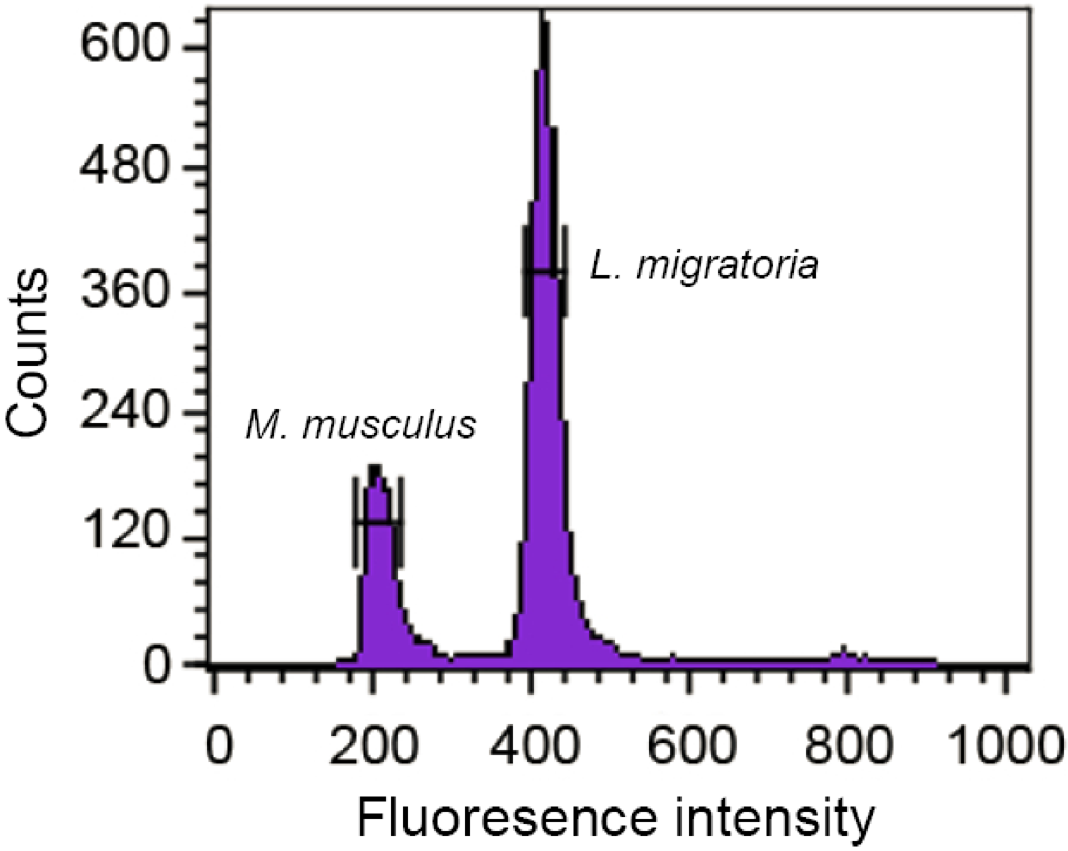

Supplementary Figure S3 Estimate of genome size based on flow cytometry.

The genome size of *L. migratoria* (peak 414.24) was estimated to be ~6.3 Gb (414.24/209.46 * 3.25 * 0.978). Data on the *M. musculus* (*Mus musculus*) genome are provided for comparison (peak 209.46, genome size 3.25 pg).

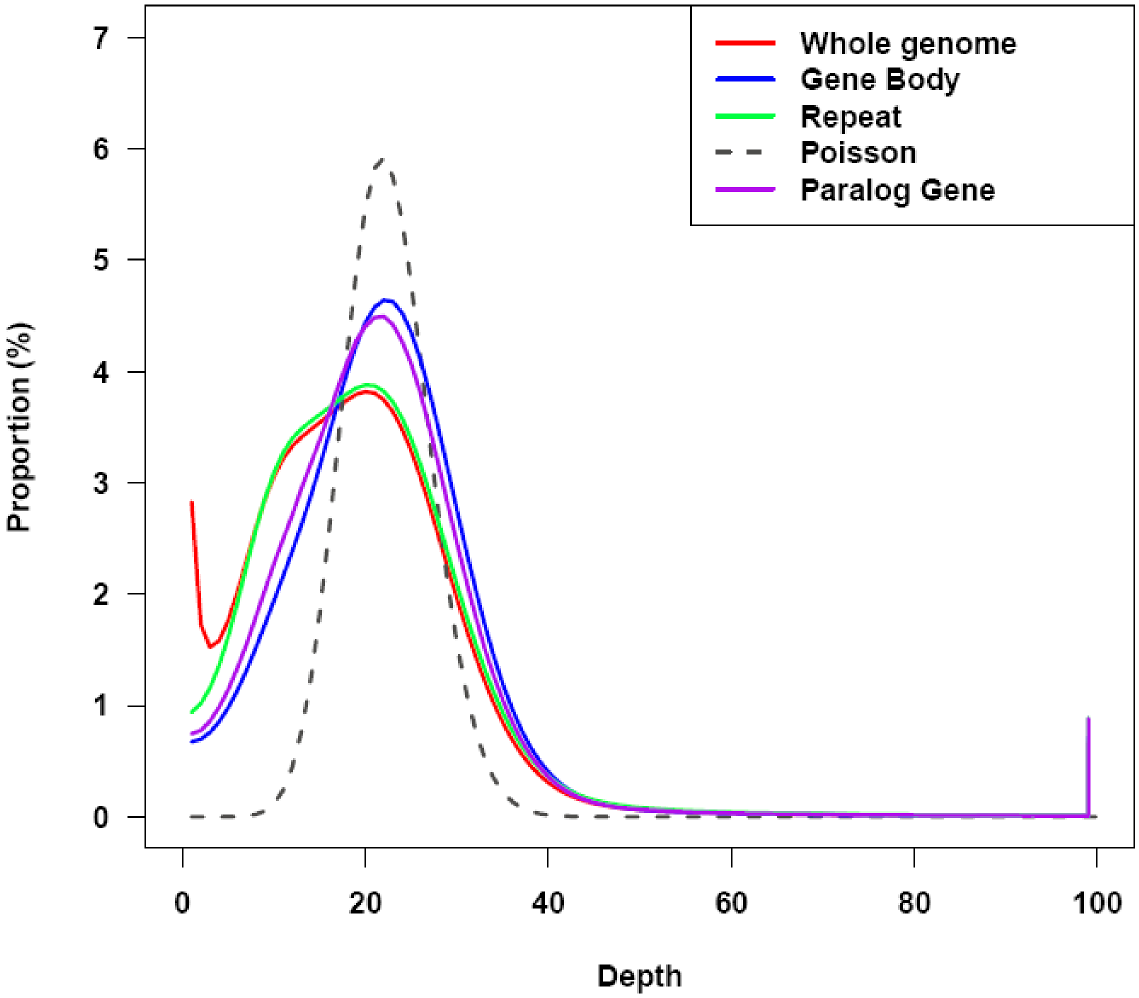

Supplementary Figure S4 Sequencing depth distribution of the *L. migratoria* genome.

The used reads was 135 Gb (~22X) high quality reads with insert sizes of 200 bp. The depth distributions were plotted for the whole genome (red), gene body region including intron (blue), repeat (green) and gene body region of paralog genes (purple). The theoretical poisson distribution was plotted with λ=22.34.

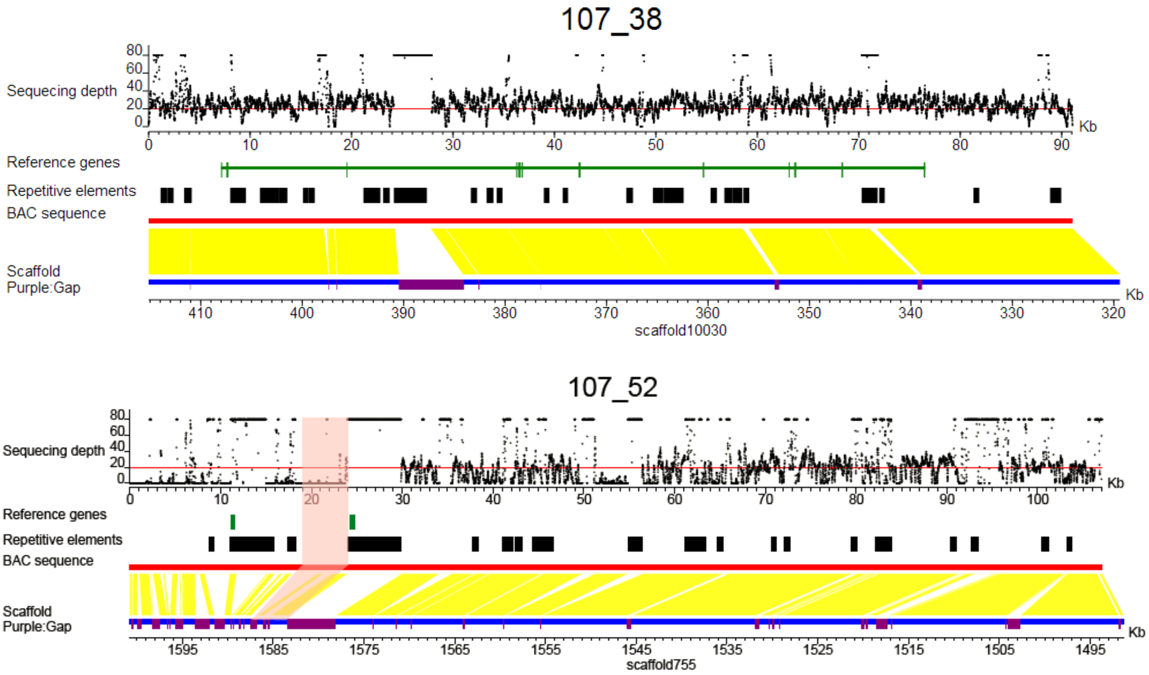

Supplementary Figure S5 Comparison of the assembled genome with BAC sequences.

Sequencing depth on the BAC (Bacterial Artificial Chromosome) was calculated by mapping the Illumina HiSeq 2000 short reads onto the BAC sequence using BWA (version 0.6.2) with default parameters. Here we performed single-end mapping and reported all repetitive hits. The red line is the average depth across the genome. The predicted genes and annotated TEs on the BAC sequence are shown in green and black, respectively. The TEs were annotated by RepeatMasker using the locust repeat consensus sequence generated by RepeatModeler. The genes were annotated using proteins from 4 species, *Drosophila melanogaster*, *Apis mellifera*, *Acyrthosiphon pisum* and *Pediculus humanus*, with GeneWise. The remaining unclosed gaps on the scaffolds are marked as purple blocks.

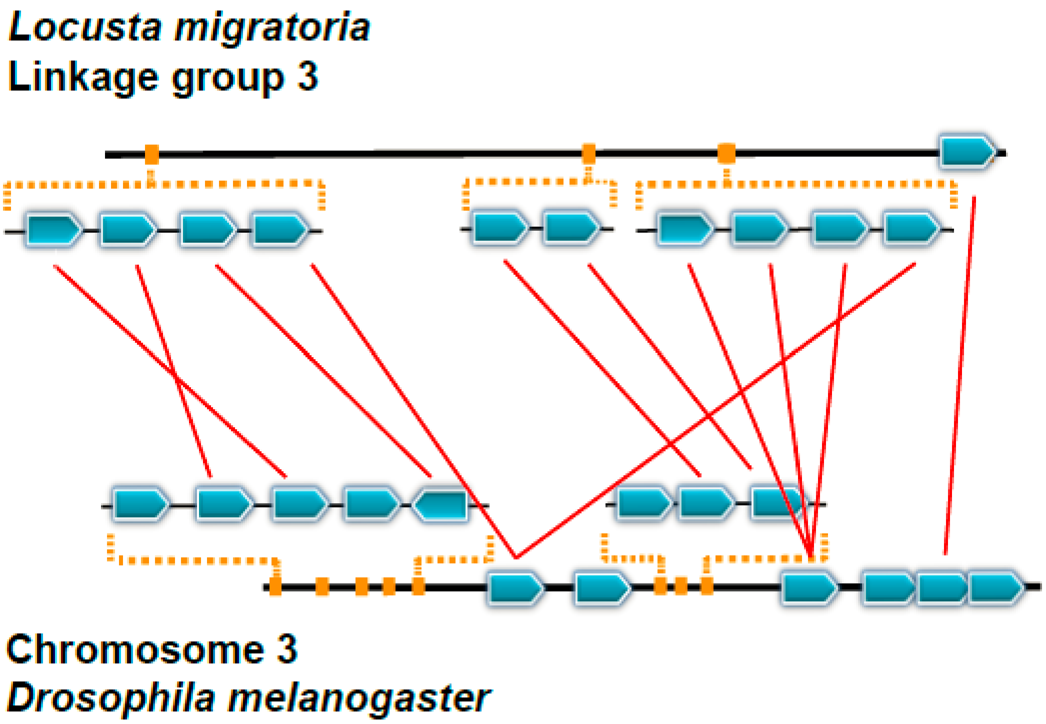

Supplementary Figure S6 Homologous regions between the locust and fly genome based on an Osiris gene family which is conserved and syntenic in insects. The homologous relationships were determined by reciprocal best hits of BLASTP searches.

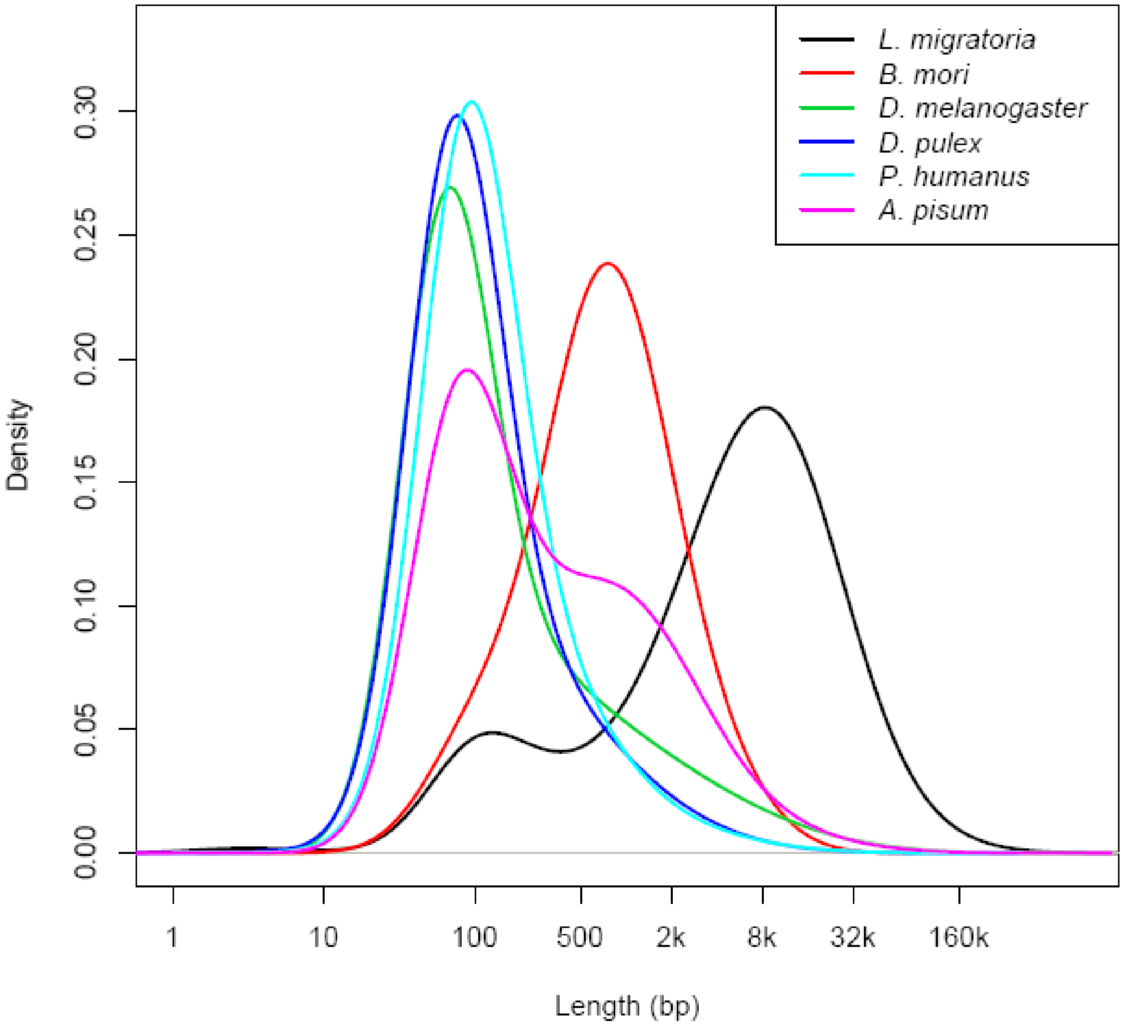

Supplementary Figure S7 Intron length distribution of 6 insect species. The density estimation of intron length was determined for each species.

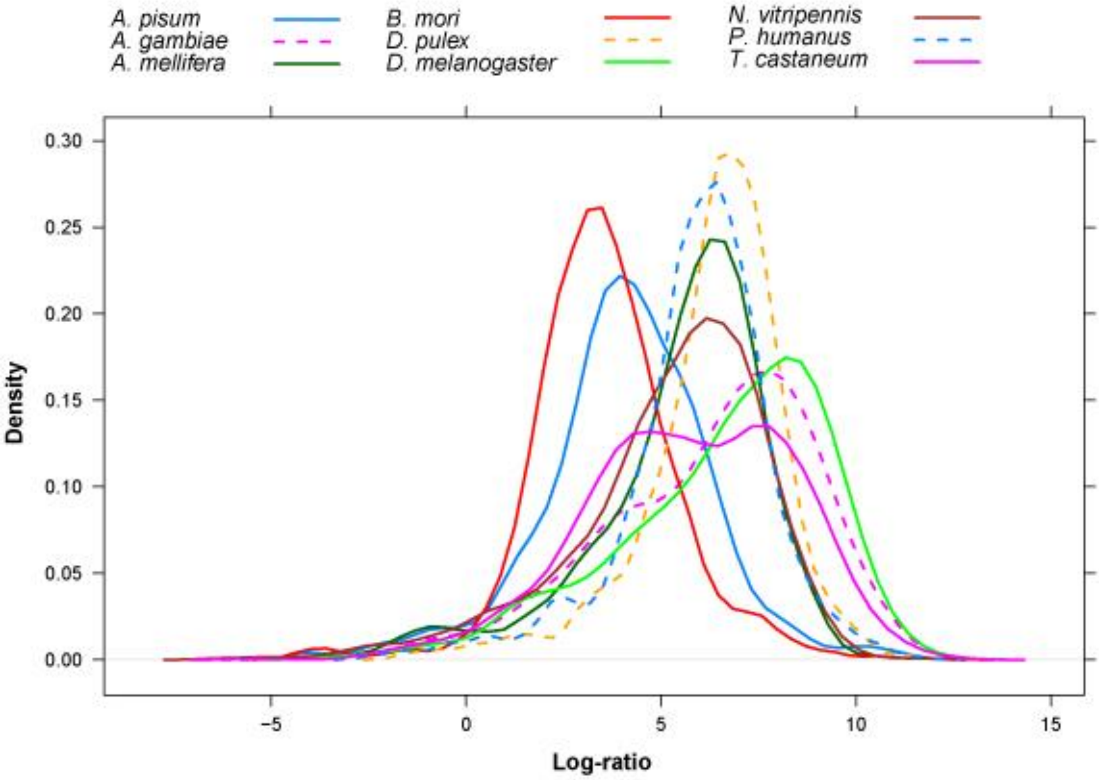

Supplementary Figure S8 Comparison of intron size expansion across insects.

Pairwise comparisons between *L. migratoria* and other insects were visualized using the log expansion/contraction ratios of introns in the 1,046 conserved homologous genes.

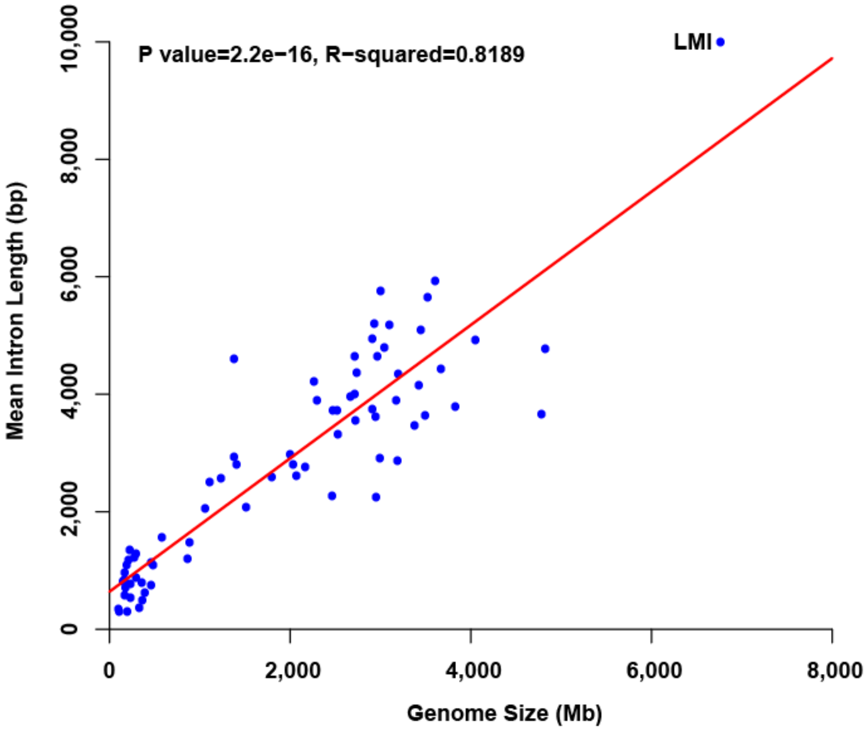

Supplementary Figure S9 Correlation of genome size and average intron length.

The vertical and horizontal axes show the average intron size and the genome size, respectively. Pearson's correlation test is used to test the relationships between variables.

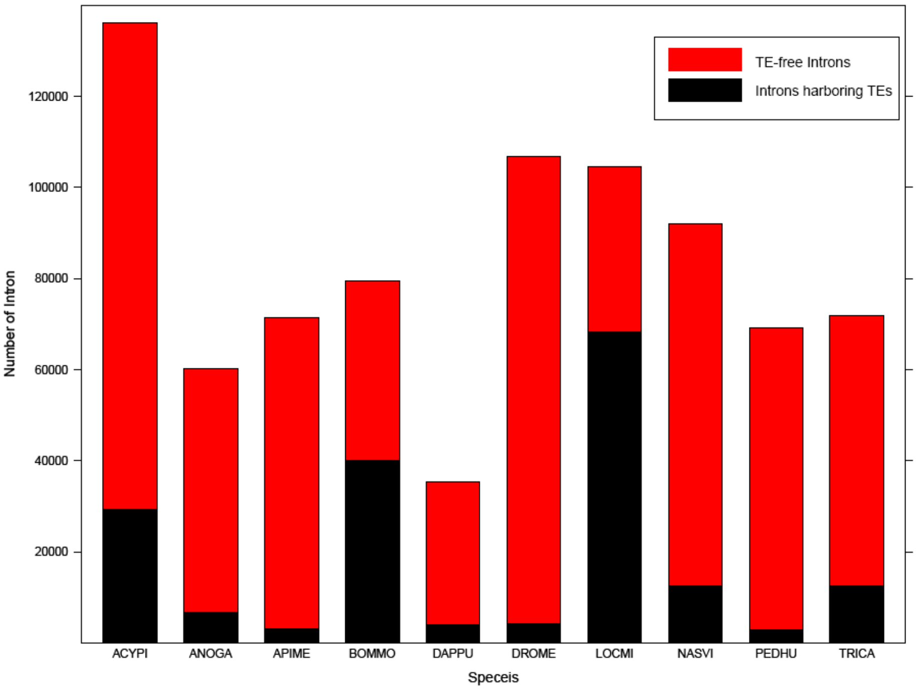

Supplementary Figure S10 Statistics of TE-harboring and TE-free introns across 10 arthropod species.

The fraction of TEs in introns was calculated from the aligned genome sequences of RepeatMasker screenings.

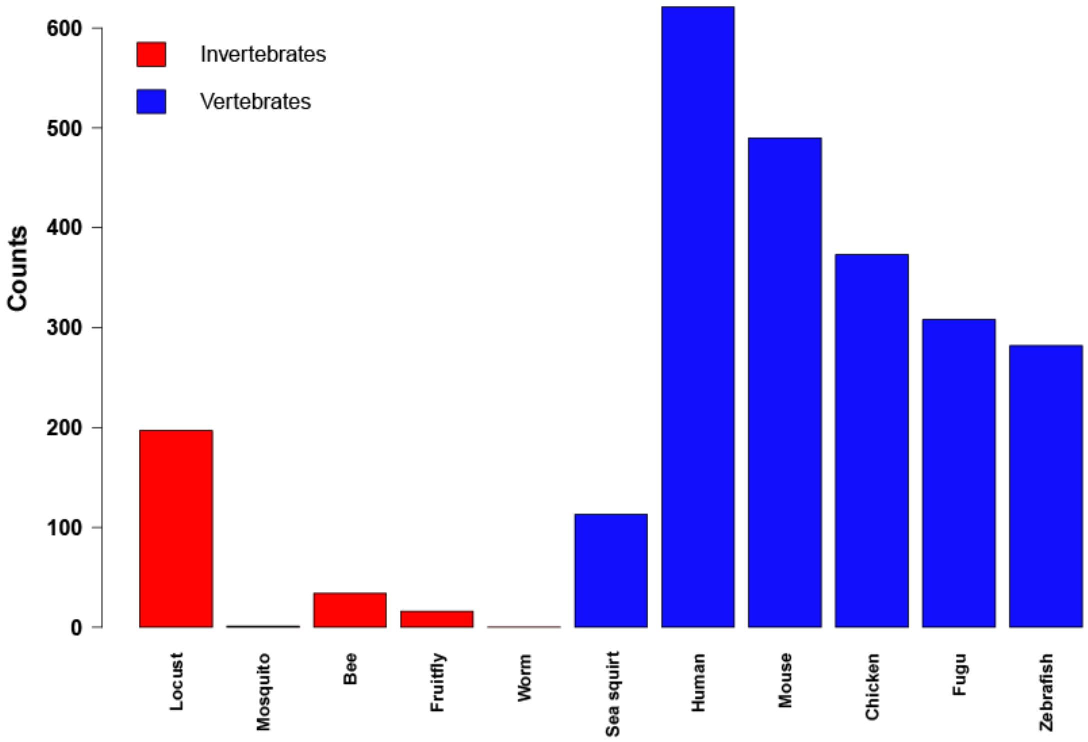

Supplementary Figure S11 Counts of introns that are orthologous to 621 human U12-type introns in different species.

The counts for other species were determined based on information in the U12db database. Locust, *Locusta migratoria*; Mosquito, *Anopheles gambiae*; Bee, *Apis mellifera*; Fruitfly, *Drosophila melanogaster*; Worm, *Caenorhabditis elegans*; Sea squirt, *Ciona intestinalis*; Human, *Homo sapiens*; Mouse, *Mus musculus*; Chicken, *Gallus gallus*; Fugu, *Fugu rubripes*; Zebrafish, *Danio rerio*.

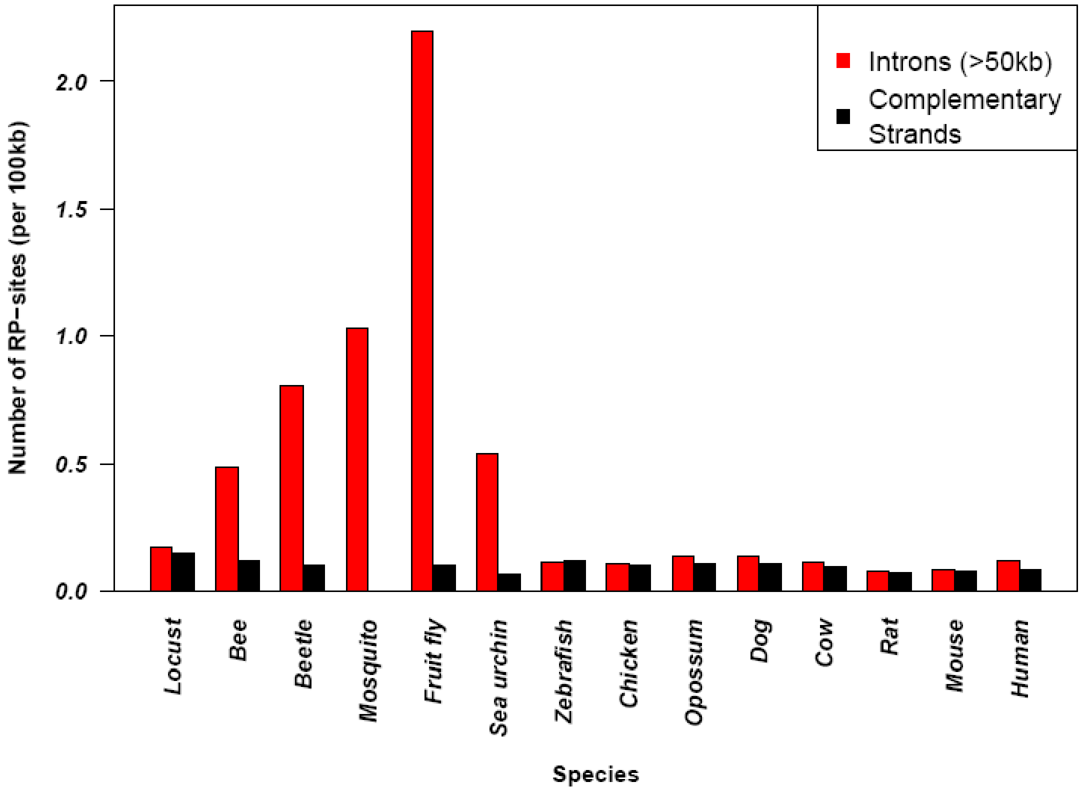

Supplementary Figure S12 Number of RP-sites per 100 kb inside large introns and their complementary sequences.

Data for other species were retrieved from a previous study[26]. Locust, *Locusta migratoria*; Bee, *Apis mellifera*; Beetle, Tribolium castaneum; Mosquito, *Anopheles gambiae*; Fruitfly, *Drosophila melanogaster*; Sea squirt, *Ciona intestinalis*; Zebrafish, *Danio rerio*; Chicken, *Gallus gallus*; Opossum, *Monodelphis domestica*; Dog, Canis familiaris; Cow, Bos Taurus; Rat, *Rattus norvegicus*; Mouse, *Mus musculus*; Human, *Homo sapiens*.

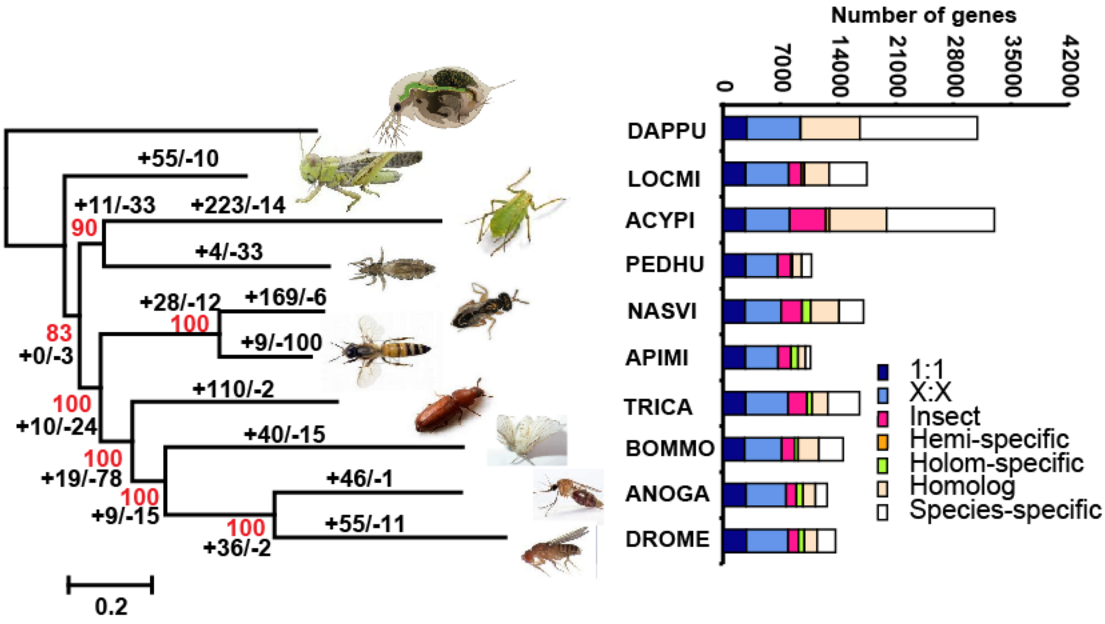

Supplementary Figure S13 Phylogenetic relationships of *L. migratoria*, *D. pulex* and other sequenced insects (left), and insect gene orthology (right).

A) Phylogenetic relationships were inferred based on the concatenated data set from universal single-copy genes. The number of gains (1) and losses (2) of gene families is indicated as inferred by the CAFE program. The bootstrap values are shown in red. B) Comparison of the gene repertoire of nine insect and crustacean genomes. Bars are subdivided to represent different types of orthology relationships. 1:1 indicates universal single-copy genes (allowing absence and/or duplication for a single genome); X:X indicates orthologues present in multiple copies in all species (allowing one loss); homologue indicates a patchy orthologous relationship in the involved genomes. LOCMI: *Locusta migratoria*; DAPPU: *Daphnia pulex*; PEDHU: *Pediculus humanus*; ACYPI: *Acyrthosiphon pisum*; APIME: *Apis mellifera*; NASVI: *Nasonia vitripennis*; TRICA: *Tribolium castaneum*; BOMMO: *Bombyx mori*; ANOGA: *Anopheles gambiae*; DROME: *Drosophila melanogaster*.

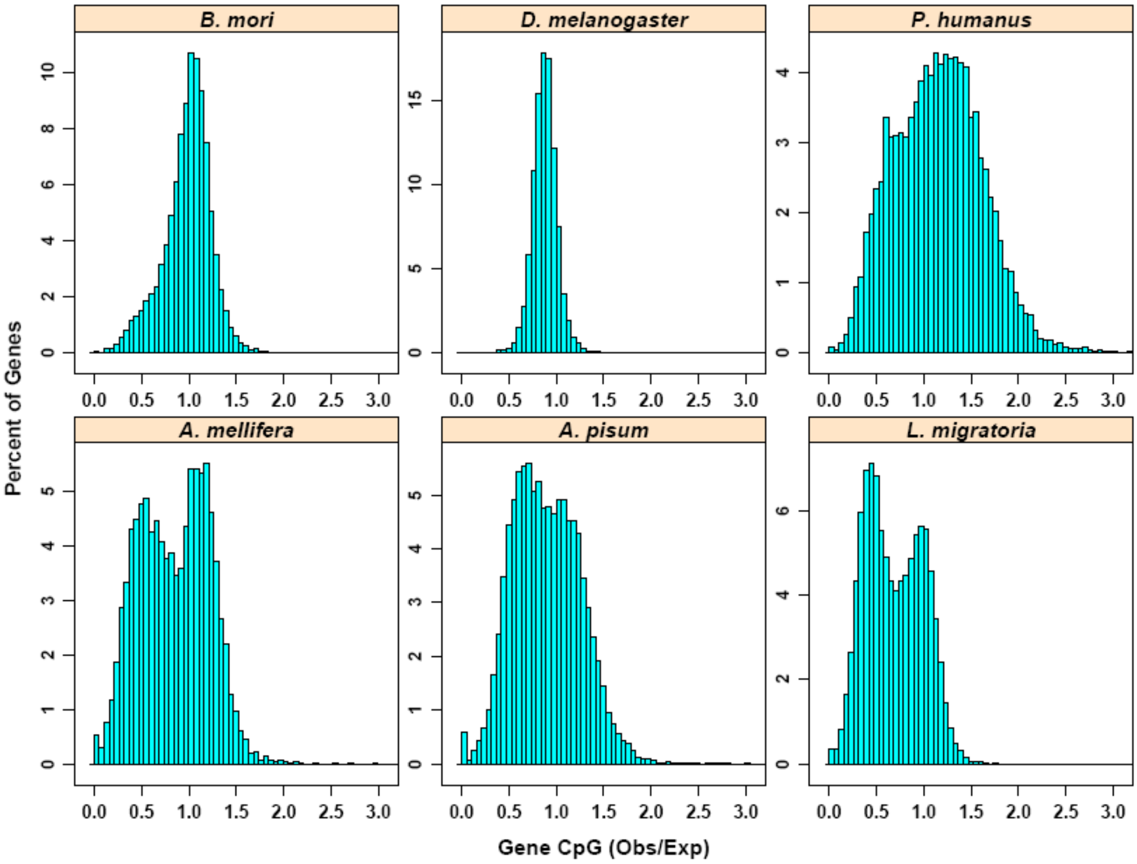

Supplementary Figure S14 Gene CpGo/e distribution of the 6 insect species.

The observed/expected (Obs/Exp) ratio of CpG dinucleotides, based on G+C content, was calculated for each annotated gene in the six insect genomes. Similar to *A. mellifera*, *L. migratoria* also displays a bimodal distribution, with a clearly distinct class of low-CpG genes. *L. migratoria*: *Locusta migratoria*, *P. humanus*: *Pediculus humanus*, *A. pisum*: *Acyrthosiphon pisum*, *A. mellifera*: *Apis mellifera*, *B. mori*: *Bombyx mori*, and *D. melanogaster*: *Drosophila melanogaster*.

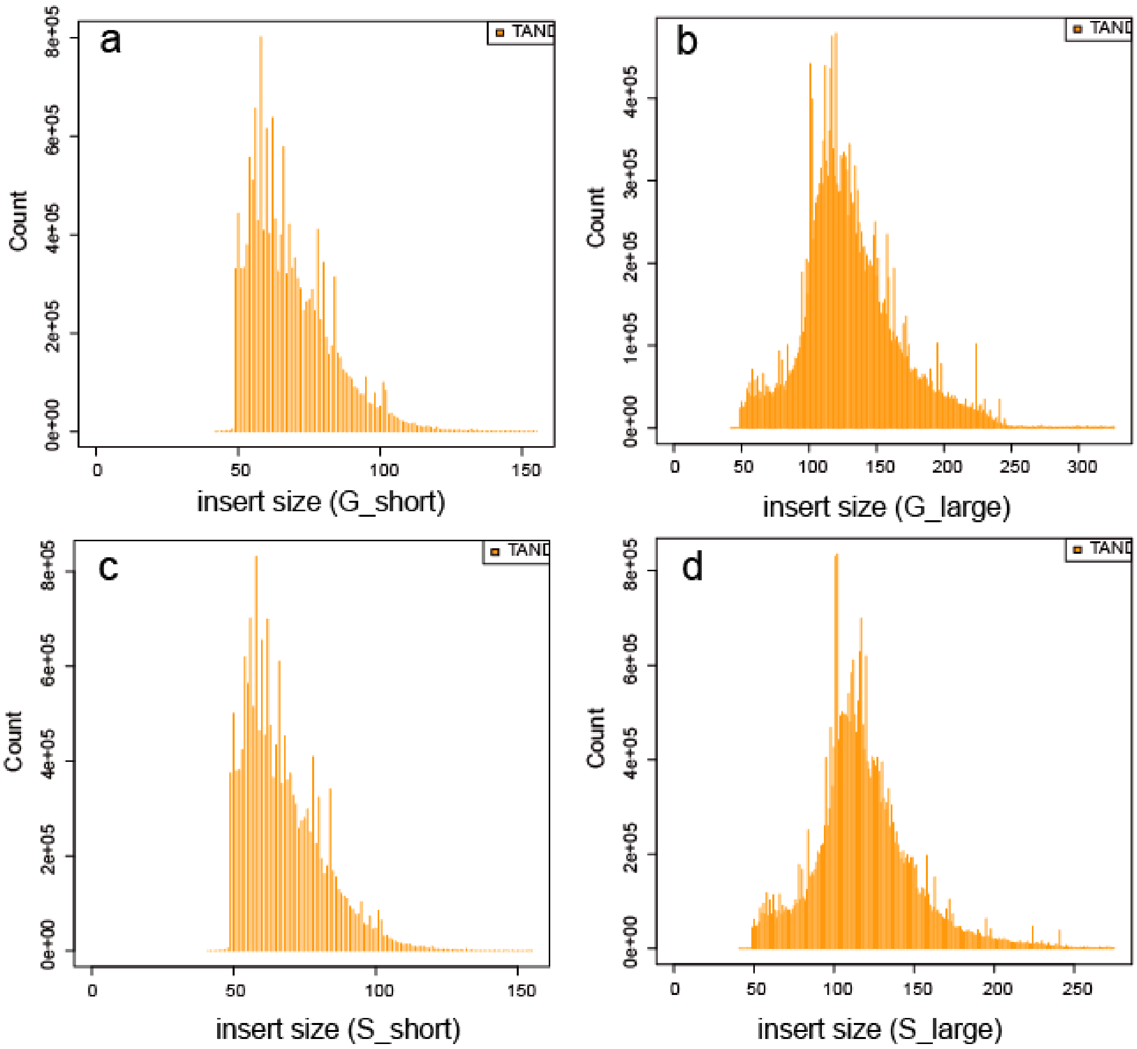

Supplementary Figure S15 Insert size distribution of RRBS libraries.

X axis denotes insert size of RRBS sequencing libraries, Y axis denotes the counts of read pairs with that insert size. (a) and (b) were libraries for gregarious, (c) and (d) were solitarious, (a) and (c) were libraries with short insert size (40-120bp), (b) and (d) were libraries with large insert size (120-220 bp). From these pictures, we can conclude that the insert size distributed as expected.

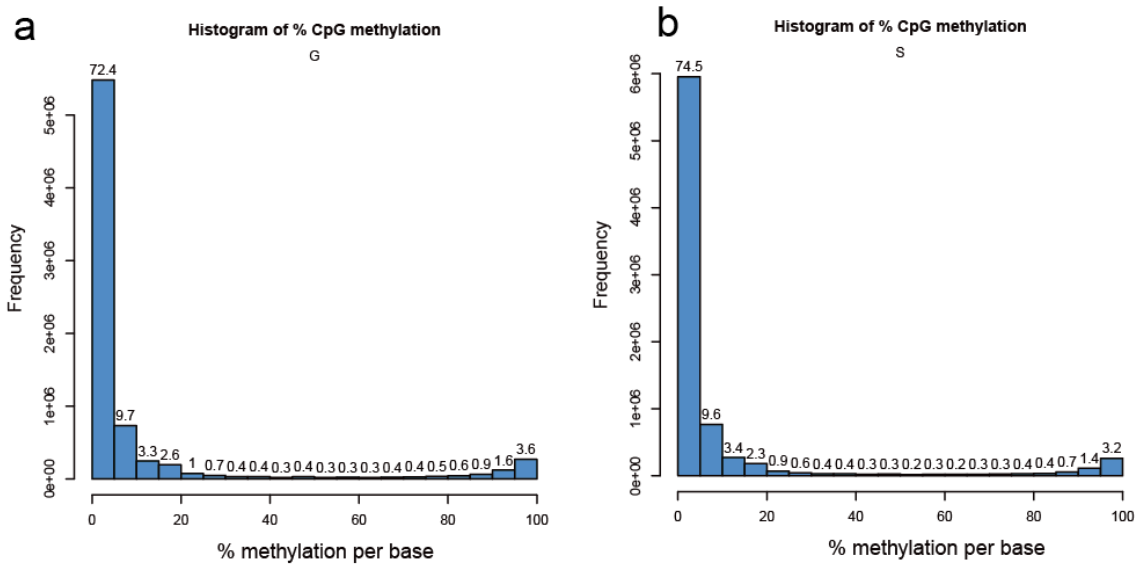

Supplementary Figure S16 Methylation levels across all CpGs.

X axis denotes the methylation levels of CpGs, binned at every 5 percent step. Y axis denotes the frequencies of CpGs at each bin. (a) Gregrarious and (b) solitarious samples were plotted.

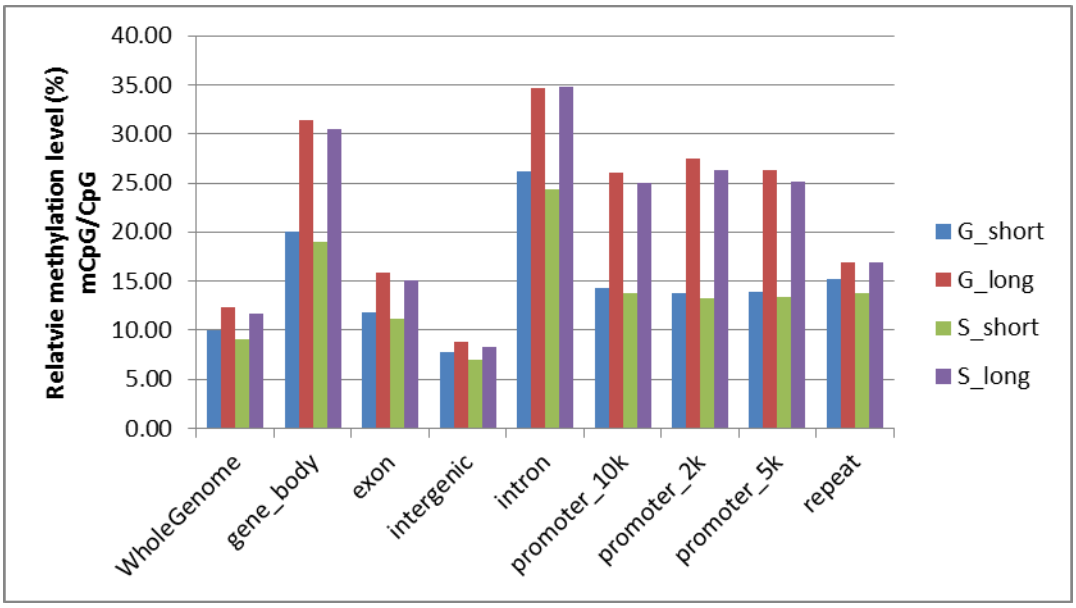

Supplementary Figure S17 Relative methylation level of CpG across different genomic regions.

The promoter was defined as the upstream 2kb, 5kb and 10kb of start codon. Short and long denote the libraries of insert sizes 40-120 bp and 120-220 bp respectively.

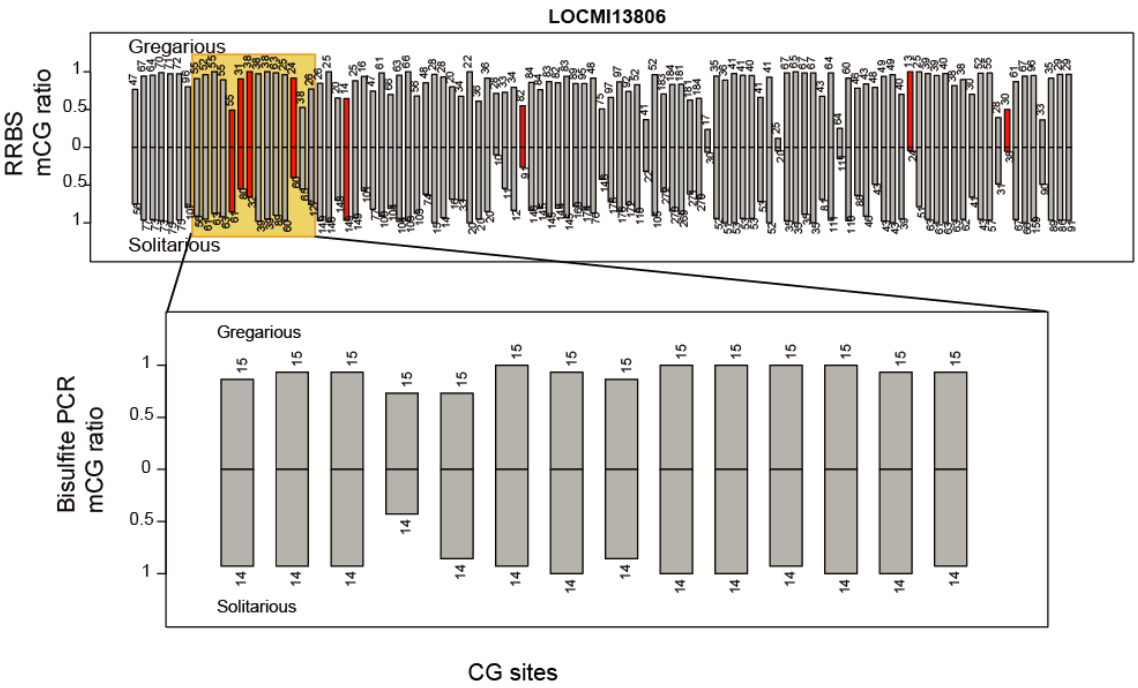

Supplementary Figure S18 RRBS and bisulfite PCR validation of the differences in CG site methylation ratio of LOCMI13806 between the brains of gregarious and solitarious locusts.

The barplot at the top was produced from RRBS data and the bottom displayed the Bisulfite PCR validation of the yellow region of the top.

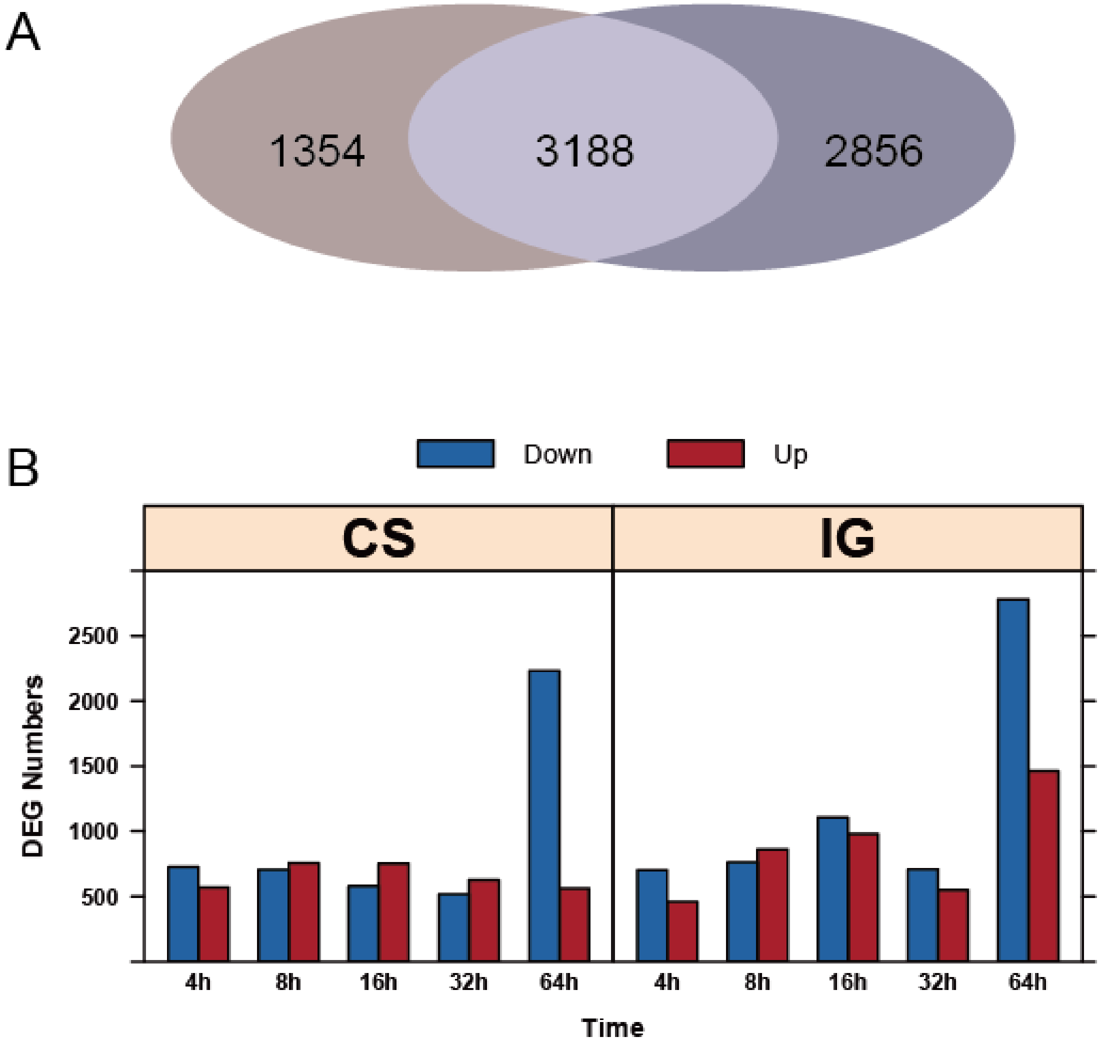

Supplementary Figure S19 The number of differentially expressed genes during isolation of gregarious locusts (IG) and crowding of solitarious locusts (CS).

The number of differentially expressed genes in the two conditions in total (A) and at every time point compared to control (B).

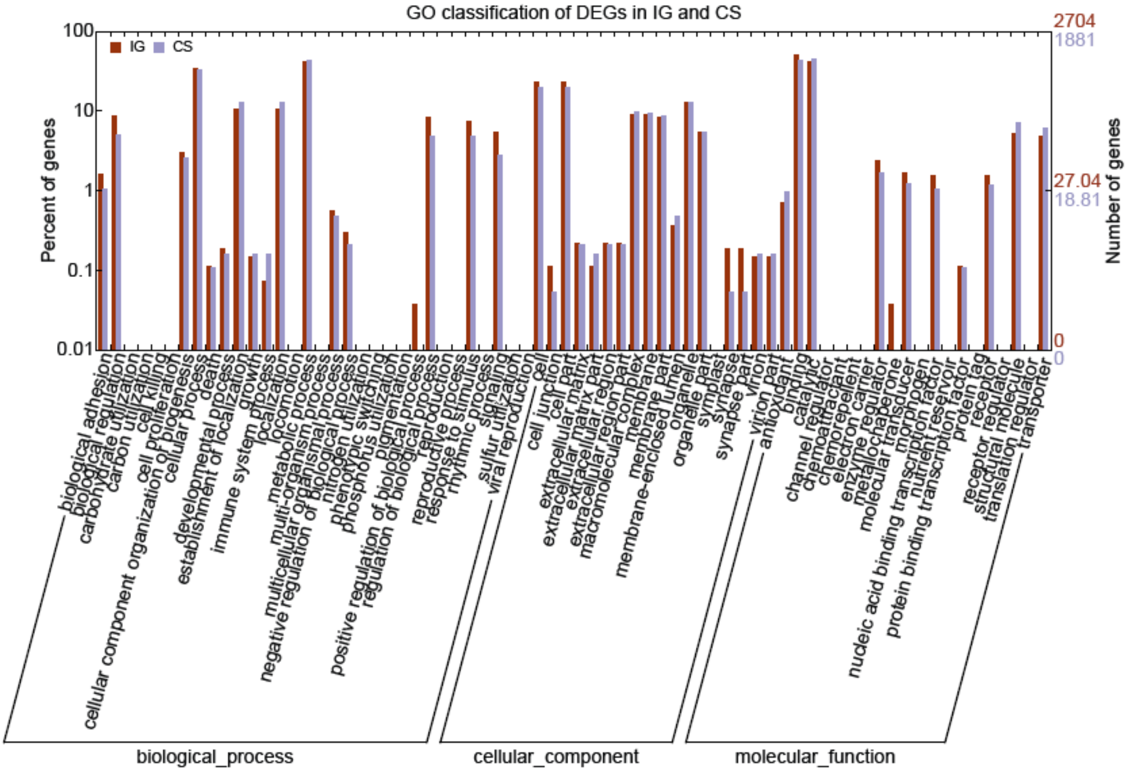

Supplementary Figure S20 GO classification of the differentially expressed genes in the IG and CS processes.

Schematic diagram showing GO classification of the differentially expressed genes in the IG and CS processes produced using the web-based tool WEGO[72].

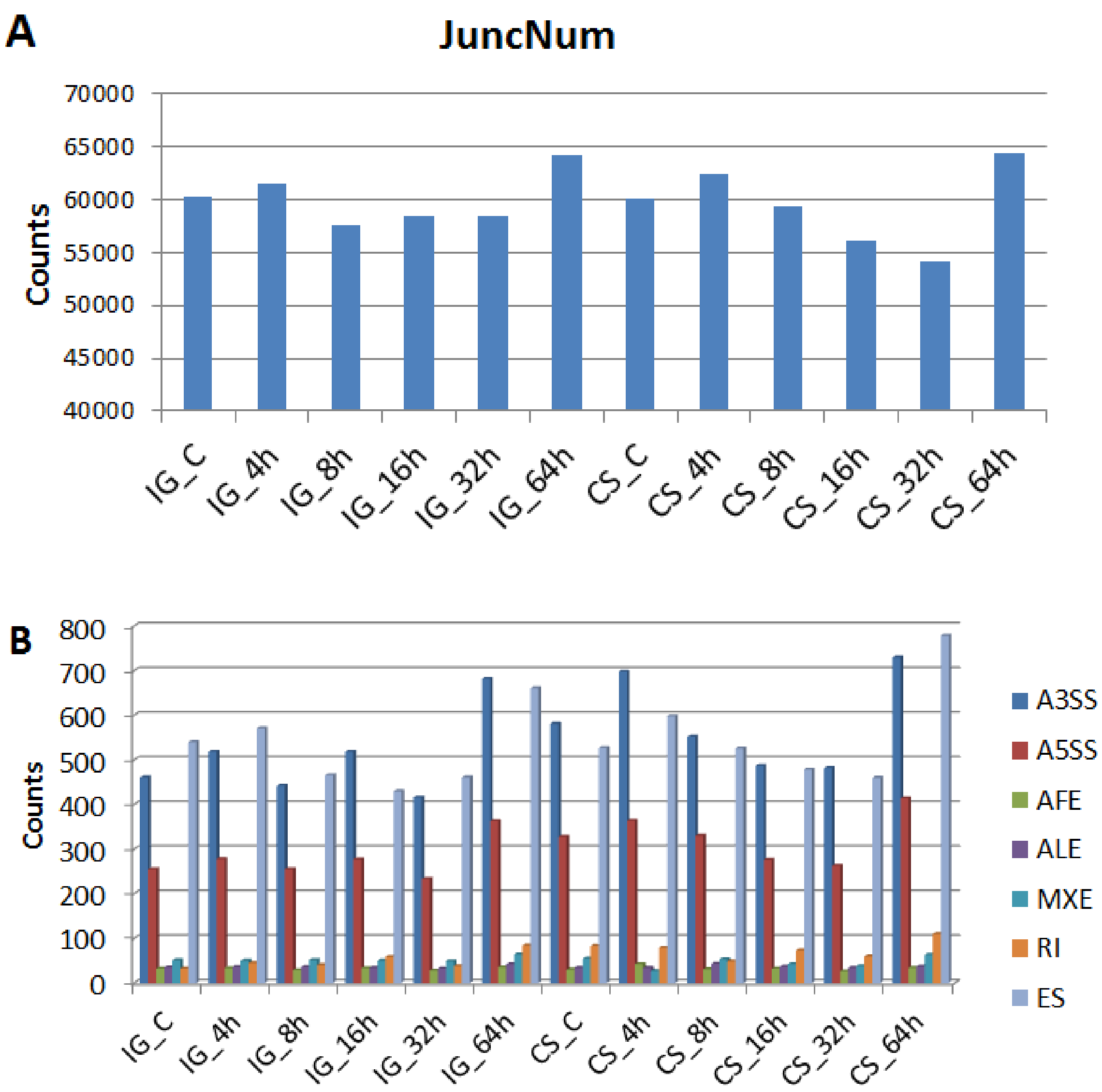

Supplementary Figure S21 Statistics of splicing junctions and classification of alternative splicing across IG and CS processes.

The junction numbers (A) were calculated based on the TopHat mapping result. The method of alternative splicing classification (B) was described at Supplementary methods. IG: Isolation of Gregarious locust; CS: Crowding of Solitarious locust.

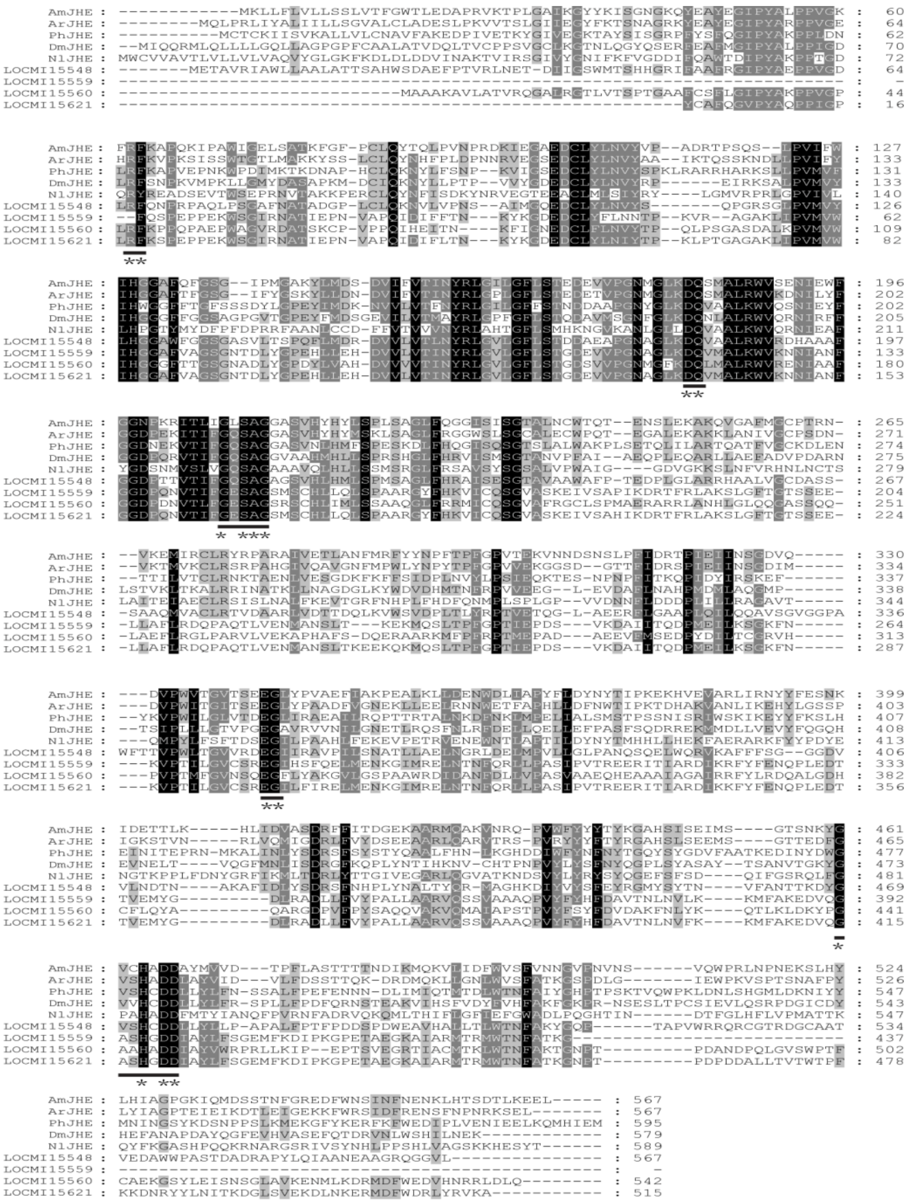

Supplementary Figure S22 Amino acid sequence alignment of *L. migratoria* and other insect JHEs.

Numbers on the right side of the alignment indicate the position of residues in the sequence of each protein. The five catalytic motifs which are conserved in insect JHEs are underlined and marked with asterisks. Similar amino acid residues are shaded. AmJHE (*Apis mellifera*, NP_001011563), ArJHE (*Athalia rosae*, BAD91554), PhJHE (*Psacothea hilaris*, BAE94685), DmJHE (*Drosophila melanogaster*, NP_523758) and NlJHE (*Nilaparvata lugens*, ACB14344) were used in the alignment.

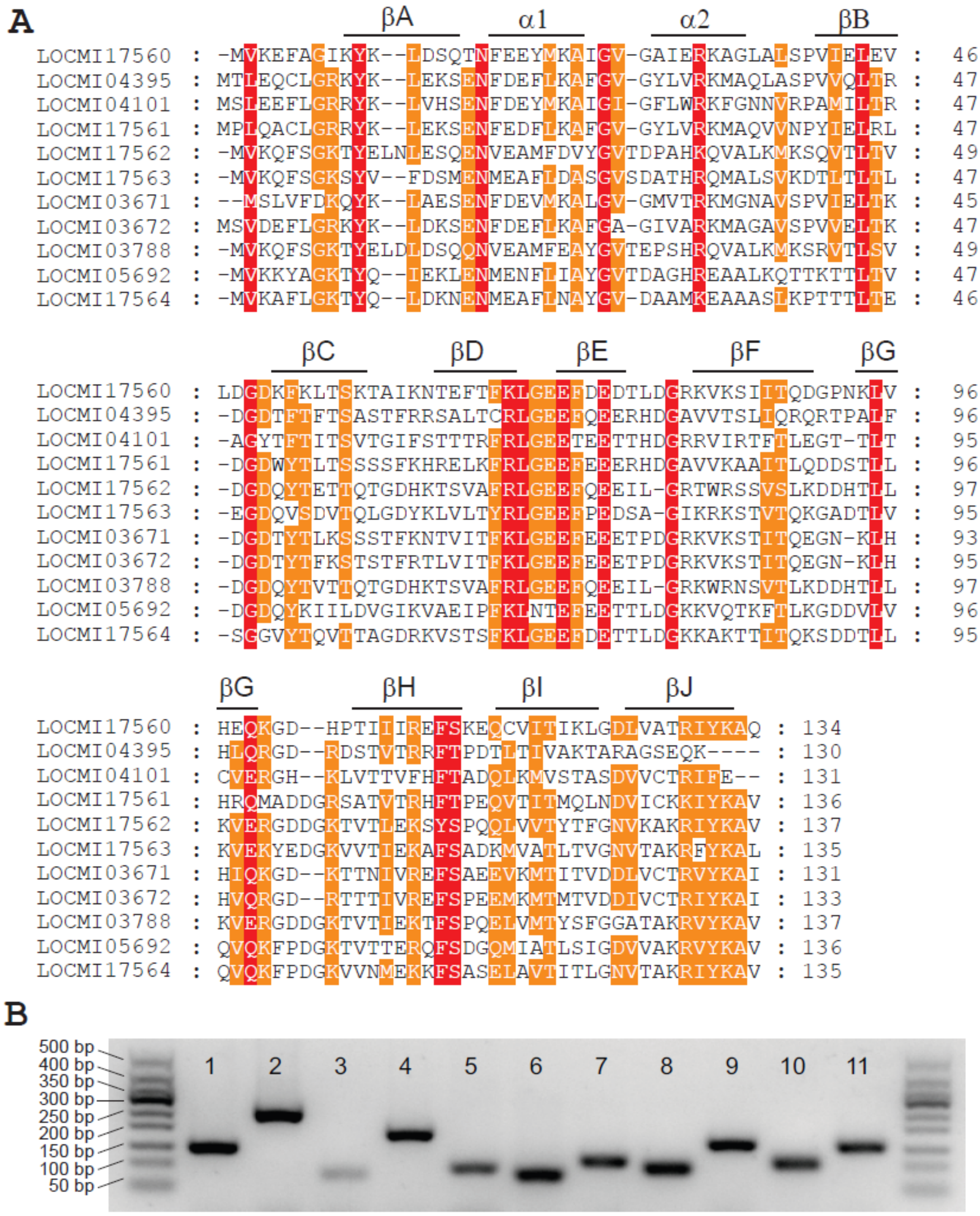
A
βA
α1
α2
βB
LOCMI17560 : -MVKEFAGIKYK--LDSQTNFEEYMKAIGV-GAIERKAGLALSPVIELEV : 46
LOCMI04395 : MTLEQCLGRKYK--LEKSENFDEFLKAFGV-GYLVRKMAQLASPVVQLTR : 47
LOCMI04101 : MSLEEFLGRRYK--LVHSENFDEYMKAIGI-GFLWRKFGNNVRPAMILTR : 47
LOCMI17561 : MPLQACLGRRYK--LEKSENFEDFLKAFGV-GYLVRKMAQVVNPYIELRL : 47
LOCMI17562 : -MVKQFSGKTYELNLESQENVEAMFDVYGVTDPAHKQVALKMKSQVTLTV : 49
LOCMI17563 : -MVKQFSGKSYV--FDSMENMEAFLDASGVSDATHRQMALSVKDTLTLTL : 47
LOCMI03671 : --MSLVFDKQYK--LAESENFDEVMKALGV-GMVTRKMGNAVSPVIELTK : 45
LOCMI03672 : MSVDEFLGRKYK--LDKSENFDEFLKAFGA-GIVARKMAGAVSPVVELTK : 47
LOCMI03788 : -MVKQFSGKTYELDLDSQQNVEAMFEAYGVTEPSHRQVALKMKSRVTLSV : 49
LOCMI05692 : -MVKKYAGKTYQ--IEKLENMENFLIAYGVTDAGHREAALKQTTKTTLTV : 47
LOCMI17564 : -MVKAFLGKTYQ--LDKNENMEAFLNAYGV-DAAMKEAAASLKPTTTLTE : 46
βC
βD
βE
βF
βG
LOCMI17560 : LDGDKFKLTSKTAIKNTEFTFKLGEEFDEDTLDGRKVKSIITQDGPNKLV : 96
LOCMI04395 : -DGDTFTFTSASTFRRSALTCRLGEEFQEERHDGAVVTSLIQRQRTPALF : 96
LOCMI04101 : -AGYTFTITSVTGIFSTTTRFRLGEETEETTHDGRRVIRTFTLEGT-TLT : 95
LOCMI17561 : -DGDWYTLTSSSSFKHRELKFRLGEEFEEERHDGAVVKAAITLQDDSTLL : 96
LOCMI17562 : -DGDQYTETTQTGDHKTSVAFRLGEEFQEEIL-GRTWRSSVSLKDDHTLL : 97
LOCMI17563 : -EGDQVSDVTQLGDYKLVLTYRLGEEFPEDSA-GIKRKSTVTQKGADTLV : 95
LOCMI03671 : -DGDTYTLKSSSTFKNTVITFKLGEEFEEETPDGRKVKSTITQEGN-KLH : 93
LOCMI03672 : -DGDTYTFKSTSTFRTLVITFKLGEEFEEETPDGRKVKSTITQEGN-KLH : 95
LOCMI03788 : -DGDQYTVTTQTGDHKTSVAFRLGEEFQEEIL-GRKWRNSVTLKDDHTLL : 97
LOCMI05692 : -DGDQYKIILDVGIKVAEIPFKLNTEFEETTLDGKKVQTKFTLKGDDVLV : 96
LOCMI17564 : -SGGVYTQVTTAGDRKVSTSFKLGEEFDETTLDGKKAKTTITQKSDDTLL : 95
βG
βH
βI
βJ
LOCMI17560 : HEQKGD--HPTIIIREFSKEQCVITIKLGDLVATRIYKAQ : 134
LOCMI04395 : HLQRGD--RDSTVTRRFTPDTLTIVAKTARAGSEQK---- : 130
LOCMI04101 : CVERGH--KLVTTVFHFTADQLKMVSTASDVVCTRIFE-- : 131
LOCMI17561 : HRQMADDGRSATVTRHFTPEQVTITMQLNDVICKKIYKAV : 136
LOCMI17562 : KVERGDDGKTVTLEKSYSPQQLVVTYTFGNVKAKRIYKAV : 137
LOCMI17563 : KVEKYEDGKVVTIEKAFSADKMVATLTVGNVTAKRFYKAL : 135
LOCMI03671 : HIQKGD--KTTNIVREFSAEEVKMTITVDDLVCTRVYKAI : 131
LOCMI03672 : HVQRGD--RTTTIVREFSPEEMKMTMTVDDIVCTRIYKAI : 133
LOCMI03788 : KVERGDDGKTVTIEKTFSPQELVMTYSFGGATAKRVYKAV : 137
LOCMI05692 : QVQKFPDGKTVTTERQFSDGQMIATLSIGDVVAKRVYKAV : 136
LOCMI17564 : QVQKFPDGKVVNMEKKFSASELAVTITLGNVTAKRIYKAV : 135
B
500 bp
400 bp
350 bp
300 bp
250 bp
200 bp
150 bp
100 bp
50 bp
1
2
3
4
5
6
7
8
9
10
11

Supplementary Figure S23 Protein alignments and PCR validation of *L. migratoria* FABPs.

(A) Amino acid residues that are identical in all sequences are shaded red, while orange shadow indicates at least 50% identical amino acids in all sequences. The secondary structure is indicated as α (α-helix) and β (β-strands). (B) PCR validation of all identified FABP genes. Genes are arranged in the same order as in the alignment (A). Primers are listed in Supplementary Table S30.

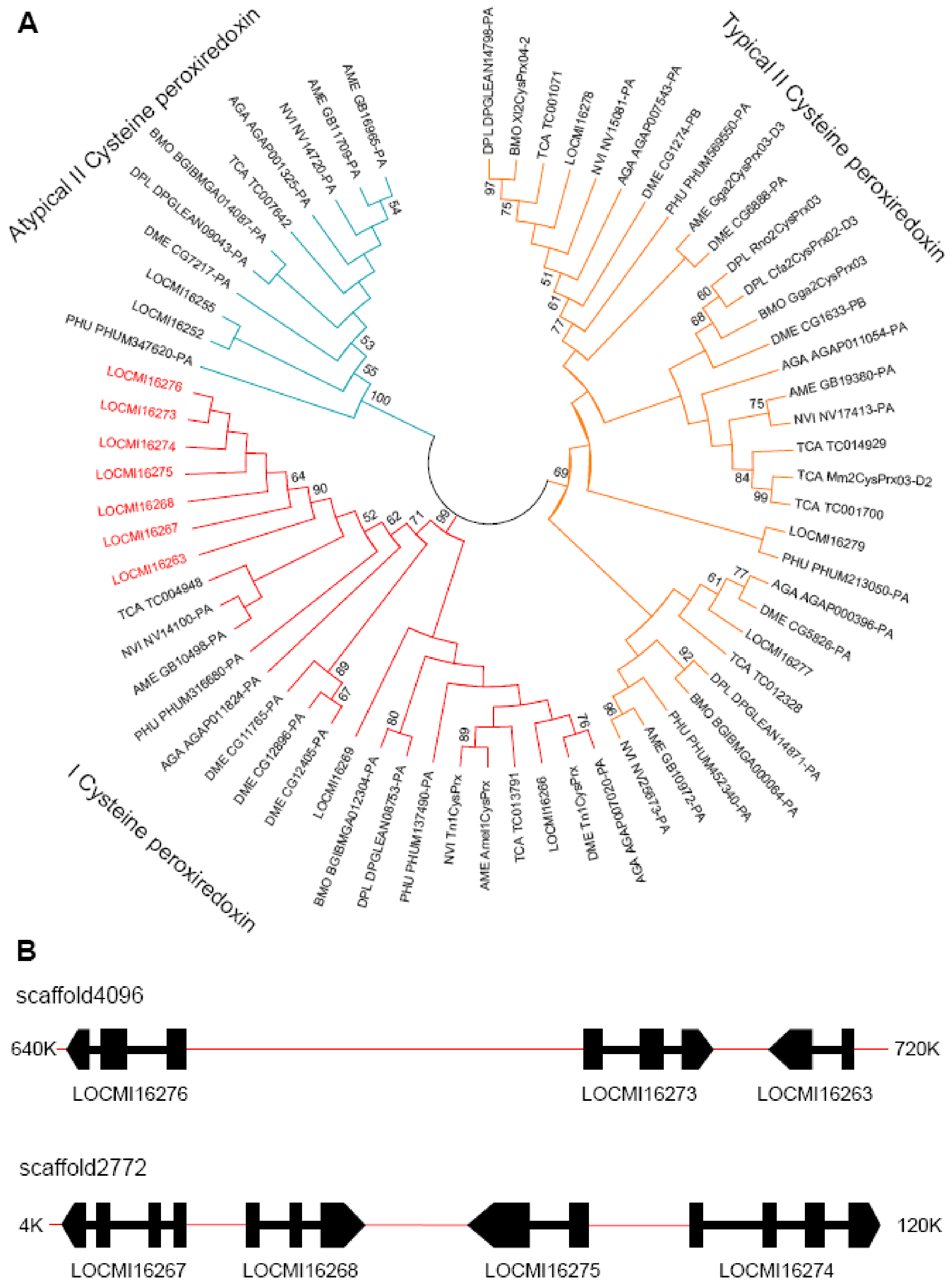

Supplementary Figure S24 Expansion of antioxidant genes in the *L. migratoria* genome.

(A) Phylogenetic tree of peroxiredoxin genes. The neighbor-joining algorithm was used with 500 bootstraps. The percentages of replicate trees (over 50%) in which the associated taxa clustered together in the bootstrap test (500 replicates) are shown next to the branches. Evolutionary distances were computed using the Poisson correction method and are expressed in units of number of amino acid substitutions per site. Rate variation among sites was modeled with gamma distribution (shape parameter = 1). (B) Organization of the expanded I cysteine peroxiredoxin (Prdx6) genes in the *L. migratoria* genome.

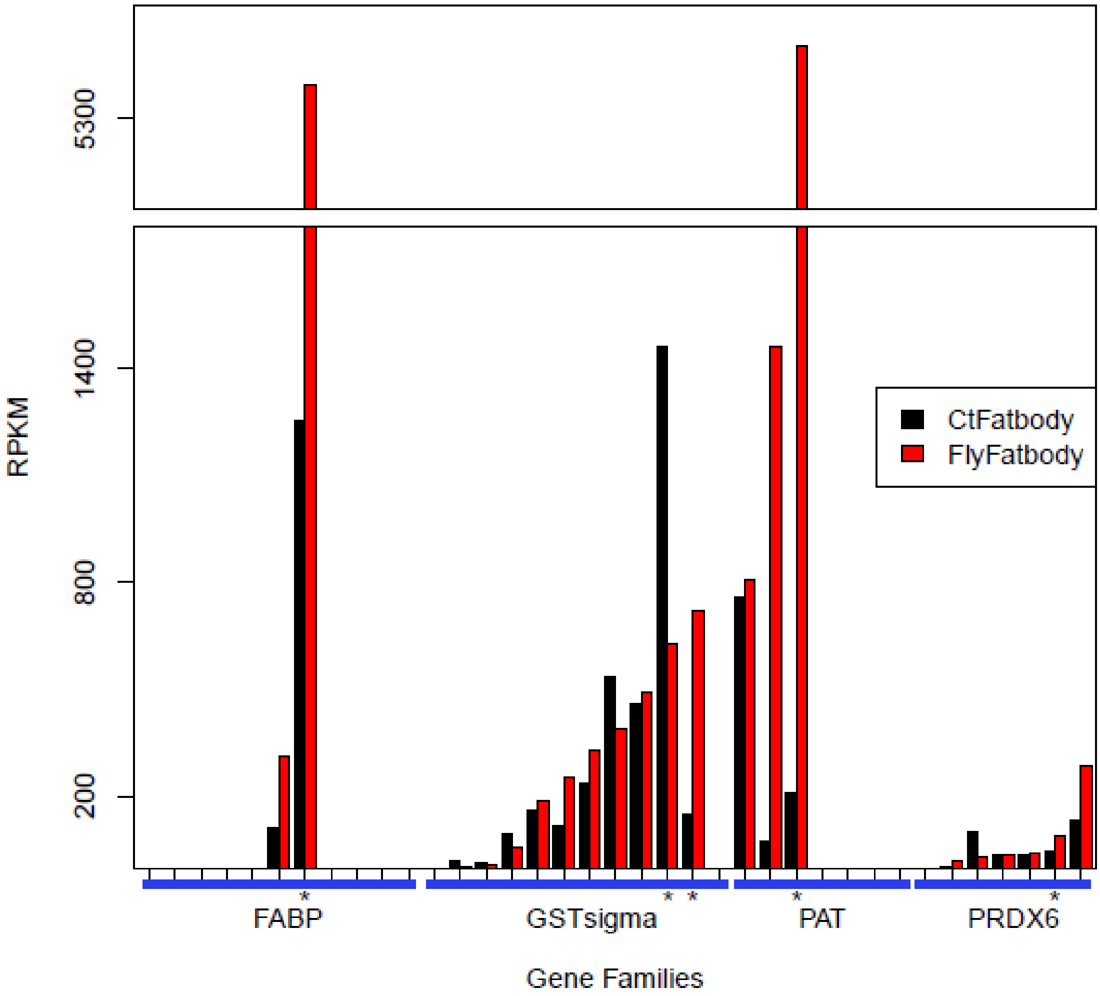

Supplementary Figure S25 Expression levels of expanded gene families in *L. migratoria* in the energy mobilization processes.

The red denotes the fat body samples before flying and the black denotes samples after flying. The asterisks at the bottom of the bar denote the significantly differentially expressed genes between these two samples.

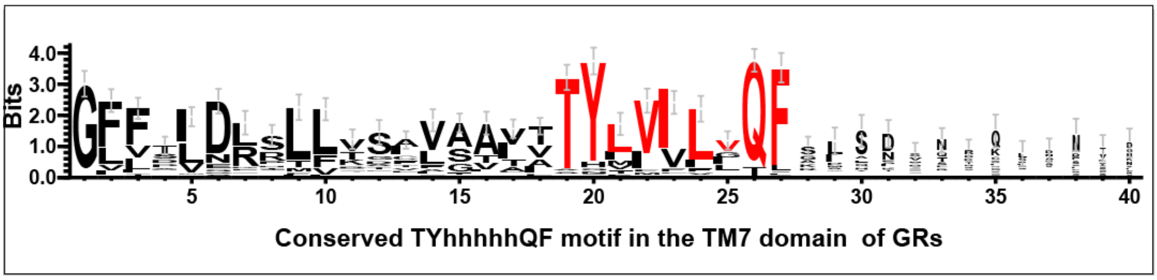

Supplementary Figure S26 The conserved TYhhhhhQF motif in the TM7 domain of GRs.

Consensus sequences of the UGT motifs were created and displayed using the WebLogo server at http://weblogo.berkeley.edu/. Error bars indicate an approximate, Bayesian 95% confidence interval. The TM7 domain for the 75 gustatory receptors were used to construct the TYhhhhhQF motif.

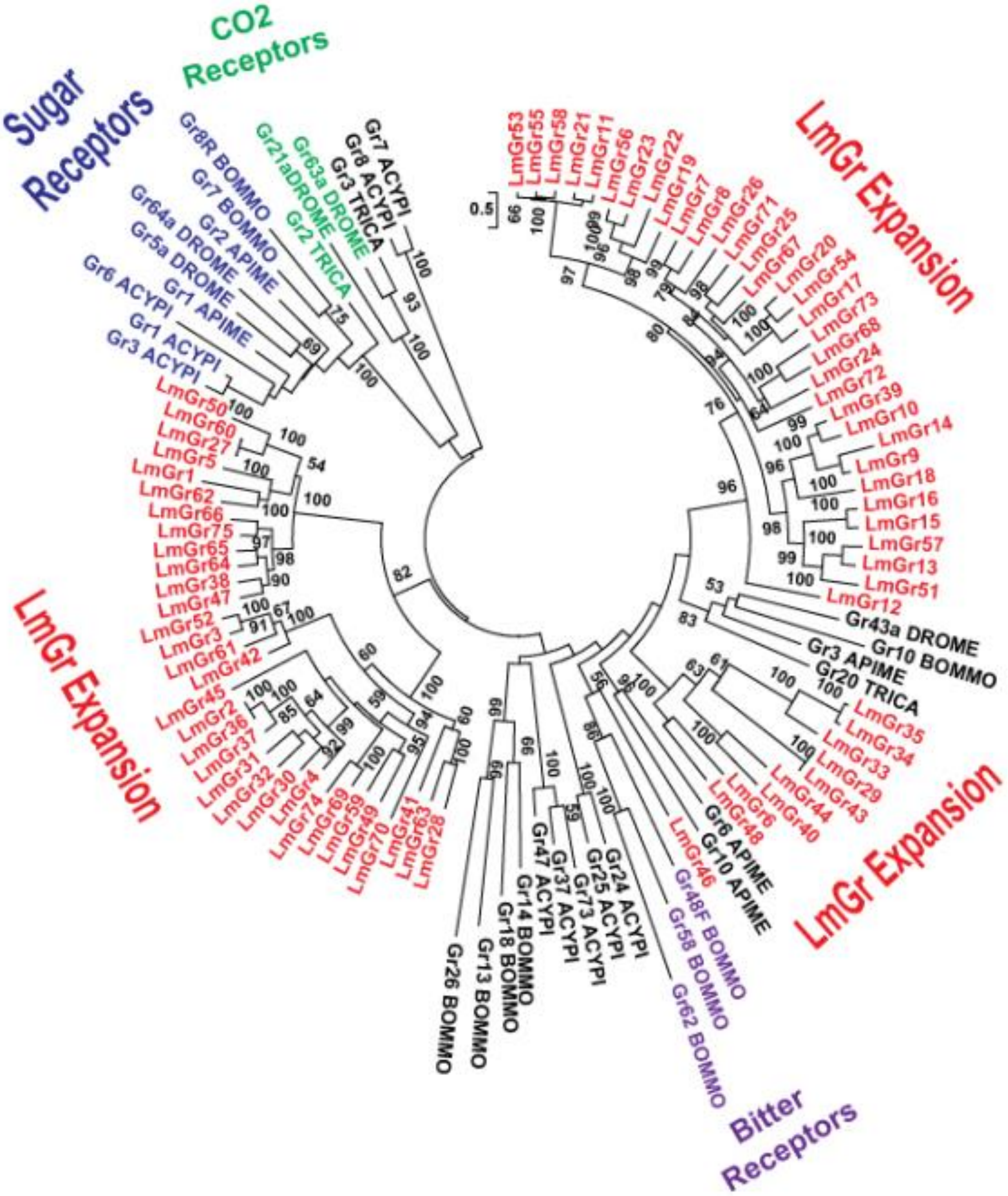

Supplementary Figure S27 A phylogenetic tree of *L. migratoria* GRs with representative GRs from other insects.

Nodes with >50% bootstrap support (100 replicates) are indicated. APIME, *Apis mellifera*, TRICA, *Tribolium castaneum*, BOMMO, *Bombyx mori*, DROME, *Drosophila melanogaster*, and ACYPI, *Acyrthosiphon pisum*.

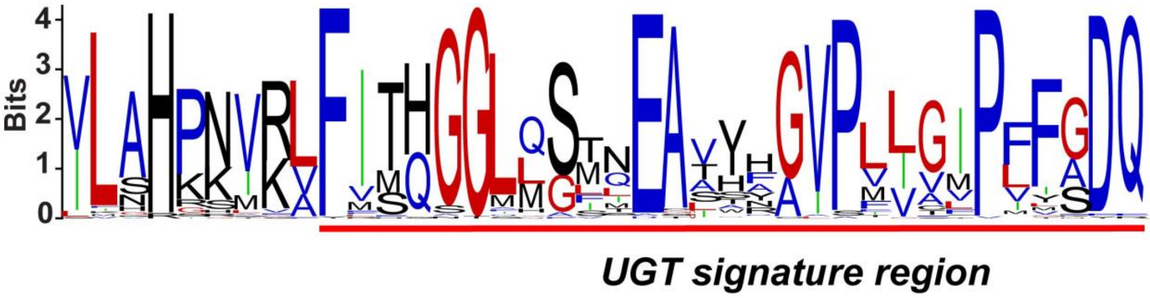

Supplementary Figure S28 WebLogos representing the signature motif of *L. migratoria* UGT genes.

UGT genes include a conserved C-terminal region that contain the UGT signature motif [FVA]-[LIVMF]-[TS]-[HQ]-[SGAC]-G-X[2]-[STG]-X[2]-[DE]-X[6]-P-[LIVMFA]-[LIVMFA]-X[2]- P-[LMVFIQ]-X[2]-[DE]-Q, where X is any amino acid [73]. The UGT signature motifs are underlined in red. Consensus sequences of the UGT motifs were created and displayed using the WebLogo server (http://weblogo.berkeley.edu/).

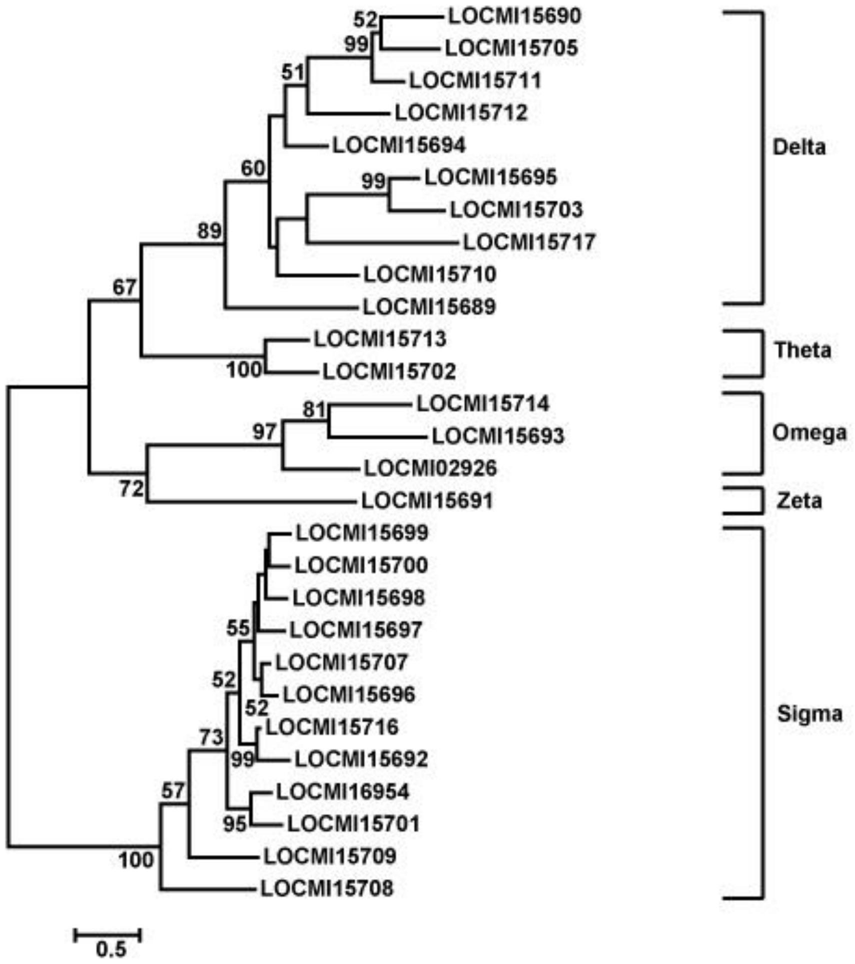

Supplementary Figure S29 The phylogenetic tree of glutathione S-transferases in *L. migratoria*.

The six subclasses are indicated on the right panel. Bootstrap values greater than 50 are labelled at the nodes. Scale bar shows the inferred amino acid distance.

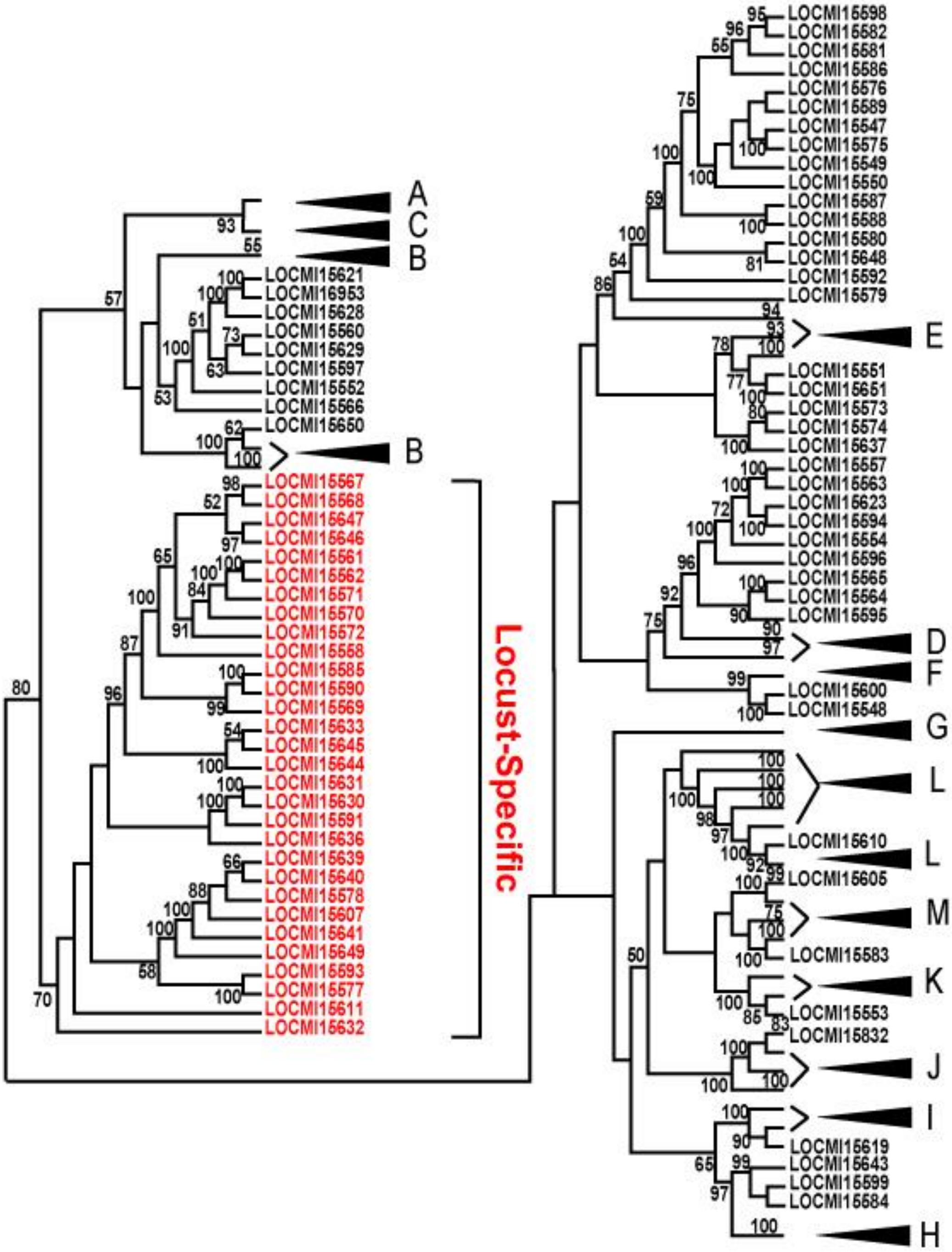

Supplementary Figure S30 The phylogenetic tree of *L. migratoria* CCE genes with representatives of CCE genes from different subclasses.

Numbers at nodes indicate bootstrap values, and only values greater than 50% are shown. Nomenclature of the clades was done based on previous studies[74].

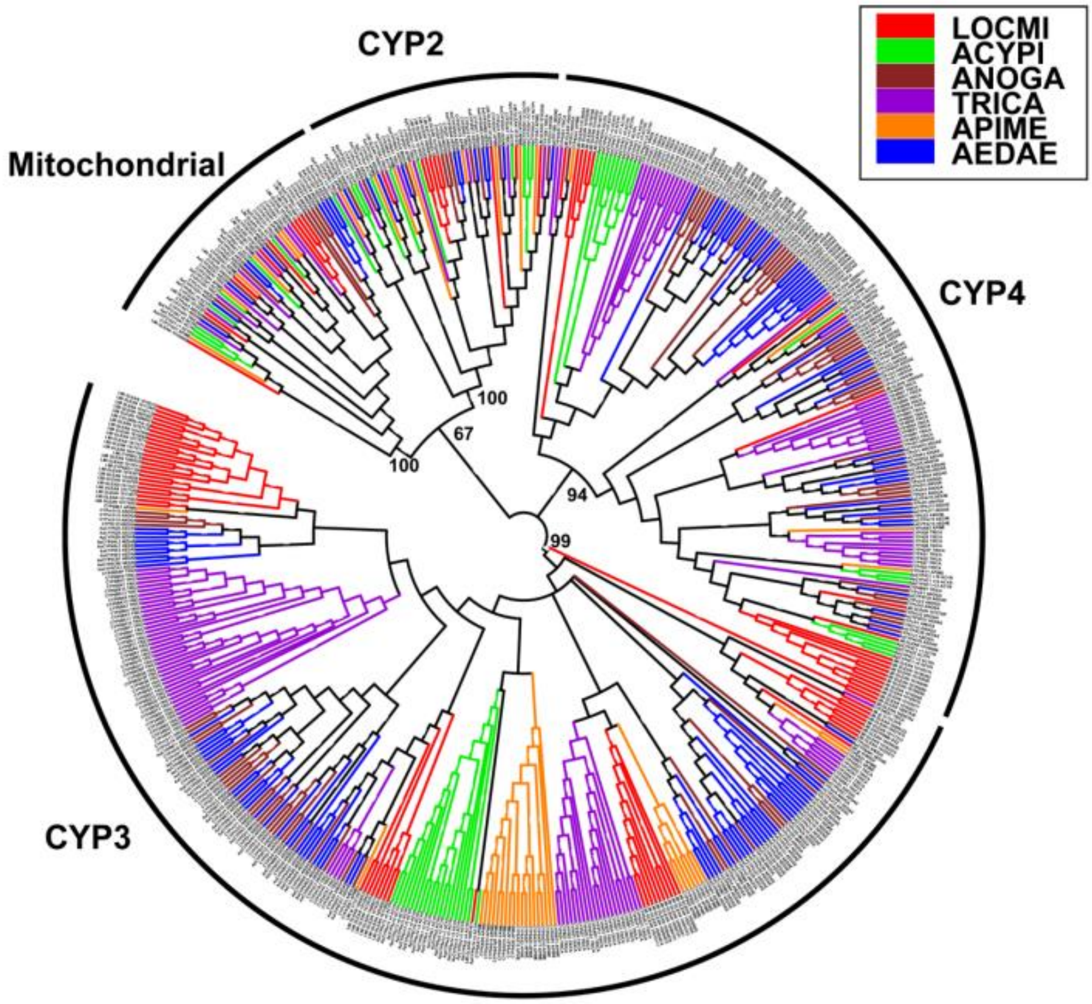

Supplementary Figure S31 The insect P450 gene family.

The four distinct branches of the phylogenetic tree corresponding to the known four clades of insect P450 genes. Bootstrap values are indicated for the four insect clades. LOCMI: *Locusta migratoria*; ACYPI: *Acyrthosiphon pisum*; APIME: *Apis mellifera*; AEDAE:, *Aedes aegypti*; TRICA: *Tribolium castaneum* and ANOGA: *Anopheles gambiae*.

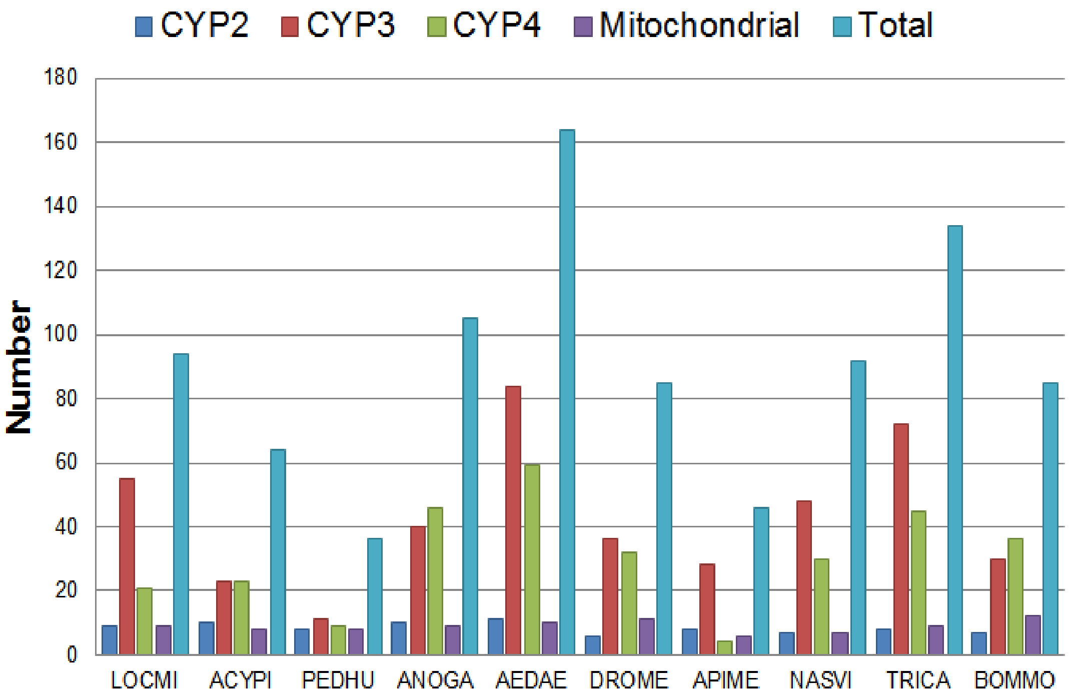

Supplementary Figure S32 Comparison of CYP gene numbers across several insect species.

The number of identified insect CYP genes in each P450 clade was retrieved from a previous study[75]. LOCMI: *Locusta migratoria*; ACYPI: *Acyrthosiphon pisum*; PEDHU: *Pediculus humanus*; APIME: *Apis mellifera*; NASVI: *Nasonia vitripennis*; TRICA: *Tribolium castaneum*; AEDAE, *Aedes aegypti*; BOMMO: *Bombyx mori*; DROME: *Drosophila melanogaster* and ANOGA: *Anopheles gambiae*.

Supplementary Tables

Supplementary Table S1 Illumina sequencing data for *L. migratoria* genome assembly.

Insert Size	Reads Length	Raw			Filter		
		Total Data (G)	Sequence coverage (X)	Physical coverage (X)	Total Data (G)	Sequence coverage (X)	Physical coverage (X)
170	100	38.57	6.12	10.41	30.23	4.8	8.59
200	150	54.63	8.67	11.56	44.51	7.07	9.81
200	100	277.47	44.04	88.09	218.36	34.66	74.4
500	100	252.93	40.15	200.74	168.41	26.73	144.9
800	100	165.23	26.23	209.82	103.02	16.35	139.61
2000	49	76.87	12.2	498.06	54.76	8.69	354.78
5000	49	84.75	13.45	1,372.72	42.16	6.69	682.84
10000	90	14.32	2.27	252.52	9.57	1.52	168.84
10000	49	39.96	6.34	1294.6	18.34	2.91	593.96
20000	49	80.46	12.77	5,212.82	21.77	3.46	1,410.63
20000	90	19.03	3.02	671.15	4.5	0.71	158.75
40000	49	30.81	4.89	3,992.78	5.15	0.82	667.3
Total		1,135.06	180.17	13,815.27	720.79	114.41	4,414.41

Note: For raw data, PCR duplication, low quality and adaptor contamination have been filtered. Physical coverage was calculated as insert size x paired-end reads number / genome size. The genome size is assumed to be 6.3 Gb.

Supplementary Table S2 Genome size estimation of *L. migratoria* based on 17-mer analysis.

k-mer size	#Total *k*-mer	*k*-mer depth	Genome size (bp)
17	146,642,996,731	23	6,375,782,466

Note: See Supplementary Supplementary Figure S2 for detailed description of the methods used.

Supplementary Table S3 Statistics of the assembly of *L. migratoria* genome.

	Contig		Scaffold	
	Size(bp)	**Number**	**Size(bp)**	**Number**
N90	1,933	672,695	17,393	39,025
N80	3,763	463,944	56,676	19,124
N70	5,527	338,619	107,724	10,783
N60	7,349	248,612	187,295	6,135
N50	9,338	179,233	322,681	3,440
Total size (bp)	5,748,086,465		6,524,990,357	
Longest (bp)	106,221		7,902,988	
Total number (>100 bp)	1,438,086		551,270	
Total number (>2 kb)	661,979		97,233	

N50 is the size above which the additive length occupies 50% of the total length of the assembly sequences. The total sizes of the contigs and scaffold were 5.7 Gb and 6.5 Gb respectively, with 0.78 Gb Ns (12% of the total assembly).

Supplementary Table S4 Statistics of Sanger sequencing reads aligned to the BAC sequences assembled using Solexa reads.

Library	Ratio mismatch	#Reads	Coverage>90%	Coverage>80%
107-88	0.09%	261	98.85%	100.00%
107-50	0.03%	286	94.76%	99.65%
107-16	0.04%	251	97.21%	98.01%
107-74	0.02%	284	91.90%	94.01%
107-86	0.03%	287	97.91%	98.26%
107-25	0.03%	198	93.43%	94.44%
Average	0.04%	261	95.68%	97.40%

The alignment was performed using BLAT.

Supplementary Table S5 Assembly quality validation by BAC coverage estimation.

BAC ID	Length (bp)	Coverage (%)	#Inconsistent	#Scaffold	Scaffold length (bp)
107-14	94,424	99.83	11	1	108,004
107-2	57,640	99.79	27	3	159,089
107-25	83,390	99.37	21	4	160,334
107-38	91,133	99.93	12	1	98,802
107-52	109,069	98.67	37	1	115,718
107-73	87,904	91.76	35	11	417,471
107-74	51,544	99.16	5	1	51,857
107-86	58,464	95.03	22	3	174,224
107-88	84,676	95.00	21	5	157,623
Average	79,678	94.00	22	4	206,414

Supplementary Table S6 Assembly quality validation by EST coverage estimation.

	Total Number	Total Match		>50%		>90%	
		Number	Percent	Number	Percent	Number	Percent
>200	41,880	41,547	99.2%	41,360	98.76%	39,625	94.62%
>500	23,408	23,242	99.29%	23,162	98.95%	22,647	96.75%

Supplementary Table S7 Comparison of assembled scaffolds with 71 *L. migratoria* complete CDS sequences in GenBank.

ID	Length (bp)	% bases covered by single best piece	ID	Length (bp)	% bases covered by single best piece
AB583233.1	1,446	100.00%	FJ609648.1	2,075	89.69%
AB698670.1	2,233	100.00%	FJ609649.1	1,848	98.48%
AB698671.1	2,625	100.00%	FJ609738.1	2,089	99.52%
AB698672.1	2,142	100.00%	FJ609739.1	2,156	100.00%
AF049136.1	2,401	87.51%	FJ609741.1	2,144	97.81%
AF083951.1	2,360	98.18%	FJ771024.1	2,471	99.07%
AF083952.1	2,031	97.29%	FJ771025.1	2,388	98.91%
AF083953.1	1,944	68.47%	FJ795020.1	1,953	98.46%
AF107732.1	579	99.83%	GU067730.1	5,116	95.72%
AF107733.1	700	99.86%	GU067731.1	5,116	95.72%
AF115777.1	1,850	90.05%	GU593056.1	939	95.95%
AF136372.1	4,677	99.64%	GU722575.1	1,055	80.76%
AY040537.1	3,926	96.03%	GU722576.1	469	96.59%
AY077627.1	1,835	96.84%	GU722577.1	517	97.29%
AY077628.1	1,469	98.16%	GU722578.1	459	99.78%
AY299637.3	1,968	99.54%	GU722579.1	483	100.00%
AY348873.1	4,752	99.54%	HM131834.1	657	100.00%
AY445913.2	2,465	96.80%	HM131835.1	645	99.84%
DQ340870.1	3,774	95.95%	HM131836.1	615	99.67%
DQ355963.1	883	95.58%	HM131837.1	615	100.00%
DQ355964.1	1,802	98.28%	HM131838.1	615	100.00%
DQ355965.1	773	96.25%	HM131839.1	615	100.00%
DQ355966.1	1,660	98.19%	HM131840.1	609	100.00%
DQ513322.1	2,052	98.73%	HM131841.1	615	99.02%
DQ848565.1	1,313	99.77%	HM131842.1	615	100.00%
EF090723.1	1,604	96.38%	HM131843.1	696	99.71%
EU131894.1	2,806	98.68%	HM153425.1	1,917	78.46%
EU231603.1	2,255	69.09%	HM153426.1	1,895	98.47%
FJ215322.1	607	95.22%	HQ213937.1	2,271	98.90%
FJ472841.1	2,863	90.95%	J03888.1	672	100.00%
FJ472842.1	2,395	97.58%	JN129988.1	599	59.93%
FJ472843.1	2,583	98.61%	JN247410.1	465	82.80%
FJ609646.1	2,488	99.12%	JN661173.1	1,600	98.69%
FJ609647.1	1,766	98.36%	M36206.1	938	95.42%
U90609.1	2,193	96.58%	U74469.1	4,016	91.38%
Z22805.1	603	99.34%			
Sum	Length:	127,771	Covered%:	95.72%	

Supplementary Table S8 Comparison of gene parameters among the sequenced insects and *H. sapiens*.

species	GN	CO	%	SE	%	ATL	ACL	AEG	AEL	AIL
L. migratoria	17,307	14,805	85.54	3,079	17.79	54,341	1,160	5.77	201	11,159
A. pisum	33,486	32,316	96.51	8,967	26.78	4,333	899	4.06	221	1,121
P. humanus	10,775	10,646	98.80	353	3.28	3,139	1,545	6.43	240	294
A. mellifera	11,062	10,411	94.11	847	7.66	8,976	1,627	6.46	252	1,347
D. melanogaster	13,689	13,608	99.41	2,761	20.17	4,261	1,621	3.97	408	888
A. gambiae	14,324	14,324	100	1,667	11.64	5,955	1,583	4.21	376	1,363
B. mori	14,623	14,623	100	2,260	15.46	6,030	1,224	5.44	225	1,082
D. pulex	30,907	30,907	100	5,341	17.28	2,009	976	4.62	211	285
N. vitripennis	17,369	17,369	100	2,598	14.96	6,934	1,412	5.30	267	1,286
T. castaneum	16,531	15,733	95.17	2,937	17.77	5,289	1,351	4.34	311	1,179
H. sapiens	22,389	20,098	89.77	3,318	14.82	44,855	1,560	8.96	174	5,436

Abbreviations: GN: Gene set number; CO: Number of genes with complete open reading frames; SE: Single Exon Gene Number; ATL: Average transcript length (bp); ACL: Average CDS length (bp); AEG: Average exon number per gene; AEL: Average exon length (bp); AIL: Average intron length (bp).

Supplementary Table S9 Gene functional annotation.

		Number	**%genes**
Total		17,307	100
Annotated	Swissprot	11,513	66.52%
	TrEMBL	12,101	69.92%
	KEGG	10,687	61.75%
	InterPro	10,268	59.33%
	GO	8,459	48.88%
	NR	12,343	71.32%
	All annotated	12,963	74.90%
Unknown		4,344	25.10%

Supplementary Table S10 Number of base pairs occupied by transposable element derived sequences in the genomes of four species.

	L. migratoria		*D. melanogaster*		*H. sapiens*	
Types	**Length (bp)**	**P%**	**Length (bp)**	**P(%)**	**Length (bp)**	**P(%)**
DNA	1,480,538,225	22.69	4,849,763	2.87	99,797,428	3.18
LINE	1,332,720,207	20.42	12,119,904	7.18	637,919,432	20.33
LTR	508,675,263	7.80	21,849,378	12.95	267,738,295	8.53
nonLTR	63,892,419	0.98	-	-	-	-
Retro	153,548,453	2.35	-	-	-	-
Unknown	406,097,360	6.22	11,211,970	6.64	1,298,163	0.04
SINE	141,176,698	2.16	52,841	0.03	397,225,496	12.66
Simple_repeat	13,026,240	0.20	2,733	0.00	26,240,511	0.84
Other	32,017	0.00	698,554	0.41	4,153,812	0.13
Total	3,840,808,141	58.86	50,785,143	30.00	1,434,373,137	46.00

Supplementary Table S11 Top 10 dominant repeat families.

#	Copy number	Length (bp)	Percentage (%)	
1	611,942	260,834,265	4.00	NonLTR/LINE/RTE-BovB
2	1,434,794	235,189,848	3.60	NonLTR/SINE/LM1
3	440,451	172,763,602	2.65	NonLTR/LINE/CR1
4	216,915	77,610,704	1.19	NonLTR/LINE/CR1
5	117,885	56,089,356	0.86	DNA/TcMar-Tc1
6	144,881	51,843,228	0.79	DNA
7	87,352	37,702,822	0.58	Satellite
8	209,668	34,698,742	0.53	NonLTR/SINE/ID
9	143,144	24,029,149	0.37	NonLTR/SINE/MIR
10	48,432	18,584,822	0.28	NonLTR/LINE/CR1

Supplementary Table S12 Statistics of intronic expansion/contraction in 1,046 conserved single copy orthologous genes.

Species	Contraction%	Expansion%
Bombyx mori	2.4%	97.6%
Pediculus humanus	1.5%	98.5%
Anopheles gambiae	2.3%	97.7%
Tribolium castaneum	2.3%	97.7%
Drosophila melanogaster	2.0%	98.0%
Apis mellifera	3.8%	96.2%
Acyrthosiphon pisum	4.2%	95.8%
Nasonia vitripennis	3.9%	96.1%
Daphnia pulex	0.9%	99.1%
Average	2.6%	97.3%

Supplementary Table S13 IPR enrichment of hemi/holo-metabolous insect-specific gene families.

IPR ID	IPR Title	FDR
Holometabolous Specific gene families		
IPR013087	Zinc finger, C2H2-type/integrase, DNA-binding	2.49E-32
IPR007087	Zinc finger, C2H2-type	2.85E-30
IPR015880	Zinc finger, C2H2-like	2.30E-28
IPR004117	Olfactory receptor, Drosophila	1.63E-21
IPR009057	Homeodomain-like	1.09E-10
IPR012287	Homeodomain-related	7.61E-08
IPR012934	Zinc finger, AD-type	9.29E-08
IPR020479	Homeobox, eukaryotic	1.49E-07
IPR013653	FR47-like	3.23E-06
IPR007614	Retinin-like protein	5.68E-06
IPR001356	Homeobox	7.99E-06
IPR006625	Insect pheromone/odorant binding protein PhBP	2.21E-05
IPR006631	Protein of unknown function DM4/12	5.20E-05
IPR006170	Pheromone/general odorant binding protein, PBP/GOBP	7.79E-05
IPR023316	Pheromone/general odorant binding protein, PBP/GOBP, domain	1.14E-04
IPR005520	Attacin, N-terminal	1.14E-04
IPR000010	Proteinase inhibitor I25, cystatin	1.14E-04
IPR000219	Dbl homology (DH) domain	2.80E-04
IPR013069	BTB/POZ	4.93E-04
IPR002557	Chitin binding domain	5.73E-04
IPR005521	Attacin, C-terminal	1.28E-03
IPR011526	Helix-turn-helix, Psq-like	1.55E-03
IPR022773	Siva	1.78E-03
IPR011333	BTB/POZ fold	2.38E-03
IPR007889	Helix-turn-helix, Psq	4.48E-03
IPR022727	Pupal cuticle protein C1	5.86E-03
IPR000237	GRIP	2.63E-02
IPR020381	Proteinase inhibitor I25, cystatin, conserved region	2.79E-02
IPR008837	Serendipity locus alpha	2.79E-02
IPR008422	Homeobox KN domain	2.79E-02
IPR010562	Haemolymph juvenile hormone binding	2.99E-02
IPR012464	Protein of unknown function DUF1676	2.99E-02
IPR016179	Insulin-like	3.59E-02
IPR001159	Double-stranded RNA-binding	3.59E-02
IPR006593	Cytochrome b561/ferric reductase transmembrane	4.57E-02
IPR004877	Cytochrome b561, eukaryote	4.57E-02
IPR011993	Pleckstrin homology-type	4.57E-02
Hemimetabolous Specific gene families		

IPR006578	MADF domain	1.47E-33
IPR006612	Zinc finger, C2CH-type	3.11E-12
IPR000618	Insect cuticle protein	7.92E-03
IPR003961	Fibronectin, type III	7.92E-03
IPR002298	DNA polymerase A	1.08E-02
IPR008957	Fibronectin type III domain	1.08E-02
IPR004210	BESS motif	1.59E-02
IPR002156	Ribonuclease H domain	3.75E-02
IPR002350	Proteinase inhibitor I1, Kazal	4.53E-02
IPR012337	Ribonuclease H-like	4.53E-02
IPR004911	Gamma interferon inducible lysosomal thiol reductase GILT	4.91E-02
IPR015689	Tachykinin-like receptor	4.91E-02

FDR: false discovery rate.

Supplementary Table S14 IPR annotation of the expanded families in *L. migratoria*.

IPR annotation	API	LMI	PHU	AGA	AME	BMO	DPU	DME	NVI	TCA	FDR
IPR006578: MADF domain;	41	64	0	3	1	4	0	1	1	2	0
no ipr annotation	27	41	0	0	0	0	0	0	0	0	0
IPR009072: Histone-fold;IPR000558: Histone H2B;IPR007125: Histone core;	0	26	0	0	0	0	0	0	0	0	0
IPR004117: Olfactory receptor, Drosophila;	0	96	0	0	0	0	0	0	0	0	0
IPR001005: SANT domain, DNA binding;IPR012287: Homeodomain-related;IPR006578: MADF domain;	4	29	0	0	0	0	0	0	0	3	0
IPR002018: Carboxylesterase, type B;	19	78	5	29	16	52	9	19	30	35	0
IPR005055: Insect pheromone-binding protein A10/OS-D;	9	51	6	6	5	16	2	4	9	18	0
IPR013604: 7TM chemoreceptor;	0	33	0	0	0	0	0	0	0	0	0
IPR013087: Zinc finger, C2H2-type/integrase, DNA-binding;IPR007087: Zinc finger, C2H2-type;	133	46	2	2	0	11	1	0	2	24	1.0E-06
IPR001360: Glycoside hydrolase, family 1;IPR013781: Glycoside hydrolase, subgroup, catalytic core;	7	34	1	6	1	21	2	1	5	8	1.0E-06
IPR002213: UDP-glucuronosyl/UDP-glucosyltransferase;	45	70	4	23	11	33	24	33	19	27	4.0E-06
IPR018272: PRANC domain; IPR020683: Ankyrin repeat-containing domain;	0	16	0	0	0	0	0	0	11	0	6.2E-05
IPR001128: Cytochrome P450;	23	69	10	42	31	27	12	34	45	68	1.6E-04
IPR013788: Arthropod hemocyanin/insect	2	27	3	13	5	9	1	7	10	12	2.00E-04

LSP;IPR005204: Hemocyanin, N-terminal;IPR000896: Hemocyanin, copper-containing;IPR005203: Hemocyanin, C-terminal;										
IPR003663: Sugar/inositol transporter;IPR020846: Major facilitator superfamily;	17	43	9	17	16	20	1	13	23	41	3.84E-04
IPR002347: Glucose/ribitol dehydrogenase;IPR016040: NAD(P)-binding domain;	12	20	1	8	5	3	1	10	19	17	6.07E-03
IPR010562: Haemolymph juvenile hormone binding;	19	29	16	12	7	21	1	22	8	30	7.72E-03
IPR016187: C-type lectin fold;IPR001304: C-type lectin;	0	8	0	0	0	4	0	0	12	0	1.25E-02
IPR001071: Cellular retinaldehyde binding/alpha-tocopherol transport;IPR001251: Cellular retinaldehyde-binding/triple function, C-terminal;IPR011074: Phosphatidylinositol transfer protein-like, N-terminal;	10	24	4	11	4	20	6	14	10	26	1.87E-02
IPR003439: ABC transporter-like;IPR011527: ABC transporter, transmembrane domain, type 1;IPR001140: ABC transporter, transmembrane domain;	10	20	2	7	5	8	1	11	18	32	2.59E-02

Abbreviations: LMI: *Locusta migratoria*, DPU: *Daphnia pulex*, PHU: *Pediculus humanus*, API: *Acyrthosiphon pisum*, AME: *Apis mellifera*, NVI: *Nasonia vitripennis*, TCA: *Tribolium castaneum*, BMO: *Bombyx mori*, AGA: *Anopheles gambiae* and DME: *Drosophila melanogaster*.

Supplementary Table S15 Members of DNA methyltransferase (DNMT) genes in various arthropod species.

Species	DNMT1	DNMT2	DNMT3
Daphnia pulex	1	1	1
Locusta migratoria	2	1	1
Acyrthosiphon pisum	2	1	2
Pediculus humanus	2	1	0
Apis mellifera	2	1	1
Nasonia vitripennis	3	1	1
Camponotus floridanus	1	1	2
Harpegnathos saltator	1	1	2
Solenopsis invicta	1	1	1
Pogonomyrmex barbatus	1	1	1
Atta cephalotes	1	1	1
Tribolium castaneum	1	1	0
Bombyx mori	1	1	0
Danaus plexippus	1	1	0
Drosophila melanogaster	0	1	0

Supplementary Table S16 Mapping statistics of RRBS and whole genome test reads.

Samples	WholeGenome	Gregarious		Solitarious	
Library		**short_lib**	**Long_lib**	**Short_lib**	**Long_lib**
Insert Size	400	62	125	62	113
Read length	100	49	49	49	49
#Reads (M)	22	127	149	108	155
Total bp (Mb)	2,222	6,246	7,278	5,307	7,600
#AfterFilter_Reads (M)	22	106	132	99	151
#AfterFilter_bp (Mb)	2,134	5,148	6,449	4,817	7,378
Unique Mapped (%)	52.18%	39.73%	46.21%	42.34%	50.00%

The whole genome test Bisulfite sequencing reads was sequenced using the gregarious brain samples. The Short_lib represents the libraries with 40-120 bp insert sizes and the Long_lib represents the libraries with 120-240 bp insert sizes. The insert size here was estimated by mapping the reads to the reference genome.

Supplementary Table S17 Summary of methylation types in the *L. migratoria* genome by RRBS and whole genome test.

SampleName	WholeGenome	Gregarious brain	Solitarious brain
TotalC	184,180,721	583,516,064	664,905,454
CpGC	2,670,788	21,132,528	23,593,345
CHGC	93,696	1,088,326	1,310,445
CHHC	304,983	1,767,250	2,019,361
CpGCT	28,722,148	166,599,320	197,011,225
CHGCT	37,376,081	137,895,310	160,519,740
CHHCT	115,013,025	255,033,330	280,451,338
PctCpG	8.50%	11.26%	10.69%
PctCHG	0.30%	0.78%	0.81%
PctCHH	0.30%	0.69%	0.71%

TotalC include three kinds cytosine, CpG, CHG and CHH. PctCpG was calculated as the ratio of methylated CpG (CpGC) to the sum of CpGC and CpGCT, which was the number of C that was converted to T in the CpG context. The same for PctCHG and PctCHH.

Supplementary Table S18 statistics of covered CpG sites and related genes in the genome.

	Gregarious	Solitarious	Merge	Intersect
#CoveredCpG	7,568,981	7,996,483	9,311,972	4,345,168
#CoveredCpG_genebody	935,461	940,919	1,092,751	783,629
%CoveredCpG_genebody	12.36%	11.77%	11.73%	18.03%
#genes_covered_⩾1_CpG	11,970	11,802	12,202	11,570
#genes_covered_⩾4_CpG	11,447	11,337	11,743	11,041

The minimum depth of covered CpG sites was 10X. Merge: at any samples.

Supplementary Table S19 The 90 differentially methylated genes between the gregarious and solitarious locust brains.

GeneID	[1]#DMCG	[2]#CovCG	[3]RPKM G-B	[4]RPKM S-B	[5]Adjpv (S-B/G-B)	Annotation
LOCMI01552	4	22	6.55	6.28	0.81	Neuroglobin
LOCMI02733	6	24	4.23	4.87	0.42	NA
LOCMI02892	6	87	147.55	94.15	0.00	Mitogen-activated protein-binding protein-interacting protein homolog
LOCMI03529	4	64	6.98	6.54	0.66	NA
LOCMI03618	7	43	0.40	2.34	0.00	NA
LOCMI03849	4	330	33.39	56.35	0.00	SAP domain-containing ribonucleoprotein
LOCMI04268	5	534	10.59	11.42	0.54	Kinesin-associated protein 3
LOCMI04715	4	110	1.90	2.28	0.47	NA
LOCMI05065	5	93	28.11	34.45	0.00	Sterile alpha and TIR motif-containing protein 1
LOCMI05203	4	5	20.73	20.02	0.70	NA
LOCMI05982	5	49	13.11	18.46	0.00	Early endosome antigen 1
LOCMI06392	4	75	14.91	20.56	0.00	MAGUK p55 subfamily member 7
LOCMI06494	12	97	60.17	51.91	0.00	Unc-112-related protein
LOCMI06973	5	274	16.43	18.02	0.32	UPF0614 protein C14orf102
LOCMI07217	5	126	6.41	3.97	0.00	Transmembrane protein 194A
LOCMI07377	9	422	176.42	157.21	0.00	Basement membrane-specific heparan sulfate proteoglycan core protein
LOCMI07716	4	100	8.53	7.75	0.50	Protein FAN
LOCMI07961	4	99	1.04	3.23	0.00	NA
LOCMI08088	4	189	56.34	41.44	0.00	Probable protein-cysteine N-palmitoyltransferase porcupine
LOCMI08168	4	15	0.00	2.40	0.00	Ankyrin-2
LOCMI08308	5	233	64.88	56.36	0.00	E3 ubiquitin-protein ligase hyd
LOCMI08333	5	424	16.37	17.61	0.45	Polyhomeotic-like protein 1

LOCMI08659	11	160	4.36	6.85	0.00	Zinc finger protein 91
LOCMI08753	4	8	0.63	5.55	0.00	
LOCMI08782	18	228	0.89	1.54	0.14	Inversin
LOCMI08848	4	344	4.32	3.46	0.25	
LOCMI08885	4	218	4.15	3.26	0.20	Switch-associated protein 70
LOCMI08924	4	125	26.63	22.97	0.04	NA
LOCMI08951	4	51	10.70	14.04	0.01	PR domain zinc finger protein 4
LOCMI09066	10	150	13.18	9.94	0.01	Transmembrane protein 183
LOCMI09161	6	273	2.00	3.48	0.01	RNA exonuclease 1 homolog
LOCMI09176	7	177	11.07	16.64	0.00	Rho GTPase-activating protein 190
LOCMI09218	5	255	29.82	25.77	0.03	HEAT repeat-containing protein 5B
LOCMI09288	4	159	0.00	0.04	0.59	NA
LOCMI09354	5	322	22.62	22.90	0.90	NA
LOCMI09607	4	110	5.02	9.02	0.00	Zinc finger protein 106 homolog
LOCMI09748	9	184	24.75	22.43	0.20	NA
LOCMI09749	7	364	11.38	14.10	0.03	RING finger protein unkempt
LOCMI09785	7	234	9.15	11.97	0.01	Probable uridine-cytidine kinase
LOCMI09797	22	216	9.70	15.50	0.00	Telomerase-binding protein EST1A
LOCMI09866	4	75	97.52	111.95	0.00	Eukaryotic translation initiation factor 4B
LOCMI09918	8	244	51.84	57.26	0.04	Serine/threonine-protein kinase SRPK3
LOCMI09987	10	439	32.77	28.37	0.03	NA
LOCMI10093	7	201	14.02	14.79	0.61	GRIP and coiled-coil domain-containing protein 1
LOCMI10164	4	145	15.86	17.44	0.30	Protein Daple
LOCMI10228	5	256	1.95	3.27	0.02	Uncharacterized protein KIAA0467
LOCMI10293	6	176	46.96	29.62	0.00	Collagen alpha-1(XXVII) chain
LOCMI10351	6	140	25.40	30.67	0.00	Brefeldin A-inhibited guanine nucleotide-exchange protein 3

LOCMI10509	5	60	17.58	12.03	0.00	ATP-binding cassette sub-family D member 3
LOCMI10788	4	58	1.76	1.15	0.18	Tubulin glycylase 3B
LOCMI11004	9	115	43.14	31.20	0.00	Phosphatidylinositol glycan anchor biosynthesis class U protein
LOCMI11005	8	51	9.64	12.00	0.05	Ribosome biogenesis protein BOP1 homolog
LOCMI11060	5	68	4.41	4.15	0.77	Ankyrin-2
LOCMI11711	5	586	8.87	7.10	0.09	Ubiquitin-protein ligase E3B
LOCMI12126	4	73	3.63	5.64	0.01	Uncharacterized protein C10orf118 homolog
LOCMI12132	5	55	5.47	8.75	0.00	Protein FAM91A1
LOCMI12604	4	25	0.42	0.04	0.04	Putative ankyrin repeat protein RBE_0921
LOCMI12740	4	210	0.58	1.25	0.04	
LOCMI12853	5	142	42.90	45.55	0.30	Phosphatidylinositol-4-phosphate 5-kinase type-1 alpha
LOCMI13295	4	80	0.00	0.00	1.00	Sialin OS=Homo sapiens
LOCMI13328	4	119	29.86	31.06	0.58	Calcium-binding and coiled-coil domain-containing protein 2
LOCMI13357	4	95	29.17	39.62	0.00	Endophilin-B1
LOCMI13712	4	300	43.42	40.68	0.26	Glycyl-tRNA synthetase
LOCMI13714	6	358	2.82	3.99	0.08	NA
LOCMI13789	5	76	10.96	13.58	0.04	Probable phospholipid-transporting ATPase IA
LOCMI13989	4	101	0.59	0.05	0.00	Netrin-G1 ligand
LOCMI14004	4	19	9.60	17.88	0.00	Serine--pyruvate aminotransferase, mitochondrial
LOCMI14187	4	145	22.85	21.61	0.51	Polyphosphoinositide phosphatase
LOCMI14270	4	41	104.11	97.50	0.07	Dynein heavy chain, cytoplasmic
LOCMI14289	4	85	4.18	6.25	0.01	Dedicator of cytokinesis protein 7
LOCMI14667	11	102	4.75	4.87	0.92	Aladin

LOCMI14843	6	44	0.04	0.07	1.00	NA
LOCMI14963	4	78	4.80	11.27	0.00	Hyaluronan mediated motility receptor
LOCMI15522	4	59	35.13	46.27	0.00	NA
LOCMI15740	5	123	0.11	0.36	0.17	NA
LOCMI15751	7	499	9.29	10.32	0.40	Protein son of sevenless
LOCMI15754	4	226	6.10	11.38	0.00	NA
LOCMI15756	5	72	32.96	53.96	0.00	NA
LOCMI15961	4	288	11.51	12.66	0.41	NA
LOCMI16020	7	95	25.43	17.96	0.00	NA
LOCMI16380	6	38	49.61	38.72	0.00	Serine/threonine-protein kinase mTOR
LOCMI16558	4	140	2.59	1.58	0.05	NA
LOCMI16680	4	275	9.07	12.70	0.00	NA
LOCMI17108	4	77	143.47	116.71	0.00	NA
LOCMI17214	4	165	2.56	2.34	0.75	Serine/threonine-protein kinase DCLK1
LOCMI17232	5	172	66.60	51.17	0.00	Niemann-Pick C1 protein
LOCMI17328	7	120	13.76	15.05	0.36	NUAK family SNF1-like kinase 1
LOCMI17336	4	106	17.77	13.89	0.01	Vacuolar protein sorting-associated protein 16 homolog
LOCMI17416	6	23	3.26	1.80	0.01	NA
LOCMI13806	8	107	6.15	7.60	0.13	Phosphatidylinositol-4,5-bisphosphate 3-kinase catalytic subunit delta isoform

Notes: 1. Number of differentially methylated CG sites of one gene. 2. Number of Covered CG sites of one gene; 3. The expression level (RPKM value) in the brain of gregarious locust. 4. The expression level (RPKM value) in the brain of solitarious locust. 5. False discovery rate of the significant level of the differential expression in the brains between gregarious and solitarious locusts.

Supplementary Table S20 Transcriptome data and mapping statistics.

Sample	Total reads	Mapped reads	Map%	RPKM		
				>0	>=1	>=5
Gegg	3,763,045	1,513,052	40.21%	12,231	11,735	8,512
G1_2	4,484,110	2,026,623	45.20%	12,339	11,668	8,010
G3	16,895,730	11,229,663	66.46%	14,392	12,046	8,056
G4	20,617,698	15,806,218	76.66%	14,925	13,265	9,713
G5	5,589,216	2,983,675	53.38%	13,375	12,628	8,656
Gadult	3,908,336	1,931,045	49.41%	11,977	11,639	9,148
Segg	5,612,745	2,464,268	43.90%	12,763	12,010	8,728
S1_2	4,117,835	1,701,616	41.32%	12,226	11,716	8,152
S3	16,669,884	11,209,294	67.24%	14,209	11,910	7,679
S4	19,959,546	16,142,892	80.88%	14,235	12,067	8,307
S5	5,111,368	2,601,197	50.89%	12,654	11,809	7,661
Sadult	4,974,685	2,650,487	53.28%	12,985	12,043	7,684
G-B	70,619,250	56,173,778	79.54%	14,637	12,584	9,783
S-B	76,275,942	58,821,271	77.12%	14,470	12,535	9,879
IG-C	85,275,914	68,065,130	79.82%	14,649	11,680	7,183
IG-4h	91,007,586	72,991,150	80.20%	14,385	11,766	7,529
IG-8h	75,905,038	59,360,007	78.20%	14,238	11,447	6,881
IG-16h	67,089,958	54,110,697	80.65%	14,324	11,714	7,599
IG-32h	77,311,238	57,580,234	74.48%	14,529	11,369	6,859
CS-C	88,614,074	69,474,148	78.40%	14,374	11,535	7,153
CS-4h	89,207,696	69,680,045	78.11%	14,623	11,921	7,981
CS-8h	80,837,168	63,208,282	78.19%	14,541	12,042	8,210
CS-16h	88,387,552	67,905,408	76.83%	14,239	11,199	6,568
CS-32h	79,676,856	65,032,909	81.62%	14,114	11,071	6,327
Antenna	126,501,261	101,230,019	80.02%	15,759	13,053	10,557
Brain	92,782,188	76,978,395	82.97%	14,378	12,103	9,719
Gangalia	114,664,633	90,319,596	78.77%	14,671	11,805	8,709
Hind leg	112,788,727	90,072,088	79.86%	14,104	10,399	6,510
Hemolymph	127,040,788	103,708,042	81.63%	15,083	12,119	9,237
Middle gut	95,655,682	74,337,067	77.71%	14,088	11,021	8,422
Muscle	99,234,003	84,745,107	85.40%	13,166	8,159	4,238
Ovary	109,948,380	89,723,778	81.61%	15,081	11,794	9,693
Testis	101,957,854	82,362,842	80.78%	14,933	11,747	8,847
Wing	134,083,093	107,204,353	79.95%	15,311	12,281	9,353
Mixed	120,544,806	100,795,136	83.62%	15,659	13,415	9,730
Total	1,202,457,276	935,458,225	78.31%	16,913	16,244	14,940

Data in the first 12 lines were retrieved from a report by Chen *et al*[70], who has studied the developmental time course (egg, 1_2, 3, 4, 5 and adult developmental stages) of gregarious (G) and solitarious (S) *L. migratoria* using RNA-seq. G-B and S-B were

RNA-seq data for samples used for the RRBS study. The RNA-seq data of time course (control, 4, 8, 16 and 32 hour) of isolation of gregarious (IG) and crowding of solitarious (CS) locusts was produced in this study. Mixed samples from various organs and developmental stages were used to assist gene annotation.

Supplementary Table S21 GO enrichment of differentially expressed genes (DEGs) in the process of isolation of gregarious locust.

GO_ID	GO_Term	GO_Class	AdjustedPv	GOlevl
IG-4h.down				
GO:0008236	serine-type peptidase activity	MF	7.06E-68	5
GO:0005975	carbohydrate metabolic process	BP	4.55E-62	4
GO:0070011	peptidase activity, acting on L-amino acid peptides	MF	6.90E-51	5
GO:0006508	proteolysis	BP	3.66E-37	5
GO:0004175	endopeptidase activity	MF	6.27E-37	6
GO:0004252	serine-type endopeptidase activity	MF	3.27E-29	6
GO:0016787	hydrolase activity	MF	2.62E-26	3
GO:0004553	hydrolase activity, hydrolyzing O-glycosyl compounds	MF	1.46E-25	5
GO:0044238	primary metabolic process	BP	5.52E-20	3
GO:0008152	metabolic process	BP	2.65E-17	2
IG-4h.up				
GO:0044430	cytoskeletal part	CC	9.21E-05	4
GO:0005856	cytoskeleton	CC	9.21E-05	5
GO:0016491	oxidoreductase activity	MF	7.79E-04	3
GO:0015630	microtubule cytoskeleton	CC	9.79E-04	6
GO:0005874	microtubule	CC	2.25E-03	4
GO:0007017	microtubule-based process	BP	3.61E-03	3
GO:0007018	microtubule-based movement	BP	3.61E-03	4
GO:0016758	transferase activity, transferring hexosyl groups	MF	4.14E-03	5
GO:0051258	protein polymerization	BP	1.91E-02	7
GO:0034622	cellular macromolecular complex assembly	BP	3.88E-02	6
IG-8h.down				
GO:0005975	carbohydrate metabolic process	BP	9.25E-40	4
GO:0008236	serine-type peptidase activity	MF	3.67E-34	5
GO:0070011	peptidase activity, acting on L-amino acid peptides	MF	4.30E-30	5
GO:0006508	proteolysis	BP	5.34E-23	5
GO:0004175	endopeptidase activity	MF	4.03E-20	6
GO:0004553	hydrolase activity, hydrolyzing O-glycosyl compounds	MF	1.13E-19	5
GO:0004252	serine-type endopeptidase activity	MF	6.24E-17	6
GO:0016787	hydrolase activity	MF	8.06E-15	3
GO:0044238	primary metabolic process	BP	4.08E-14	3

GO:0008061	chitin binding	MF	3.47E-10	5
IG-8h.up				
GO:0009308	amine metabolic process	BP	1.31E-11	4
GO:0005976	polysaccharide metabolic process	BP	1.32E-10	4
GO:0006022	aminoglycan metabolic process	BP	1.22E-09	5
GO:0008061	chitin binding	MF	3.45E-08	5
GO:0006030	chitin metabolic process	BP	3.15E-07	6
GO:0005975	carbohydrate metabolic process	BP	3.15E-07	4
GO:0005576	extracellular region	CC	1.60E-05	2
GO:0016491	oxidoreductase activity	MF	6.52E-05	3
GO:0006816	calcium ion transport	BP	6.52E-05	8
GO:0005262	calcium channel activity	MF	2.22E-04	8
IG-16h.down				
GO:0004553	hydrolase activity, hydrolyzing O-glycosyl compounds	MF	2.55E-30	5
GO:0005975	carbohydrate metabolic process	BP	2.62E-29	4
GO:0008236	serine-type peptidase activity	MF	3.89E-24	5
GO:0004252	serine-type endopeptidase activity	MF	2.83E-22	6
GO:0008152	metabolic process	BP	1.21E-20	2
GO:0044238	primary metabolic process	BP	8.70E-20	3
GO:0008233	peptidase activity	MF	1.88E-17	4
GO:0070011	peptidase activity, acting on L-amino acid peptides	MF	2.88E-17	5
GO:0006508	proteolysis	BP	6.49E-11	5
GO:0004175	endopeptidase activity	MF	9.92E-11	6
IG-16h.up				
GO:0016491	oxidoreductase activity	MF	1.55E-06	3
GO:0005856	cytoskeleton	CC	1.74E-05	5
GO:0008061	chitin binding	MF	1.74E-05	5
GO:0020037	heme binding	MF	1.74E-05	4
GO:0042302	structural constituent of cuticle	MF	1.74E-05	3
GO:0004601	peroxidase activity	MF	1.93E-05	3
GO:0006979	response to oxidative stress	BP	1.93E-05	4
GO:0044430	cytoskeletal part	CC	2.79E-05	4
GO:0006030	chitin metabolic process	BP	5.88E-05	6
GO:0005976	polysaccharide metabolic process	BP	1.08E-04	4
IG-32h.down				
GO:0005975	carbohydrate metabolic process	BP	5.54E-07	4
GO:0009628	response to abiotic stimulus	BP	1.51E-06	3
GO:0055114	oxidation-reduction process	BP	5.31E-05	3
GO:0016491	oxidoreductase activity	MF	5.31E-05	3

GO:0009408	response to heat	BP	1.05E-04	4
GO:0070011	peptidase activity, acting on L-amino acid peptides	MF	1.26E-04	5
GO:0004175	endopeptidase activity	MF	1.76E-04	6
GO:0004252	serine-type endopeptidase activity	MF	4.30E-04	6
GO:0006508	proteolysis	BP	7.19E-04	5
GO:0016620	oxidoreductase activity, acting on the aldehyde or oxo group of donors, NAD or NADP as acceptor	MF	1.49E-03	5
IG-32h.up				
GO:0005975	carbohydrate metabolic process	BP	9.06E-18	4
GO:0003824	catalytic activity	MF	9.06E-18	2
GO:0009055	electron carrier activity	MF	4.92E-16	2
GO:0016491	oxidoreductase activity	MF	2.00E-12	3
GO:0004497	monooxygenase activity	MF	3.40E-11	4
GO:0020037	heme binding	MF	8.81E-10	4
GO:0008152	metabolic process	BP	3.57E-09	2
GO:0004553	hydrolase activity, hydrolyzing O-glycosyl compounds	MF	1.46E-08	5
GO:0016758	transferase activity, transferring hexosyl groups	MF	1.48E-08	5
GO:0016757	transferase activity, transferring glycosyl groups	MF	1.61E-08	4
IG-b-64h.down				
GO:0008152	metabolic process	BP	5.03E-33	2
GO:0008233	peptidase activity	MF	2.69E-32	4
GO:0070011	peptidase activity, acting on L-amino acid peptides	MF	8.53E-32	5
GO:0008236	serine-type peptidase activity	MF	8.48E-31	5
GO:0004252	serine-type endopeptidase activity	MF	1.79E-28	6
GO:0003735	structural constituent of ribosome	MF	6.41E-28	3
GO:0005840	ribosome	CC	1.19E-27	4
GO:0030529	ribonucleoprotein complex	CC	7.96E-24	3
GO:0005975	carbohydrate metabolic process	BP	2.76E-23	4
GO:0006508	proteolysis	BP	4.13E-23	5
IG-b-64h.up				
GO:0005515	protein binding	MF	4.89E-19	3
GO:0008270	zinc ion binding	MF	6.40E-10	7
GO:0007165	signal transduction	BP	4.51E-09	3
GO:0007154	cell communication	BP	1.44E-08	3
GO:0051716	cellular response to stimulus	BP	1.88E-08	3

GO:0030695	GTPase regulator activity	MF	2.00E-08	4
GO:0050794	regulation of cellular process	BP	2.87E-08	3
GO:0065007	biological regulation	BP	8.68E-08	2
GO:0005488	binding	MF	1.92E-07	2
GO:0051056	regulation of small GTPase mediated signal transduction	BP	1.93E-07	5

Both down and up represent the down-regulated and up-regulated genes at time 4, 8, 16, 32 and 64 hours compared with typical gregarious locust. Only top 10 most significant GO terms were listed according to AdjustedPv (false discover ratio, which was calculated according to Benjamini and Hochberg[237]).

Supplementary Table S22 GO enrichment of the differentially expressed genes (DEGs) in the process of crowding of solitarious locusts.

GO_ID	GO_Term	GO_Class	AdjustedPv	GOlevl
CS-4h.down				
GO:0016491	oxidoreductase activity	MF	5.94E-14	3
GO:0042302	structural constituent of cuticle	MF	4.12E-13	3
GO:0009055	electron carrier activity	MF	1.16E-11	2
GO:0004497	monooxygenase activity	MF	1.62E-09	4
GO:0020037	heme binding	MF	2.92E-08	4
GO:0005975	carbohydrate metabolic process	BP	8.82E-07	4
GO:0005198	structural molecule activity	MF	1.52E-06	2
GO:0016758	transferase activity, transferring hexosyl groups	MF	1.44E-05	5
GO:0055114	oxidation-reduction process	BP	1.82E-05	3
GO:0008061	chitin binding	MF	6.60E-05	5
CS-4h.up				
GO:0070011	peptidase activity, acting on L-amino acid peptides	MF	1.15E-30	5
GO:0004175	endopeptidase activity	MF	8.65E-28	6
GO:0006508	proteolysis	BP	3.41E-25	5
GO:0008236	serine-type peptidase activity	MF	6.86E-23	5
GO:0004252	serine-type endopeptidase activity	MF	8.63E-23	6
GO:0016787	hydrolase activity	MF	5.69E-09	3
GO:0005975	carbohydrate metabolic process	BP	2.65E-06	4
GO:0003824	catalytic activity	MF	6.31E-05	2
GO:0008061	chitin binding	MF	6.51E-05	5
GO:0006030	chitin metabolic process	BP	2.18E-04	6
CS-8h.down				
GO:0016491	oxidoreductase activity	MF	9.58E-47	3
GO:0020037	heme binding	MF	2.71E-32	4
GO:0009055	electron carrier activity	MF	1.37E-30	2
GO:0055114	oxidation-reduction process	BP	5.34E-29	3
GO:0016757	transferase activity, transferring glycosyl groups	MF	6.57E-29	4
GO:0005506	iron ion binding	MF	4.29E-26	7
GO:0003824	catalytic activity	MF	2.88E-22	2
GO:0004497	monooxygenase activity	MF	7.04E-18	4
GO:0016758	transferase activity, transferring hexosyl groups	MF	3.63E-15	5
GO:0008152	metabolic process	BP	2.11E-13	2

CS-8h.up				
GO:0008236	serine-type peptidase activity	MF	2.23E-25	5
GO:0004175	endopeptidase activity	MF	2.15E-18	6
GO:0070011	peptidase activity, acting on L-amino acid peptides	MF	2.86E-15	5
GO:0004252	serine-type endopeptidase activity	MF	2.93E-14	6
GO:0006508	proteolysis	BP	9.92E-13	5
GO:0005975	carbohydrate metabolic process	BP	2.62E-12	4
GO:0006022	aminoglycan metabolic process	BP	1.14E-11	5
GO:0008061	chitin binding	MF	6.66E-11	5
GO:0006030	chitin metabolic process	BP	9.42E-11	6
GO:0030246	carbohydrate binding	MF	9.36E-10	3
CS-16h.down				
GO:0042302	structural constituent of cuticle	MF	1.19E-08	3
GO:0016758	transferase activity, transferring hexosyl groups	MF	2.09E-07	5
GO:0016757	transferase activity, transferring glycosyl groups	MF	2.37E-07	4
GO:0051920	peroxiredoxin activity	MF	8.29E-07	5
GO:0016209	antioxidant activity	MF	1.42E-06	2
GO:0005198	structural molecule activity	MF	9.98E-06	2
GO:0016491	oxidoreductase activity	MF	2.39E-03	3
GO:0004497	monooxygenase activity	MF	1.28E-02	4
GO:0020037	heme binding	MF	3.20E-02	4
GO:0009055	electron carrier activity	MF	3.84E-02	2
CS-16h.up				
GO:0070011	peptidase activity, acting on L-amino acid peptides	MF	3.48E-27	5
GO:0004175	endopeptidase activity	MF	7.02E-24	6
GO:0006508	proteolysis	BP	1.41E-19	5
GO:0008236	serine-type peptidase activity	MF	1.84E-17	5
GO:0004252	serine-type endopeptidase activity	MF	2.29E-17	6
GO:0016787	hydrolase activity	MF	3.75E-06	3
GO:0005576	extracellular region	CC	1.18E-04	2
GO:0000786	nucleosome	CC	1.23E-04	4
GO:0005975	carbohydrate metabolic process	BP	1.29E-04	4
GO:0006334	nucleosome assembly	BP	1.29E-04	7
CS-32h.down				
GO:0016491	oxidoreductase activity	MF	1.10E-09	3
GO:0042302	structural constituent of cuticle	MF	6.88E-08	3
GO:0016209	antioxidant activity	MF	1.47E-07	2

GO:0016758	transferase activity, transferring hexosyl groups	MF	1.47E-07	5
GO:0051920	peroxiredoxin activity	MF	8.61E-07	5
GO:0016705	oxidoreductase activity, acting on paired donors, with incorporation or reduction of molecular oxygen	MF	6.36E-05	4
GO:0004497	monooxygenase activity	MF	1.81E-04	4
GO:0055114	oxidation-reduction process	BP	3.22E-04	3
GO:0020037	heme binding	MF	6.87E-04	4
GO:0005198	structural molecule activity	MF	1.81E-03	2
CS-32h.up				
GO:0070011	peptidase activity, acting on L-amino acid peptides	MF	2.12E-06	5
GO:0008236	serine-type peptidase activity	MF	2.12E-06	5
GO:0006508	proteolysis	BP	1.57E-05	5
GO:0004252	serine-type endopeptidase activity	MF	5.72E-05	6
GO:0004175	endopeptidase activity	MF	1.08E-03	6
GO:0006026	aminoglycan catabolic process	BP	1.08E-03	6
GO:0006022	aminoglycan metabolic process	BP	2.40E-03	5
GO:0016614	oxidoreductase activity, acting on CH-OH group of donors	MF	3.16E-03	4
GO:0016491	oxidoreductase activity	MF	3.16E-03	3
GO:0008745	N-acetylmuramoyl-L-alanine amidase activity	MF	3.16E-03	6
CS-b-64h.down				
GO:0003735	structural constituent of ribosome	MF	7.51E-42	3
GO:0005840	ribosome	CC	9.96E-42	4
GO:0016491	oxidoreductase activity	MF	8.29E-40	3
GO:0005198	structural molecule activity	MF	1.64E-34	2
GO:0005506	iron ion binding	MF	2.23E-34	7
GO:0020037	heme binding	MF	4.21E-32	4
GO:0004497	monooxygenase activity	MF	7.42E-30	4
GO:0044444	cytoplasmic part	CC	1.32E-25	4
GO:0009055	electron carrier activity	MF	2.01E-24	2
GO:0055114	oxidation-reduction process	BP	1.15E-23	3
CS-b-64h.up				
GO:0005515	protein binding	MF	8.84E-03	3

Both down and up represent the down-regulated and up-regulated genes at time 4, 8, 16, 32 and 64 hours compared with typical solitarious locust. Only top 10 most significant GO terms were listed according to AdjustedPv (false discover ratio, which was calculated according to Benjamini and Hochberg[236]).

Supplementary Table S23 Differentially spliced genes between gregarious and solitarious brain samples.

GeneID	JuncStart	JuncEnd	FDR	RatioDiff	Annotation
LOCMI01089	9,503	9,731	2.9E-88	79%	Ubiquitin
LOCMI01289	208,041	208,185	8.5E-03	41%	Microtubule-associated protein futsch
LOCMI01289	212,936	213,003	2.6E-03	24%	Microtubule-associated protein futsch
LOCMI01929	352	949	3.9E-02	24%	Heterogeneous nuclear ribonucleoprotein F
LOCMI02112	25,158	29,945	4.7E-02	44%	S-adenosylmethionine decarboxylase proenzyme
LOCMI02840	56,175	56,247	1.9E-02	30%	NA
LOCMI03690	46,327	54,871	5.7E-14	38%	Ankyrin repeat domain-containing protein 50
LOCMI03696	63,788	84,710	8.9E-07	50%	39S ribosomal protein L22, mitochondrial
LOCMI03875	114,742	115,138	2.6E-03	69%	Neurofilament heavy polypeptide
LOCMI06132	17,002	19,880	1.7E-05	26%	Tankyrase-2
LOCMI06300	237,941	248,085	1.3E-02	34%	Orphan sodium- and chloride-dependent neurotransmitter transporter NTT4
LOCMI06515	38,336	44,550	2.4E-06	38%	Myosin light chain alkali
LOCMI06569	120,498	138,528	1.3E-03	42%	Calcium-transporting ATPase sarcoplasmic/endoplasmic reticulum type
LOCMI07192	360,229	367,172	8.8E-03	55%	Arrestin homolog
LOCMI07498	358,962	370,733	1.5E-03	28%	GatC-like protein
LOCMI08053	257,589	349,754	9.5E-02	24%	
LOCMI08665	412,452	412,638	5.6E-22	25%	Selenide, water dikinase 1
LOCMI08665	412,452	412,792	2.1E-08	22%	Selenide, water dikinase 1
LOCMI08748	592,833	599,356	6.8E-02	29%	NA
LOCMI09211	250,251	250,481	2.2E-09	22%	tRNA (uracil-5-)-methyltransferase homolog A
LOCMI09348	520,566	527,423	5.9E-03	32%	Troponin T
LOCMI09800	351,323	400,625	4.1E-04	21%	TM2 domain-containing protein almondex

LOCMI10443	210,105	214,365	4.0E-20	33%	Cytochrome c
LOCMI10825	901,123	901,507	5.9E-23	30%	S-adenosylmethionine synthetase
LOCMI11033	279,947	288,905	4.0E-02	23%	Mucosa-associated lymphoid tissue lymphoma translocation protein 1 homolog
LOCMI11116	145,059	145,606	4.6E-02	91%	Sorting nexin-9
LOCMI11537	390,510	500,197	1.8E-13	20%	NA
LOCMI11822	189,207	189,732	3.1E-09	24%	Growth hormone-inducible transmembrane protein
LOCMI11956	123,414	123,616	1.1E-35	93%	NA
LOCMI12061	127,789	128,009	8.4E-02	80%	NA
LOCMI12462	953,700	956,713	1.8E-09	24%	Chromodomain-helicase-DNA-binding protein Mi-2 homolog
LOCMI12462	954,372	973,680	5.8E-08	21%	Chromodomain-helicase-DNA-binding protein Mi-2 homolog
LOCMI13014	1,639,012	1,661,291	3.9E-03	31%	Protein turtle
LOCMI13647	715,041	715,533	1.2E-04	43%	NA
LOCMI13701	986,125	986,395	1.1E-38	21%	Y-box factor homolog
LOCMI14075	324,079	334,455	3.7E-14	21%	Histone H3.3
LOCMI14096	1,537,431	1,537,510	1.0E-37	23%	Eukaryotic translation initiation factor 4 gamma 2
LOCMI14124	664,510	695,269	4.0E-03	21%	Elongation factor Ts, mitochondrial
LOCMI14302	444,762	454,682	4.2E-02	21%	Catenin delta-2
LOCMI14384	2,763,226	2,767,020	2.1E-02	67%	Sodium-dependent phosphate transporter 1-A
LOCMI14503	1,179,102	1,180,309	9.3E-04	25%	Synaptobrevin
LOCMI15369	3,450,741	3,461,535	1.0E-04	20%	Tyrosine-protein phosphatase 99A
LOCMI15498	255,468	255,569	0.0E+00	25%	Elongation factor 1-alpha
LOCMI16160	133,512	138,870	3.5E-02	29%	NA
LOCMI16195	1,504,719	1,505,088	1.7E-02	28%	Cytochrome P450 4C1

Supplementary Table S24 Genes related to the contraction/relaxation activity of flight muscle.

Gene ID	LMI	API	AGA	AME	DME	DPL	NVI	PHU	BMO	TCA
CG12408-PA	0	0	0	0	1	0	0	0	0	0
CG15920-PA	1	0	0	1	1	1	1	0	1	0
CG1915-PC	1	1	1	1	1	1	2	1	2	1
CG32019-PF	1	1	1	1	1	1	1	1	1	2
CG3725-PD	2	1	1	1	1	1	1	1	1	1
CG7107-PA	1	1	1	1	1	2	1	1	1	1

Note: Abbreviation: LMI: *Locusta migratoria*, PHU: *Pediculus humanus*, API: *Acyrthosiphon pisum*, AME: *Apis mellifera*, NVI: *Nasonia vitripennis*, TCA: *Tribolium castaneum*, BMO: *Bombyx mori*, AGA: *Anopheles gambiae*, DME: *Drosophila melanogaster* and DPL: *Danaus plexippus*.

Supplementary Table S25 Genes related to wing vein morphogenesis and wing vein specification.

Gene ID	LMI	API	AGA	AME	DME	DPL	NVI	PHU	BMO	TCA
CG1004-PA	0	0	0	1	1	0	1	0	0	0
CG10079-PB	1	1	1	1	1	1	1	1	1	1
CG1007-PA	1	1	2	1	1	1	1	1	1	1
CG10197-PC	1	2	1	1	1	1	1	1	1	1
CG10491-PA	0	1	1	1	1	1	1	0	1	0
CG10571-PA	1	0	0	0	1	0	0	1	0	0
CG10595-PB	1	2	1	2	1	1	2	1	1	1
CG10605-PA	0	0	0	1	1	0	1	0	0	0
CG1064-PA	1	1	1	1	1	2	1	1	1	1
CG10917-PA	0	0	1	0	1	2	0	1	1	1
CG11450-PB	0	1	1	1	1	1	0	1	1	1
CG11990-PB	1	2	1	1	1	2	1	1	1	1
CG12399-PA	1	2	1	2	1	2	3	3	2	4
CG12559-PF	2	1	1	1	3	1	3	0	1	1
CG14080-PB	1	1	1	1	1	1	1	1	1	1
CG15154-PB	1	1	0	1	1	1	1	1	1	1
CG15671-PA	2	1	1	1	1	1	4	2	1	1
CG1696-PA	1	1	1	1	1	2	2	1	1	1
CG17090-PA	1	2	1	1	1	1	1	0	1	1
CG17149-PA	1	2	1	1	1	3	2	2	2	1
CG17596-PA	1	1	1	1	1	1	1	2	1	1
CG17998-PA	1	1	1	1	1	2	1	1	1	1
CG18250-PC	1	1	1	1	1	1	1	1	1	1
CG18497-PA	1	1	1	1	1	1	1	1	1	1
CG18740-PA	2	1	1	1	1	2	1	1	1	1
CG30115-PE	1	0	1	1	1	1	1	0	1	1
CG31000-PO	1	1	1	1	1	1	1	1	1	1
CG32062-PD	1	0	0	0	1	1	0	0	1	1
CG32372-PA	1	1	2	1	1	1	1	1	1	1
CG3274-PA	1	1	1	1	1	1	1	1	1	1
CG3411-PA	1	1	1	1	1	1	1	1	0	1
CG34157-PH	2	2	1	2	1	1	1	1	0	1
CG34389-PC	0	1	1	1	1	1	1	1	1	2
CG3497-PA	1	2	1	1	1	1	2	1	1	1
CG3619-PA	1	1	1	1	1	1	1	1	1	2
CG3936-PA	3	1	1	1	1	1	1	1	1	2
CG40129-PB	1	1	1	1	1	2	1	1	1	1
CG4244-PA	1	1	1	1	1	1	1	1	1	1
CG4426-PA	1	1	1	1	1	2	2	1	1	1
CG4444-PA	1	1	1	1	1	1	0	1	1	1

CG4531-PA	1	4	0	1	1	1	1	1	1	2
CG4547-PB	1	1	1	0	1	1	0	1	1	1
CG4637-PA	1	2	1	1	1	1	1	1	1	1
CG4713-PA	1	0	1	1	1	3	1	2	1	1
CG4881-PB	0	0	0	0	1	0	0	0	0	0
CG4974-PA	0	1	1	1	1	1	1	1	1	1
CG5067-PB	0	1	1	1	1	0	0	0	1	1
CG5441-PA	0	1	1	0	1	0	0	0	0	2
CG5460-PD	0	0	1	0	1	0	0	0	1	0
CG5562-PA	1	2	2	1	1	2	2	1	1	2
CG5591-PA	1	0	1	1	1	1	1	0	1	0
CG5942-PA	5	1	1	1	1	1	2	8	1	0
CG6148-PA	4	2	1	1	1	1	2	2	1	2
CG6464-PA	1	0	1	0	1	0	0	1	0	0
CG6677-PD	2	1	1	1	1	1	3	1	1	1
CG6863-PB	1	1	1	0	1	1	1	1	1	1
CG6868-PA	0	0	0	0	1	0	0	0	0	0
CG6964-PC	1	1	1	1	1	1	0	1	0	0
CG7467-PB	1	1	1	1	1	1	1	1	1	2
CG7595-PA	2	2	3	2	1	3	2	2	3	3
CG7734-PD	1	1	1	1	1	1	0	1	1	1
CG7890-PA	1	1	1	1	1	1	1	2	2	1
CG7892-PG	1	1	1	1	1	1	1	1	1	1
CG7935-PA	2	1	1	1	1	1	1	1	1	1
CG8339-PA	1	2	1	1	1	1	1	1	1	1
CG8709-PA	1	1	1	1	1	1	1	1	1	1
CG9139-PA	1	1	1	1	1	1	1	1	1	1
CG9224-PA	1	1	1	1	1	1	0	1	1	1
CG9397-PI	0	1	0	1	1	0	1	0	0	1
CG9885-PE	1	4	1	1	1	1	1	1	1	2

Note: Abbreviation: LMI: *Locusta migratoria*, PHU: *Pediculus humanus*, API: *Acyrthosiphon pisum*, AME: *Apis mellifera*, NVI: *Nasonia vitripennis*, TCA: *Tribolium castaneum*, BMO: *Bombyx mori*, AGA: *Anopheles gambiae*, DME: *Drosophila melanogaster* and DPL: *Danaus plexippus*.

Supplementary Table S26 Juvenile hormone genes in the *L. migratoria* genome.

Genes	*L. migratoria* ID	*B. mori* ID
Biosynthesis		
Acetoacetyl-CoA thiolase	LOCMI16298 LOCMI16359 LOCMI16371	NP_001093296.1
Diphosphomevalonate decarboxylase	LOCMI03890 LOCMI05712	NP_001093300.1
Epoxidase	LOCMI16177	CYP15C1
Farnesol dehydrogenase	LOCMI05376 LOCMI05943 LOCMI16310	BGIBMGA005248-PA
Farnesyl diphosphate synthase	LOCMI15132 LOCMI16337 LOCMI15132 LOCMI15132	NP_001036889.1 NP_001093301.1 NP_001093302.1
HMG CoA reductase	LOCMI16309	NP_001093298.1
HMG CoA synthase	LOCMI15805 LOCMI17476	NP_001093297.1
Isopentenyl diphosphate isomerase	LOCMI16436	NP_001040323.2
JHA O-Methyltransferase	LOCMI01015 LOCMI16697 LOCMI16699 LOCMI16705 LOCMI17143 LOCMI17167	BGIBMGA010392-PA BGIBMGA010393-PA BGIBMGA010563-PA BGIBMGA014014-PA NP_001036901.1
Mevalonate kinase	LOCMI07473	NP_001093299.1
Phosphomevalonate kinase	LOCMI10595	NP_001040145.1
Degradation		
juvenile hormone diol kinase	LOCMI16350 LOCMI16608 LOCMI17114	BGIBMGA006444-PA BGIBMGA008813-PA BGIBMGA008815-PA NP_001037080.1
juvenile hormone epoxide hydrolase	LOCMI04730 LOCMI16691 LOCMI17120 LOCMI17136 LOCMI16251 LOCMI16258	BGIBMGA009211-PA BGIBMGA011468-PA BGIBMGA013793-PA BGIBMGA013929-PA BGIBMGA013994-PA NP_001037201.1
juvenile hormone esterase 1	LOCMI15548 LOCMI15559 LOCMI15560 LOCMI15621	NP_001037027.1

Supplementary Table S27 Insulin metabolic pathway.

GenesGene	*L. migratoria*	*D. melanogaster*
Ligands and secreted factors		
convoluted	LOCMI12686	CG8561-PA
short neuropeptide F receptor	LOCMI16723	CG7395-PA
Ecdysone-inducible gene L2	ND[1]	CG15009-PC
Insulin-like peptide	LOCMI16379	CG14173-PA CG13317-PA CG14049-PA CG14167-PA CG33273-PA CG6736-PA CG8167-PA
Insulin-like receptor and its substrates		
Insulin-like receptor	LOCMI16333 LOCMI07370 LOCMI07679	CG18402-PA
Pi3K21B	LOCMI07824	CG2699-PA
Pi3K92E	LOCMI13806	CG4141-PA
chico	LOCMI16419	CG5686-PA
Signal transduction pathway		
target of rapamycin	LOCMI16380	CG5092-PA
nucleostemin 3	LOCMI06145	CG14788-PA
twins	LOCMI07527	CG6235-PF
widerborst	LOCMI12365	CG5643-PA
pten	LOCMI16332	CG5671-PB
CHARYBDE	LOCMI16625	CG7533-PC
melted	LOCMI16412	CG8624-PC
Akt1	LOCMI16427	CG4006-PC
focal adhesion kinase	LOCMI16428	CG10023-PD
Tsc1	LOCMI16439	CG6147-PA
RPS6-p70-protein kinase	LOCMI16450	CG10539-PA
SCYLLA	LOCMI16625	CG7590-PA
Targets		
ribosomal protein S6	LOCMI00728 LOCMI09740	CG10944-PB
gigas (TSC2)	LOCMI13246	CG6975-PA
spargel	LOCMI16312	CG9809-PB
thor	LOCMI16388	CG8846-PA
diminutive	ND	CG10798-PA
forkhead box, sub-group O	LOCMI16409	CG3143-PA

[1] ND: not detected.

Supplementary Table S28 PAT genes in insect genomes.

Species	**PLIN1**	**PLIN2**	**PLIN3**	**PLIN4**	**PLIN5**
H. sapiens	NP_002657	NP_001113.2	NP_005808	NP_001073869.1	NP_001013728
L. migratoria	LOCMI16244	LOCMI16243 LOCMI16245 LOCMI16246 LOCMI16247 LOCMI16248 LOCMI16250			
P. humanus	PHUM299200				
A. pisum	ACYPI007905				
T. castaneum	XP_966587	XP_976120			
D. melanogaster	CG10374	CG9057			
A. gambiae	AGAP002890	AGAP000167			
B. mori	BGIBMGA013593	BGIBMGA013612			
D.plexippus	DPGLEAN05949	DPGLEAN15300			
A. mellifera	GB15498	GB14434			

Supplementary Table S29 Conserved domains of *L. migratoria* PAT proteins.

Locust ID	From	To	E-Value	Bitscore
LOCMI16244	6	338	9.40E-54	184.591
LOCMI16243	47	200	8.44E-06	44.7633
LOCMI16245	10	239	2.78E-26	105.24
LOCMI16246	66	177	0.0003606	38.6001
LOCMI16247	66	154	3.17E-05	41.6817
LOCMI16248	65	176	0.0002675	38.9853
LOCMI16250	10	237	1.82E-20	88.2909

The conserved domains of the PAT proteins were identified through the NCBI Batch CD-Search (http://www.ncbi.nlm.nih.gov/Structure/cdd/cdd.shtml). The conserved PAT domain was identified in all the predicted candidates (PSSM-ID: 190508; accession: cl03851, Perilipin superfamily). In the two sequence lengths m and n, the statistics of high-scoring segment pair scores are characterized by two parameters, K and lambda. The E-value of high-scoring segment pairs with score at least S is given by the formula $E=Kmne^{-\Lambda s}$.

Supplementary Table S30 Primers for *L. migratoria* FABP genes.

Gene ID	Forward	Reverse	Length	Position
LOCMI17560	GCCGCAAGGTCAAGTCTATC	TATTCTCGTCGCCACCAAGT	152	239-390
LOCMI04395	GGCTACCTGGTCCGTAAGAT	CCTCTGCCGCTGGATCAGT	189	85-273
LOCMI04101	TCTCGGTCGCAGGTACAAA	TCCGCCACAGAAAGCCAAT	83	18-100
LOCMI17562	AAGACCTCTGTGGCGTTCC	TGTGGTCGTCCTTGAGTGA	94	190-283
LOCMI17563	AAGCTCGTGCTCACCTACC	TGACGGTGCTCTTCCTCTT	76	184-259
LOCMI03671	CACCCTCAAGTCCTCGTCG	GCCCTTCTGGATGTGGTGC	145	150-294
LOCMI03672	GTTTGGAGCGGGCATAGTG	CGATGGTGGTGGTCCTGTC	245	75-319
LOCMI03788	AAGACCTCTGTGGCGTTCC	CGACCTTGAGCAGCGTGT	109	190-298
LOCMI05692	CAAGCAGACGACCAAGACG	TGAAAGGGATCTCCGCCAC	92	111-202
LOCMI17564	AGCCGACGACGACCCTGAC	TCGCTCTTCTGGGTGATGG	157	116-272
LOCMI17561	GTCACCAGGCACTTCACGC	GTCACATCGGTCCTTACAGC	111	181-291

Supplementary Table S31 Comparison of antioxidant genes in insects.

Type	LMI	PHU	TCA	DME	AGA	BMO	DPL	AME	NVI
SOD [Mn]	1	1	1	1	1	1	2	1	1
SOD [Cu-Zn]	4	4	4	4	4	4	4	2	4
Copper chaperone for SOD	1	0	1	1	1	1	2	1	1
General animal peroxidase	17	10	14	10	16	20	12	10	10
Catalase superfamily	2	1	3	2	1	9	6	3	1
Glutathione Peroxidase Superfamily	4	2	3	2	3	2	1	1	3
General Peroxiredoxin Superfamily	14	7	8	9	7	5	6	8	6
Prdx6	9	2	2	4	2	1	1	2	2
NADPH oxidase V	1	0	1	1	1	1	1	1	1
Thioredoxinreductase	2	3	2	2	1	1	1	1	1
Thioredoxin	14	12	10	15	10	10	9	12	9
Glutaredoxin	7	6	5	6	4	3	4	4	4
Methionine-R-sulphoxidereductase	3	3	2	2	3	2	2	2	2

Abbreviations: LMI: *Locusta migratoria*, DPL: *Danaus plexippus*, PHU: *Pediculus humanus*, AME: *Apis mellifera*, NVI: *Nasonia vitripennis*, TCA: *Tribolium castaneum*, BMO: *Bombyx mori*, AGA: *Anopheles gambiae* and DME: *Drosophila melanogaster*.

Supplementary Table S32 List of glutathione S-transferase (GST) genes in the insect genomes.

	AAE	AGA	DME	AME	NVI	TCA	BMO	API	PHU	LMI
Delta	8	12	11	1	5	3	4	10	4	10
Epsilon	8	8	14	0	0	19	8	0	0	0
Omega	1	**1**	5	1	2	4	4	0	1	3
Sigma	1	1	1	4	8	7	2	6	4	12
Theta	4	2	4	1	3	1	1	2	1	2
Zeta	1	1	2	1	1	1	2	0	1	1
Others	3	3	0	0	0	1	2	0	0	0
Total	26	28	37	8	19	36	23	18	11	28

Abbreviations: LMI: *Locusta migratoria*, PHU: *Pediculus humanus*, API: *Acyrthosiphon pisum*, AME: *Apis mellifera*, NVI: *Nasonia vitripennis*, TCA: *Tribolium castaneum*, BMO: *Bombyx mori*, AAE:, *Aedes aegypti*, AGA: *Anopheles gambiae*, DME: *Drosophila melanogaster*.

Supplementary Table S33 Summary of carboxyl/cholinesterase genes in insect genomes.

Species	**AAE**	**AGA**	**DME**	**AME**	**NVI**	**TCA**	**BMO**	**API**	**PHU**	**LMI**
Dietary/detoxification										
A class (hymenopteran metabolising)	0	0	0	8	8	0	0	0	0	0
B class (α-esterases)	22	16	13	0	5	14	55	5	3	9
C class(microsomalα-esterases)	0	0	0	0	0	12	0	0	0	0
Locust-Specific	0	0	0	0	0	0	0	0	0	**30**
Hormone/semiochemical processing										
D class (integument esterases)	0	0	3	1	4	2	2	0	0	9
E class (β-esterases)	2	4	3	2	11	7	2	18	1	**21**
F class (dipteran JH esterases)	6	6	2	2	2	2	0	0	0	2
G class (lepidopteran JH esterases)	6	4	0	0	0	0	4	0	0	0
Neuro/developmental										
H class (glutactins)	7	10	4	1	1	1	0	0	1	3
I class (unknown)	1	1	1	1	1	1	2	1	1	1
J class (acetylcholinesterases)	2	2	1	2	2	2	2	2	2	1
K class (gliotactins)	1	1	1	1	1	1	1	1	1	2
L class (neuroligins)	5	5	5	5	5	5	6	3	5	1
M class (neurotactins)	2	2	2	1	1	2	2	0	3	1
Total	54	51	35	24	41	48	76	30	17	80

Note: Numbers of CCE genes in other insects were retrieved from a previous report[75]. Species involved in this analysis include LMI: *Locusta migratoria*, PHU: *Pediculus humanus*, API: *Acyrthosiphon pisum*, AME: *Apis mellifera*, NVI: *Nasonia vitripennis*, TCA: *Tribolium castaneum*, BMO: *Bombyx mori*, AAE:, *Aedes aegypti*, AGA: *Anopheles gambiae*, DME: *Drosophila melanogaster*.

Supplementary Table S34 Summary of ABC transporter subfamilies in the genomes of selected insects.

Species	ABCA	ABCB	ABCC	ABCD	ABCE	ABCF	ABCG	ABCH	Total
LOCMI	5	19	19	2	1	3	15	1	65
ACYPI	11	9	16	2	1	4	19	9	71
ANOGA	11	6	12	2	1	3	15	1	51
APIME	8	7	10	2	1	3	14	1	46
BOMMO	7	11	11	2	1	3	14	1	50
DAPPU	17	12	6	3	1	4	19	3	65
DROME	12	8	14	2	1	3	15	1	56
NASVI	10	8	20	1	1	3	11	1	55
PEDHU	6	7	5	2	1	3	13	1	38
TRICA	3	0	7	0	0	0	2	1	13

LOCMI: *Locusta migratoria*; ACYPI: *Acyrthosiphon pisum*; PEDHU: *Pediculus humanus humanus*; APIME: *Apis mellifera*; NASVI: *Nasonia vitripennis*; TRICA: *Tribolium castaneum*; BOMMO: *Bombyx mori*; DROME: *Drosophila melanogaster* and ANOGA: *Anopheles gambiae*.

Supplementary Table S35 'Lethal' insecticide target candidates in the *L. migratoria* genome.

Protein	Function	Total number
Cys-loop ligand-gated ion channels	Nicotinic acetylcholine receptor (17); GABA/Glycine chloride channel (10); Glutamate-gated chloride channel (4); Histamine-gated chloride channel (2); pH sensitive chloride channel (1)	34
GPCRs	Class A Rhodopsin-like (61); Class B Secretin receptor-like (21); Class C Metabotropic glutamate receptor-like (3); Class D Atypical GPCRs (5)	90
'Lethal' insecticide candidates	Kinase (9); Synthetase (7); receptor (6); Methyltransferase (5); Helicase (4); Polymerase (3); Transporter (3); GTPase (2); Phosphatase (2); Primase (2); Translocase (1); Peptidase (1); Ligase (1); Isomerase (1); Hydrolase (1); Dehydrogenase (1); Carboxylase (1); ATPase (1)	51

Supplementary Table S36 Immune related genes across five species.

Gene Family of Pathway	**DPU**	**LMI**	**API**	**PHU**	**DME**
Anti-microbial Peptides (AMPs)	11	9	2	4	21
Autophagy Pathway Members (APHAGs)	16	21	12	14	16
Gram-Negative Binding Proteins (GNBPs)	9	3	1	0	3
Caspases (CASPs)	22	9	6	5	7
Caspase Activators (CASPAs)	1	2	1	0	5
Catalases (CATs)	1	2	1	1	2
CLIP-domain Serine Proteases (CLIPs)	94	54	38	23	46
C-Type Lectins (CTLs)	52	27	11	13	35
Fibrinogen-Related proteins (FREPs)	26	4	1	3	13
Galectins (GALEs)	6	3	2	3	6
Glutathione Peroxidases (GPXs)	3	4	0	1	2
Heme Peroxidases (HPXs)	12	22	27	1	10
Inhibitors of Apoptosis (IAPs)	6	4	16	2	4
IMD Pathway Members	6	6	2	5	8
JAK/STAT Pathway Members	3	6	8	3	3
Lysozymes (LYSs)	0	3	0	0	12
MD2-like Proteins (MLs)	6	3	11	2	8
Peptidoglycan Recognition Proteins (PGRPs)	0	15	0	1	13
Prophenoloxidases (PPOs)	1	8	2	3	3
Rel-like NFkappa-B Proteins (RELs)	5	3	3	4	21
Scavenger Receptors (SCRs)	19	22	14	25	4
Superoxide Dismutases (SODs)	18	7	10	8	6
Spaetzle-like Proteins (SPZs)	6	6	9	5	30
Serine Protease Inhibitors (SRPNs)	5	23	10	12	14
Thio-Ester Containing Proteins (TEPs)	11	7	4	3	6
Toll Receptors (TOLLs)	6	8	7	6	9
Toll Pathway Members	7	6	3	4	5
Thioredoxin Peroxidases (TPXs)	0	10	0	0	8
Total	414	297	244	167	320

Abbreviation: LMI: *Locusta migratoria*, DPU: *Daphnia pulex*, PHU: *Pediculus humanus*, API: *Acyrthosiphon pisum* and DME: *Drosophila melanogaster*.

Supplementary Table S37 List of annotated genes of the miRNA and siRNA machinery in the *L. migratoria* genome.

miRNA pathway		siRNA pathway	
Ago1	LOCMI17227	Ago2	LOCMI17302
Loq	LOCMI16664		LOCMI16696
	LOCMI16661	R2D2	LOCMI16661
	LOCMI16590	Dicer-2	LOCMI10988
Dicer-1	LOCMI16844		LOCMI13152
Exportin-5	LOCMI17101		
Drosha	LOCMI17264		
Pasha	LOCMI17070		

Supplementary Table S38 Summary of cuticle protein genes in the *L. migratoria* genome.

Name	Type	Score	E-value[1]
LOCMI16739	RR1	141.5	5.00E-43
LOCMI16727	RR1	93.8	1.10E-28
LOCMI06228	RR1	81.1	8.00E-25
LOCMI17181	RR1	92.8	2.40E-28
LOCMI17140	RR1	23.5	1.60E-08
LOCMI01986	RR1	15	1.30E-07
LOCMI16703	RR1	33.8	1.30E-10
LOCMI16728	RR1	38.3	5.80E-12
LOCMI16731	RR1	58	7.10E-18
LOCMI16610	RR1	25.6	9.60E-09
LOCMI17322	RR1	30.4	1.50E-09
LOCMI17211	RR1	93.8	1.20E-28
LOCMI17165	RR1	22.9	1.90E-08
LOCMI16714	RR1	12.4	2.40E-07
LOCMI16609	RR1	77.2	1.10E-23
LOCMI16601	RR1	23.7	1.50E-08
LOCMI16604	RR1	68.8	3.80E-21
LOCMI03817	RR1	39.8	2.10E-12
LOCMI17205	RR1	154.5	6.00E-47
LOCMI17206	RR1	64.9	5.70E-20
LOCMI17125	RR1	20.7	3.10E-08
LOCMI01532	RR1	13.5	1.80E-07
LOCMI17128	RR1	20.4	3.40E-08
LOCMI17141	RR1	74.6	7.10E-23
LOCMI03209	RR1	27.4	6.10E-09
LOCMI16847	RR1	35.9	3.10E-11
LOCMI01460	RR1	32.8	2.70E-10
LOCMI16615	RR1	39.6	2.40E-12
LOCMI17159	RR1	36.6	1.90E-11
LOCMI17132	RR1	44.3	9.50E-14
LOCMI16800	RR1	58.4	5.30E-18
LOCMI16819	RR1	85.8	3.00E-26
LOCMI16851	RR2	100.6	1.00E-30
LOCMI16632	RR2	97.6	8.30E-30
LOCMI01688	RR2	66.1	2.50E-20
LOCMI05479	RR2	113.9	1.00E-34
LOCMI16766	RR2	21.9	4.10E-07
LOCMI04505	RR2	82.3	3.40E-25
LOCMI04506	RR2	82	4.10E-25
LOCMI05131	RR2	21.6	4.50E-07

LOCMI16617	RR2	58.5	4.80E-18
LOCMI17196	RR2	82.1	3.70E-25
LOCMI16600	RR2	112.2	3.30E-34
LOCMI16693	RR2	24.2	1.10E-07
LOCMI16599	RR2	105	5.00E-32
LOCMI12142	RR2	136.6	1.50E-41
LOCMI16606	RR2	30.2	1.70E-09
LOCMI13224	RR2	99.6	2.10E-30
LOCMI16637	RR2	99.6	2.10E-30
LOCMI16638	RR2	99.6	2.10E-30
LOCMI16718	RR2	73.2	1.80E-22
LOCMI16781	RR2	65.5	3.90E-20
LOCMI16838	RR2	103.7	1.20E-31
LOCMI07059	RR2	63.3	1.70E-19
LOCMI07060	RR2	110.2	1.40E-33
LOCMI16618	RR2	219.8	1.40E-66
LOCMI16597	RR2	91.3	6.40E-28
LOCMI17139	RR2	81.8	4.60E-25
LOCMI16612	RR2	84.7	6.40E-26
LOCMI16613	RR2	80.9	8.70E-25
LOCMI05383	RR2	67.5	9.60E-21
LOCMI16729	RR2	79.3	2.80E-24
LOCMI16621	RR2	134.2	8.30E-41
LOCMI16834	RR2	54	1.10E-16
LOCMI17147	RR2	51	8.90E-16
LOCMI16704	RR2	102.6	2.50E-31
LOCMI02816	RR2	77.3	1.00E-23
LOCMI17158	RR2	25.6	3.80E-08
LOCMI15346	RR2	24.3	9.90E-08
LOCMI16602	RR2	21.3	4.90E-07
LOCMI16626	RR2	40.2	1.60E-12
LOCMI16627	RR2	21.9	4.10E-07
LOCMI16628	RR2	29.7	2.30E-09
LOCMI16629	RR2	49.1	3.40E-15
LOCMI16630	RR2	26.4	2.30E-08
LOCMI16639	RR2	53.9	1.20E-16
LOCMI16640	RR2	28.2	6.70E-09
LOCMI16641	RR2	45.2	5.00E-14
LOCMI16648	RR2	44.2	1.00E-13
LOCMI16673	RR2	43.9	1.20E-13
LOCMI16833	RR2	30.2	1.60E-09
LOCMI16596	Others	-	-
LOCMI17145	Others	-	-
LOCMI16736	Others	-	-

LOCMI17249	Others	-	-
LOCMI16769	Others	-	-
LOCMI07701	Others	-	-
LOCMI16717	Others	-	-
LOCMI13223	Others	-	-
LOCMI16607	Others	-	-
LOCMI03719	Others	-	-
LOCMI16595	Others	-	-
LOCMI16775	Others	-	-
LOCMI16622	Others	-	-
LOCMI16611	Others	-	-
LOCMI16677	Others	-	-
LOCMI00374	Others	-	-
LOCMI16614	Others	-	-
LOCMI17157	Others	-	-
LOCMI16721	Others	-	-

[1] The E-value were determined based on the HMMER searches in the cuticleDB. An E-value (expectation value) is the number of hits that would be expected to have a score equal to or better than this by chance alone. A good E-value is much less than 1, for example, an E-value of 0.01 would mean that on average about 1 false positive would be expected in every 100 searches with different query sequences.

Supplementary Table S39 Chitinase and chitinase-like genes in the *L. migratoria* genome.

Gene	ID
LmCht2	LOCMI17199
LmCht4	LOCMI16689
LmCht5	LOCMI17048
LmCht6	LOCMI17331
LmCht7	LOCMI17356
LmCht8	LOCMI17568
LmCht9	LOCMI17569
LmCht10	LOCMI13600
LmCht11	LOCMI17267
LmIDGF1	LOCMI17185
LmIDGF2	LOCMI17170
LmIDGF3	LOCMI17127
LmIDGF4	LOCMI02015

Abbreviations: Cht, Chitinase; IDGF, chitinase-like imaginal disc growth factor.

Supplementary Table S40 Putative yellow genes of the *L. migratoria* genome.

L. migratoria	*D. melanogaster*	**Homology**
LOCMI17290	CG3757	yellow
LOCMI16530	CG17914	yellow-b
LOCMI16488	CG4182	yellow-c
LOCMI16507	CG4182	yellow-c
LOCMI17195	CG4182	yellow-c
LOCMI17293	CG4182	yellow-c
LOCMI17338	CG4182	yellow-c
LOCMI17339	CG9889	yellow-d
LOCMI17291	CG9891	yellow-d2
LOCMI16964	CG9792	yellow-e
LOCMI16526	CG18550	yellow-f
LOCMI17265	CG5717	yellow-g
LOCMI17060	CG13804	yellow-g2

Supplementary Notes

Supplementary Note 1. Genome features and evolutionary analysis

Heterogeneous distribution of heterozygosity rates

The heterozygosity rate, which was determined according to the previous studies, is the portion of heterozygous single-nucleotide polymorphisms (SNPs) between the two haploid components in the diploid genome[18,76]. It was calculated as the number of heterozygous SNPs divided by the length of corresponding genomic regions[76]. The sequencing reads (~130 GB, 20-fold genome coverage) were realigned with the assembled locust genome to identify the heterozygous SNPs. A heterogeneous distribution of heterozygosity rates was observed, possibly reflecting that the loss of heterozygous genotypes, which resulted from inbreeding line preparation of genome sequencing, varies among different genomic regions. The distribution of sequencing depth coverage and repetitive element divergence were determined to further exclude the possibility that the heterogeneous distribution of heterozygous SNPs are artifacts caused by un-equal sequencing depth coverage or high similar copies of repetitive elements. As shown in the track b of Figure 1a, the equal sequencing depth coverage indicates that the reduction of heterozygosity rates is not due to read mapping artifacts caused by low read coverage. To determine the genomic content and divergence of repetitive elements, the consensus repetitive sequences inferred from the *de novo* and homology identification were used as references to identify the genome-wide scale distribution of repetitive elements. In general, DNA transposons are the most abundant elements, and the amount of LINEs transposons is comparable to that of DNA transposons (Figure 1a track c). A homogeneous divergence distribution of these repetitive elements were observed (Figure 1a track d), and no obvious region that is of scarcity of divergent copies were detected (Figure 1a track d). Therefore, these results indicated that the results of heterozygosity rate distribution is not affected by neither sequencing overage nor repetitive element content.

Intron evolution

Comparative intron size analysis. To further elucidate the role of intron size expansion in locust evolution, pairwise comparisons between *L. migratoria* and other insects were performed using the log expansion/contraction ratios of introns of 1,046 conserved homologous genes. As shown in Supplementary Figure S8 and Supplementary Table S12, most introns (97%) experienced size expansion during locust evolution. It has been generally known that intron sizes vary widely in animals.

A previous study indicated that introns in humans are eight times as large as those in pufferfish, which is in line with the ratio of their genome sizes[77]. However, these studies were generally based on limited gene sets or assessment of relatively few species. Therefore, a broad comparison at the genome scale across divergent species is required. Here, we studied the relationship between average intron size and genome size for 73 whole genome sequenced species, including 50 vertebrates and 23 invertebrates (retrieved from Ensemble). As shown in Supplementary Figure S9, a strong positive correlation was observed between average sizes of introns and genome sizes (P value: < 2.2e-16, adjusted R-squared: 0.8206, Pearson's product-moment correlation). The trend of correlated increase in genome size with increase in average intron size was previously considered to follow a slope of 4:1 of log-transformed sizes[78]. We found that the log-transformed value of the *L. migratoria* genome size was only 2.4 times larger than that of its average intron size, implying that there were stronger selective constraints on the length of large introns. Therefore, increase in intron size in parallel with genome size expansion was likely largely responsible for the loosening of gene structures in *L. migratoria*.

TE invasions lead to intron size expansion in insects. In *L. migratoria*, the average gene size and average intron size are 42,426 bp and 10,473 bp, respectively. This average intron size is drastically larger than that of other sequenced insects (Supplementary Table S8). Most of the *L. migratoria* introns are longer than 1,000 bp, whereas most introns of other insects are about 100 bp long (Supplementary Figure S7). It is obvious that the intron size in *L. migratoria* is significantly expanded. To further elucidate intron size dynamics in insects from an evolutionary perspective, we carried out a comparison of intron length between *L. migratoria* and other insects for 1:1:1 insect orthloguous gene families that are subject to the same selection forces. We found that 97% (1,018 of 1,046) of the gene families experienced intron length expansion in the *L. migratoria* genome (Supplementary Table S12). The ratio density distribution of intron length in log2 unit showed a positive bias of ratio values and different peak location in all species, suggesting that intron size variation is associated with genome size in insects (Supplementary Figure S8).

To investigate the contribution of TE proliferation in intron size expansion, the TE content of introns was determined. We found that TE-harboring introns are more dominant in the locust genome. RepeatMasker screening indicated that a large fraction (65%, 68, 242/104,488) of locust introns contains TEs, and that this proportion is higher than that of all other insects (Supplementary Figure S10). We found a positive correlation between mean intron length and the fraction of TE-harboring introns (P value: 0.02, adjusted R-squared: 0.4364, pearson's product-moment correlation), suggesting that TE invasions likely played a key role in intron size expansion.

U12 Intron. The splicing process, which removes introns from primary transcripts, is essential for RNA maturation in eukaryotic cells. Spliceosome, a multicomponent complex, is involved in intron excision during the splicing process[79]. There are two types of introns—the U2-type and the U12-type—and they are spliced by distinct spliceosomes. The vast majority of introns are U2-dependent introns, whereas a small fraction of them are U12-dependent introns[80]. U12-type introns have an RT dinucleotide (the R indicates G or A) at the 5' splicing site and variable terminal nucleotides at the 3' splicing site. This breaks the rule observed in the U2-type introns, which have a GT dinucleotide at the 5' splicing site and an AG dinucleotide at the 3' splicing site. Further examination of U12 intron sequences revealed distinct properties compared to U2 introns, including conserved sequences (RTATCCTT nucleotide segments) at the 5' splicing site and adjacent branch site (TCTTAAC nucleotide segments) from the 3' splicing site. Both properties are required for prespliceosome complex formation[81].

U12-type introns have been identified in a wide range of eukaryotic species, indicating their early evolutionary origin[82]. Two recent studies based on comprehensive searches of genomic sequences revealed that U12 introns were lost in multiple invertebrate lineages during evolution[83,84]. Among insects, only 16 and 34 U12 introns have been identified in the *Drosophila melanogaster* and the *Apis mellifera* genomes, respectively. Of the 198 human-fruitfly orthologous genes with U12-type introns, 169 introns were lost and only sixteen cases have been maintained in the *D. melanogaster* genome.

The number of U12 introns in the locust genome was determined and was compared with those of other species reported in previous studies. Surprisingly, we identified 197 U12 introns in the *L. migratoria* genome, which is significantly higher than that of most other invertebrates ($P < 0.01$, student's *t*-test, Supplementary Figure S11), and twice as many as that of sea squirt (113), a vertebrate evolutionary ancestor, indicating the unique intron feature of *L. migratoria* genome compared to other insects.

Recursive splicing sites. The pattern of intron size can be extremely variable among different species. Although intron size expansion can be of benefit to gene expression and evolution, they also increase the potential for transcription processing errors[85]. In insects, an effective way to avoid the generation of extremely long transcripts is recursive splicing (RP), which excises long intronic transcripts into sub-fragments co-transcriptionally[86]. However, this regulatory mechanism is not observed in vertebrates[85]. Using the splice junction consensus matrix, we calculated the ratios of RP-sites within large introns (>50 kb as previously described[26]) and within their complementary strands in the *L. migratoria* genome (Supplementary Figure S12). In general, the larger introns of insects exhibited marked enrichment of RP-sites in the sense strand[85]. Contrary to the case in insects, the RP-sites of larger introns in the sense strand are less abundant in vertebrates (a ratio of 1.5 or less[85]). In *L. migratoria*, the RP-sites (with ratio of 1.14) are dramatically smaller than those of other insects, but similar to those of vertebrates. In addition, the ratio of RP-sites between the two strands was also determined in shorter introns with sequence length less than 50 kb. In *Drosophila*, the RP-sites of larger introns are significantly more abundant than those of shorter introns, whereas the ratio of RP-sites is approximately equal between the two strands in humans [85]. In *L. migratoria*, the ratio of shorter introns, 1.28, is similar to that of larger introns, indicating that the shorter introns in *L. migratoria* exhibit similar

RP-site patterns as those of humans. Taken together, these results indicate that the regulatory mechanism of introns in *L. migratoria* is similar to those in vertebrates.

Gene family analysis

Among the 17,307 genes in the *L. migratoria* genome, 7,995 are conserved across insect and daphnia, while 1,562 and 335 of them are conserved across insects and hemimetabolous animals, respectively. A total of 4,571 genes are locust specific (Supplementary Figure S13).

Supplementary Note 2. Genes related to pest and major Locust biology

Phase change

Fluctuations of CpGO/E in the coding region of genes. CpGO/E is an efficient measure of inferring the pattern of DNA methylation due to mutational mechanisms of hypermutable methylated cytosines that mutational decay of CpG di-nucleotides lead to a lower-than-expected CpGO/E from methylated region[30]. Briefly, methylated cytosines are chemically unstable and easily change to thymine via spontaneous deamination. This causes increased frequency of CpG to TpG mutations. Consequently, hypermethylated genomic regions lose CpG dinucleoties over time and have lower-than-expected CpG$_{O/E}$. Hypomethylated regions have high CpG$_{O/E}$. CpG$_{O/E}$ is expected to be negatively correlated with the levels of DNA methylation. Recent studies have demonstrated that the CpG$_{O/E}$ in several insect species that have the low level of methylation in their genomes, such as *D. melanogaster*, *T. castaneun*, *A. gambiae* has approximately normal distribution with a mean around 1. In contrast, the CpG$_{O/E}$ of genes in *A. mellirera* that has higher methylation level exhibits a striking bimodal pattern. Accordingly, CpG$_{O/E}$ can act as a indicator of the methylation level in insect genomes. We examined the distribution of CpGO/E and observed the intensity fluctuations of CpGO/E in the coding region but not in the whole genome. The depletion of CpG di-nucleotides in the coding region suggests widespread gene methylation in the locust genome.

Locust methylation system. DNA methylation is a major mechanism of epigenetic regulation and refers to the addition of a methyl group to position 5 of cytosine bases. Several studies have proposed that DNA methylation may be involved in the regulation of phenotypic plasticity in insects[87,88]. The three DNA methyltransferase genes, *Dnmt1–3*, display different functions. Dnmt3 establishes DNA methylation patterns, while Dnmt1 maintains these patterns, and Dnmt2 is involved in tRNA methylation. There have been various duplications and deletions of the three *Dnmt* genes within arthropods. Only *Dnmt2* is present in all sequenced arthropods. *Dnmt1* and *Dnmt3* have been lost in several lineages. We found two copies of *Dnmt1* in *L. migratoria*, similar to

A. mellifera and *A. pisum*. Both *Dnmt2* and *Dnmt3* exist as single copies in *L. migratoria* (Supplementary Table S15). All three *Dnmt* genes in *L. migratoria* exhibit conservation in the expected conserved domains.

Long-distance flight

Genes related to contraction/relaxation of flight muscles. Locust flight muscles are synchronous muscles[89], which are characterized by a 1:1 correspondence between neural activation and muscle contraction. Each contraction/relaxation cycle is accompanied by membrane depolarization and subsequent repolarization, release of activator calcium, attachment of cross-bridges and muscle shortening, then removal of activator calcium and cross-bridge detachment[90]. We identified the genes reported to contribute to the high frequency of flight muscle contraction and relaxation cycles in the *L. migratoria* genome. For example, calcium pumps contribute partially to the high rate of calcium removal in synchronous muscles[90,91], the troponin T subunit is possibly involved in muscle activation[90]; and resilin, one of the elastic proteins found in the wing hinge, contributes to the elastic storage of inertial energy in locust muscles[92]. The identification of these genes in the *L. migratoria* genome will help understand the function of flight muscles during long-distance flight. Comparison of these genes across insect genomes shows that there is no significant variation in their copy number across insect species, indicating that the capacity of *L. migratoria* for long-distance flight is likely supported by other genetic variations (Supplementary Table S24).

Genes related to wing vein morphogenesis and wing vein specification. In long-distance flying insects, integrity of the wings is critical for insect flight[93]. During the lifetime of a flying insect, its wings are subjected to mechanical forces and deformations for millions of cycles. Because insects control the wings remotely by transmitting forces distally via veins and areas of thickened membrane, defects in the thin membranes or veins may affect the insect's flight performance[94]. Seventy genes involved in wing vein morphogenesis (GO:0008586) and wing vein specification (GO:0007474) have been reported in *D. melanogaster* (retrieved from Amigo database: http://amigo.geneontology.org). We identified their homologues through homology-based searches (TBLASTN) in the genomes of nine other insects, including *A. pisum, A. gambiae, A. mellifera, B. mori, D. plexioppus, L. migratoria, N. vitripennis, P. humanus, T. castaneum*. Most of the genes are conserved across the insect species with only one copy in the insect genome (Supplementary Table S25). Thirty-five genes are shared by all the examined insect species, indicating that insects share a similar mechanism of vein morphogenesis and vein specification. Although wing shape and structure vary considerably between *L. migratoria* and *D. melanogaster,* 57 of the 70 genes involved in wing vein morphogenesis and wing vein specification are shared between them. This further supports a previously proposed theory that transition between different venation types may require relatively few changes in the regulatory gene networks involved[95,96].

Genes involved in biosynthesis of juvenile hormone.

Juvenile hormone (JH) plays important roles in regulating flight activity in insects[97-99].

JH is synthesized and secreted from the corpora allata, a pair of endocrine glands with neural connections to the brain. The biosynthetic pathway of JH can be divided into two steps: in the first step, farnesyl pyrophosphate (FPP) is formed from acetate through a series of chemical reactions, and in the second step, FPP is hydrolyzed by a pyrophosphatase to farnesol, and then oxidized successively to farnesal and farnesoic acid (FA) by two dehydrogenases[100].

Silkworm genes involved in JH biosynthesis were used as bait genes to identify their homologues in the *L. migratoria* genome through homology-based searches. Juvenile hormone esterase (JHE) has five essential catalytic motifs[101] which were confirmed by multiple sequence alignment with other insect JHE proteins (Supplementary Figure S22). We found that half of the JH pathway genes (7/14) in *L. migratoria* exist in more copies than their silkworm homologues do (Supplementary Table S26), which supports the idea that JH pathways function as integrators of metabolic physiology during locust flight[102].

Genes related to Insulin signalling pathway. The insulin/IGF signalling (IIS) pathway is highly conserved from yeast to worms, fruit flies, and rodents, and plays key roles in growth, metabolism, stress resistance, reproduction, and longevity in diverse organisms[103-105]. Several studies have demonstrated that the insulin signalling pathway is also involved in regulation of insect flight activity[106]. We identified most of the IIS genes in the *L. migratoria* genome using the IIS genes of *Drosophila* as bait genes (Supplementary Table S27). We only found one insulin-like peptide in the *L. migratoria* genome, which is significantly lower compared to 7 in *Drosophila*[107] and 37 in *C. elegans*[108]. In addition, a total of 3 insulin-like peptide receptors were identified in the *L. migratoria* genome.

PAT and FABP protein.

Lipid deposition, activation and transportation are critical for long-distance flight of locusts[109].

Lipid droplets are intracellular organelles enriched in adipose tissues that regulate the body fat stores of animals. PAT proteins, comprising of Perilipin, Adipose differentiation-related protein (ADRP), Tail-interacting protein of 47 kDa (TIP47), S3-12, and OXPAT[110,111], also known as PLIN1-5[111], are positioned at the surface of the lipid droplet[40]. PAT proteins manage the access of lipases to lipid esters within the lipid droplet core and interact with cellular machinery important for lipid homeostasis[112]. Members of the PAT family are present in evolutionarily distant organisms, including mammals, insects, slime molds and fungi[113]. All PAT proteins share sequence similarity and the ability to bind intracellular lipid droplets.

Using the human and *D. melanogaster* PAT homologous proteins as baits, we identified the PAT proteins of *L. migratoria* and 10 other arthropod species. The conserved domains of identified PAT proteins were further examined using Batch CD-Search[114], and only those with the perilipin domain were retained (Supplementary Table S29). Finally, 1 PLIN1 and 6 PLIN2 were identified in the *L. migratoria* genome

(Supplementary Table S28). Interestingly, the PLIN2 gene was found to be duplicated in the genome of *D. plexippus*. In *D. melanogaster*, the PLIN2 gene (Lsd2) has been reported to mainly control fat storage in fat bodies and the germ line of females[115]. Thus, duplication of PLIN2 genes might enhance the capacity of fat storage in *L. migratoria* and *D. plexippus*, which is possibly an adaptation to intensive energy demand during long-distance flight.

The fatty-acid-binding proteins (FABPs) are a family of carrier proteins for fatty acids and other lipophilic substances such as eicosanoids and retinoids. These proteins are thought to facilitate the transfer of fatty acids between extra- and intracellular membranes[116]. FABPs have been demonstrated to play key roles in the long-distance flight capacity of locusts. So we also detected these proteins in *L. migratoria* and 10 other arthropod species, using the *D. melanogaster* FABP homologous proteins as baits, we identified the number of FABP in 10 species are: 3 copies in *Pediculus humanus*, 2 copies in *Tribolium castaneum*, 1 copy in *Drosophila melanogaster*, 2 copies in *Anopheles gambiae*, 7 copies in *Bombyx mori*, 6 copies in *Danaus plexioppus*, 3 copies in *Apis mellifera*, 2 copies in *Nasonia vitripennis* and 11 copies in *Locusta migratoria*.

Antioxidants

Generation of reactive oxygen species (ROS) is a ubiquitous phenomenon in eukaryotic cells, resulting in oxidative stress, pathogenesis and aging[117]. For insects with intensive flight activity, ROS damage mitochondrial proteins and the cell membrane, and thus shorten their life span[43,118]. As defense against oxidative stress, insects have evolved a variety of antioxidant systems, such as antioxidant enzymes including superoxide dismutase, catalase and glutathione transferase, and soluble antioxidants such as ascorbate, glutathione, tocopherols, and carotenoids[119].

We searched the *L. migratoria* and 8 other insect genomes for antioxidant genes using *D. melanogaster* and *A. mellifera* antioxidant genes[120] and peroxidases from PeroxiBase[121] as bait. After homology-based searching, peroxidases were further filtered and classified using PeroxiScan[121]. The copy numbers of most antioxidant genes across the examined species are conservative except Prdx6, which belongs to the general peroxiredoxin superfamily (PS52075) (Supplementary Table S31). In contrast to the small copy number of Prdx6 in other species, nine copies were identified in the *L. migratoria* genome (Supplementary Table S31). Seven Prdx6 genes are tandemly located on two scaffolds (Supplementary Figure S24), as observed in the *D. melanogaster* genome (CG11765, CG12405, and CG12896). Prdx6 can scavenge peroxides, reduce peroxidized membrane phospholipids by using glutathione as a reductant, and protect cells against oxidant-induced plasma membrane damage[122-124]. Expansion of Prdx6 in the *L. migtratoria* genome may help alleviate the oxidative stress caused by reactive oxidative species produced during extensive flight activity[43,118].

Feeding

Odor related genes

Chemoreceptor genes. Utilizing their senses of taste (gustation) and smell (olfaction) to locate and recognize plants is a key aspect of host plant recognition in insects[125]. Environmental chemicals are detected, recognized and discriminated by chemoreceptor genes expressed in olfactory and taste sensory organs. Chemoreceptor genes include gustatory receptors (GRs), odorant receptors (ORs), and ionotropic receptors (IRs), which were identified recently[126].

The locust GRs were first identified using known insect GR proteins as templates by combined TBLASTN and GENEWISE searches[127]. Then, identified locust GRs and known insect GRs were used to perform the iterated profile searches with PSI-BLAST, because of high divergence of the GR genes[128]. These strategies were also applied in the identification of locust IRs. Known insect ORs deposited in GenBank were retrieved to identify the locust ORs by the AUGUSTUS gene prediction program[129]. Multiple alignment of the OR protein sequences were performed to construct a block profile using accompanying scripts from AUGUSTUS. The members and their exon-intron structure of the locust ORs were determined based on the protein profile extension from the block profile. Probable gene fragments of which presumed protein sequences are shorter than 250 amino acids were discarded following the strategy of a previous study[130]. For phylogenetic analysis, protein sequences were aligned with representative sequences from other insects. The phylogenetic trees were inferred by maximum likelihood methods, and were drawn using the PhyML 3.0 program with the JTT substitutional matrix[131].

By combined GLEAN gene set and predicted gene models from PSI-BLAST searches, we identified 75 *L. migratoria* GRs (LmGRs) in the draft genome sequences. To verify our gene prediction, the relative frequency of the corresponding amino acid at each position was generated using WebLogo. The WebLogo results clearly illustrated that conserved TYhhhhhQF motifs, which are representative features of GR genes, are present in the TM7 domain of most locust GRs (Supplementary Figure S26). For phylogenetic analysis, representative GRs including known carbon dioxide receptors, bitter receptors and sugar receptors were included to provide context for LmGRs. Phylogenetic relationships of the 75 LmGrs with each other are shown in Supplementary Figure S27. Most LmGRs formed three large lineages that were unique in *L. migratoria*, indicating their origin from LmGR expansion. Orthologues of the carbon dioxide and sugar receptors were not detected in the *L. migratoria* genome. In addition, no orthologue of the well-conserved DmGr43a gene lineage could be identified. Taken together with a previous report that these genes were also lost in the *A. pisum* genome[130], our results suggest that these genes are conserved only in holometabolous insects. However, the locust GR family does contain one member of the bitter receptor superfamily that is present in the silkworm moth *Bombyx mori*[132]. We also found 95 *L. migratoria* ORs and 10 *L. migratoria* IRs in the draft genome sequences. As expected, we identified a single orthologue of the Or83b gene, a highly conserved single-copy gene present in all insects studied to date.

Odorant-binding proteins. In insects, recognition of volatile compounds allows for odor and pheromone perception that is essential for feeding, survival and reproduction. Odorant-binding proteins (OBPs) are important components of the insect olfactory system[133]. The OBP genes were identified through homology searches using information from already known insect protein sequences[134]. Using the known insect OBPs as templates, the GENEWISE program was used to improve and extend the GLEAN predictions into full-length proteins. The HMMER searches using the PBP/GOBP pfam01395 profiles were conducted to determine the conserved OBP domain. Furthermore, the secondary structures including α-helices were predicted using the PSIPRED program to assist with the OBP gene annotation process[135]. We found a total of 22 putative OBPs in the *L. migratoria* genome. This indicates that compared to other known insect genomes, the *L. migratoria* genome contains a relatively low number of genes encoding OBPs.

Detoxification related genes

Families of detoxification related genes paly essential roles in interactions and defense against natural and synthetic xenobiotics, which facilitate adaptation to specific ecological niches in insects. To fully characterize these gene families, we manually annotated and compared the detoxification related genes in the *L. migratoria* genome to those in other insect genomes, including the families of genes encoding UDP-glycosyltransferases, glutathione-S-transferase, carboxyl/cholinesterase, ATP-binding cassette transporters and cytochrome P450 monooxygenases.

UDP glycosyltransferase. Potential defensive compounds of plants can act as toxins or feeding deterrents toward herbivorous insects. The detoxication of ingested plant compounds is considered to be one of the principle functions of UDP-glycosyltransferases (UGT) enzymes in insects. UGTs belong to a superfamily of metabolic enzymes that play important roles in the detoxification and elimination of a variety of endogenous and exogenous compounds[52]. Members of this superfamily are variable in sequence composition and abundance in bacteria, viruses, plants and animals, suggesting their very ancient origin and an essential role in living organisms[136]. These enzymes catalyze the conjugation of a glycosyl group from an activated sugar donor with various small lipophilic molecules, resulting in more hydrophilic products that are efficiently excreted[73,137].

We identified 68 putative UGT genes in the *L. migratoria* genome with subsequent manual curation. This number is larger than that of other insects of which genomes are determined, representing an approximately 2-fold expansion compared to *D. melanogaster* and 5.7-fold expansion relative to the number of UGTs identified in *A. mellifera*[138]. The deduced amino acid sequences showed similarity to a range of insect UGTs and included the UGT signature motif in a conserved C-terminal region: [FVA]-[LIVMF]-[TS]-[HQ]-[SGAC]-G-X[2]-[STG]-X[2]-[DE]-X[6]-P-[LIVMFA]-[LIVMFA]-X[2]- P-[LMVFIQ]-X[2]-[DE]-Q. Generally, the binding site of UDP moiety of the nucleotide sugar, also known as the UGT signature motif, is present in the conserved region of the C-terminal halves[139]. The availability of the full repertoire of putative UGT genes from *L. migratoria* makes it possible to determine the consensus sequences of the conserved region, and provides the opportunity to assess the accuracy of the UGT gene identification program. Therefore, we generated consensus sequence logos to display a graphical representation of the amino acid frequency. Supplementary Figure S28 shows the consensus amino acid sequences of locust UGT genes. The presence of consensus sequences consisting of the UGT signature motif strongly supported that the identified genes are members of the UGT superfamily. Besides the signature motif, three conserved positions ([VI], L and H in the position 1, 2 and 4, respectively) upstream of the signature motif were also detected. As the UGT superfamily has been well characterized in several insects, we included the representatives of each UGT family in our analysis to determine the members of established families in *L. migratoria*[138]. The nomenclature system was used to designate the families in the UGT phylogeny[138]. All representatives of each UGT family in other insects were retrieved from a recent study[138]. Following the UGT nomenclature guidelines, delineation of families was done on the basis of 40% or greater overall amino acid sequence identity. Within a given family, sub-families were defined by approximately 60% amino acid sequence identity. At least 31 families of UTG genes could be identified in the *L. migratoria* genome, representing the largest number of UGT families in insects. The larger number of UGT families in *L. migratoria* supports a diversified pattern of UGT gene evolution in *L. migratoria* and may reflect its specific feeding style. The putative UGTs identified in the *L. migratoria* genome were used to construct a phylogenetic tree by the neighbor-joining method (Figure 2b) that allowed clarification of the molecular evolution and structure of the superfamily of UGT genes. In total, three phylogenetic families, UGT360, UGT363 and UGT365, appear to have expanded more than the others during the evolution of the UGT superfamily in *L. migratoria*. The largest UGT family, UGT 365, contains 13 members, accounting for 19% of all UGT members. Because of the deep divergence between the *L. migratoria* and other insects, all but two members of distinct UGT families in *L. migratoria* share less than 40% amino acid identity to those of previously identified families. The phylogenetic tree also showed that the UGT genes in *L. migratoria* generally have a tendency to cluster together. Two exceptions to this are LMIUGT50E1 and LMIUGT47B1, which have similarities with UGTs of other insects. UGT50 has not been found in the *A. pisum* genome, so it had previously been considered to be common only to holometabolous insects[138]. However, the presence of the UGT50 family in *L. migratoria* suggests that this family is fairly well conserved across insects.

Glutathione-S-transferase. We identified putative glutathione-S-transferase (GST) genes by homology searches using the sequences of already known GST proteins as queries[140]. First, we identified the locust GST genes in the GLEAN gene set using BLASTP searches with an E-value threshold of 1E-5. Next, the GENEWISE program was used to improve and extend the GLEAN gene predictions into full-length proteins using GST protein sequence from other insects as a template[127]. The corresponding gene models were refined in light of supporting evidence from the expression data. The resulting gene models were verified by manual inspection using the Integrative

Genomics Viewer program[141]. Furthermore, the GST N- terminal domain (PFAM PF00043) and the C-terminal domain (PFAM PF02798) were determined with the HMMER program. This combined strategy resulted in a total of 28 putative cytosolic GST genes in the *L. migratoria* genome. Multiple sequence alignment was performed using the MAFFT program[142]. Ambiguities and gap-containing columns in alignments were excluded from phylogeny analyses. Prior to phylogeny construction, the ProtTest program was used to estimate the best model of protein evolution[143]. The resulting optimal model, the LG+I+G model, was then used for the phylogenetic analysis. Finally, maximum likelihood-based inference of the phylogenetic tree was implemented in the RAxML software[144]. Nodal support was assessed using 1000 bootstrap pseudo-replicates.

Supplementary Table S32 provides an overview of the six GST subclasses—Sigma, Theta, Omega, Zeta, Delta and Epsilon. The criteria for subclass division were obtained from published literatures and are supported by phylogenetic and BLAST-based evidence[140]. Our homology searches identified 28 GST genes in *L. migratoria*, which represents a considerable expansion in the size of this family compared with those in the other two hemimetabolous insects, *A. pisum* and *P. humanus*. No best hit was obtained for the kappa-class GSTs based on NCBI BLAST searches, which indicates that all of these locust GST genes are localized in the cytosol. The gene models of the GST genes were revised manually to improve the gene structures. Most GSTs are supported by transcriptome data in the libraries from different developmental stages. The Epsilon and Delta classes represent the insect-specific classes, which include the majority of the GSTs with a key role in metabolic detoxification of insecticides. As in the *A. psium* genome, no Epsilon class GSTs but abundant Delta class GSTs were found in the *L. migratoria* genome. In contrast to other insects involved in this study, the Sigma class is the largest GST subclass in the *L. migratoria* genome[75]. Twelve of the 28 GST genes were classified into this class. A lower divergence in several members of the Sigma GST genes in the phylogenetic tree suggested recent duplication events in the Sigma class. The reason for this duplication in the *L. migratoria* genome is unclear. Members of this class show high abundance in tissues that are either highly aerobic or particularly sensitive to oxidative damage, indicating a crucial role in protection from oxidative stress[145]. Therefore, in addition to their roles in metabolic detoxification of insecticides, their protective role against deleterious effects of oxidative stress might also have favored duplication of the Sigma class of GSTs in the *L. migratoria* genome.

Carboxyl/cholinesterase(CCE). Carboxyl/cholinesterase family members are responsible for controlling pheromone or hormone degradation, xenobiotic detoxification and neurodevelopment, and are major insecticide targets and chemical warfare agents[74]. Based on previously reported CCE genes, TBLASTN was used to identify the potential genomic loci of the locust CCE genes with an E-value threshold of 1E-5. The ClustalW program was used to perform multiple sequence alignment prior to phylogenetic analysis. The alignments were visually inspected for accuracy based on amino acid sequences. Model selection was performed with ProtTest based on Akaike Information Criterion, and the WAG model was applied in the phylogenetic reconstruction. Finally, a maximum likelihood analysis was performed in the PhyML program with 100 bootstrap iterations[131].

We have found 80 CCE genes in the *L. migratoria* genome, and this represents the largest gene family expansion of the insect genomes sequenced so far (Supplementary Table S33). As in the other insect genomes, the locust CCE genes belong to three main functional classes—dietary/detoxification, hormone/semiochemical processing, and neuro/developmental functions. The numbers of locust CCE genes in these three functional classes are 39, 32 and 9, respectively. In general, the class distribution of the locust CCE genes conformed to that of aphid CCE genes with few differences. The most notable difference between *L. migratoria* and most other insects with regard to CCE genes is the relatively high number of CCE genes of the dietary/detoxification class in the former: 39 compared to 8-26 in other insect genomes, except for *B. mori*. Locust-specific expansion largely accounted for the high number of CCE genes in the dietary/detoxification class. In addition, a large difference in the number of CCE genes could also be observed in the β-esterases subclass of the hormone/semiochemical processing class. The β-esterases subclass serves diverse functions including sex pheromone degradation, reproductive behaviour control, juvenile hormone metabolism[146,147]. This subclass has 21 representatives in *L. migratoria* but 2-18 in other insect species. In the neuro/developmental class, the *L. migratoria* genome has the same distribution of CCE genes as those found in other insects, suggesting a conserved role for this class[75]. However, variations among locust members could be identified in the J and K subclasses, which are otherwise highly consistent across insects (Supplementary Figure S30). In most cases, the insect genome contains two acetylcholinesterases and one gliotactin gene. One exception is that the *D. melanogaster* genome contains only one acetylcholinesterase and two gliotactin genes. Acetylcholinesterase is a key target of organophosphorous and carbamate insecticides[148].

ATP-binding cassette transporters. For identification of ABC transporters, we generally followed the same procedure as those used previously for the same purpose in *D. pulex*[149]. Firstly, the GLEAN gene set was searched using the BLASTP program to identify putative ABC proteins in the locust genome. Our initial query sequences were those of already identified ABC proteins from invertebrates. Protein sequences with significant matches to known ABC proteins were retained for further analysis. We also performed TBLASTN searches to identify putative genomic loci of ABC transporters using the conserved NBDs (highly conserved nucleotide-binding domains) as queries. The ABC transporters in the putative genomic loci were predicted by the GENEWISE program, and their gene structures were further refined by manual adjustment on the basis of transcriptome and homology support. In an attempt to verify our identified ABC transporters, the NBDs for each gene were determined using Interpro domain IPR003439. The domain structures of NBDs were refined using the InterProScan program[150]. To further determine ABC subfamilies, specific domains were searched against the Conserved Domain Database (CDD) using the reverse position-specific (RPS) BLAST program[151]. The CDD domains included cd03263, cd03249, cd03250, cd03223, cd03236, cd03221, cd03213 and cd03230. The subfamily assignment was further confirmed by phylogenetic analysis together with known ABC transporters. For comparison, ABC transporters of several insect genomes were also determined by the same procedure.

In total, our searches identified a total of 65 putative ABC genes in the *L. migratoria* genome (Supplementary Table S34), which includes members from all known ABC subfamilies. Of these, 19 genes were classified under the ABCB subfamily while the two ABCC subfamilies together comprised another 19 genes. These two subfamilies are involved in xenobiotic resistance and represent the largest ABC subfamilies in *L. migratoria* as well as other insects[152].

Cytochrome P450 genes. Cytochrome P450s (CYPs) form a large and diverse gene family in metabolic systems and are involved in the metabolism of xenobiotics such as pesticides, plant toxins and toxic environmental chemicals. They are also important in the regulation of endogenous lipophilic compounds, including hormones, fatty acids and steroids. To detect the CYP genes, the GLEAN gene models were searched by the TBLASTN and GENEWISE programs with known insect CYP sequences representing the four conserved CYP clades[127]. The gene models were corrected to avoid fusion with adjacent CYP genes or fragmentation when necessary. Through these manual annotation and curation of CYPs, we found 94 P450 genes in the *L. migratoria* genome. As shown in Supplementary Figure S31, this number represents an intermediate number of P450s in the insect genome but higher than that of the other two sequenced hemimetabolous insects, *A. pisum* and *P. humanus*. A phylogenetic analysis was performed to classify the locust P450s with other identified insect P450s. The amino acid sequences of the resulting P450 genes were aligned with those of other insect P450 genes by the MAFFT program with some manual adjustments[142]. A phylogenetic tree was then constructed based on the maximum likelihood algorithm using the RAxML program. Supplementary Figure S32 shows the four distinct branches of the phylogenetic tree corresponding to the known CYP clades. The locust P450s could be divided into four distinct clades—CYP2, CYP3, CYP4 and mitochondrial clades—that are also found in other insects. The number of genes in the CYP3 clade in the *L. migratoria* genome is higher than that of the typical insect with the exceptions of *A. aegypti* and *T. castaneum.* The CYP3 clade contains the largest number of insect P450 genes and considerable amount of evidence points to its role in xenobiotic metabolism and insecticide resistance, implying its critical role in locust biology[153].

Supplementary Note 3. Pest control

Established insecticide targets

Deficiency of ion channels and receptors promotes the death of insects by interfering with nervous system functions[154]. A variety of ion channels and receptors have been utilized as the major target sites of various insecticides[54]. Although a few genes of the ion channel superfamily have been reported in locusts, the full complement of locust ion channels has not yet been determined[155]. Sequencing of the *L. migratoria* genome offers a unique opportunity to characterize the complete set of potential insecticide target genes, representing a fundamental step in improving our understanding of key components of locust insecticide targets.

Genes of the cys-loop ligand-gated ion channel (cys-loop LGICs) superfamily are major molecular targets for currently approved insecticides. Their members include glutamate-gated chloride channels (GluCls), excitatory cation-permeable nicotinic acetylcholine receptors (nAChRs), γ-amino butyric acid (GABA)/glycine chloride channels, and histamine-gated chloride channels (HisCls)[156]. They have important functions in the nervous system of insects and are essential in a variety of biological processes, such as synaptic inhibition, cellular excitability and organic solute transport[157]. Several classes of insecticides specifically target cys-loop LGIC genes. For example, owing to their strong binding affinity to nAChRs, neonicotinoids, which includes imidacloprid and thiamethoxam, function as agonists that selectively act on insect nAChRs. In addition, cyclodienes (such as dieldrin) and phenylpyrazole (such as fipronil) insecticides have been shown to inhibit GABA receptors, GluCls and HisCls. Thus, interference of these genes by insecticidal chemical classes is a widely adopted management strategy for controlling agricultural pests. Using a combined strategy of GLEAN gene predictions and homology searches, 34 candidate cys-loop LGIC genes were identified in the *L. migratoria* genome and manually annotated. We determined the orthologous relationships between the cys-loop LGIC genes of *L. migratoria* and other known insect cys-loop LGIC genes. Based on their orthologues, these locust cys-loop LGIC genes were classified into four categories: GluCl, nAChR, HisCl and GABA-gated chloride channels. In general, insect genomes have only one GluCl gene[157]. Surprisingly, we found four GluCl genes in the *L. migratoria* genome. GluCl gene expansion has also been reported for the basal ancestor of arthropods, *Tetranychus urticae*, suggesting a partial loss of GluCl genes during insect evolution[157]. We identified 17 candidate nAChR subunit-encoding genes in the *L. migratoria* genome. This represents a larger nAChR gene family compared to that in *D. melanogaster*, *A. gambiae*, *A. mellifera*, *T. castaneum* and *N. vitripennis*, which contain 10, 10, 11, 12 and 16 subunits, respectively. Although there is no evidence to date that insects use glycine as a neurotransmitter, we identified 11 genes that encode proteins similar to GABA/Glycine chloride channels. These locust GABA/Glycine chloride channels include orthologues of the three known GABA-gated chloride channels (*Rdl*, *Grd* and *Lcch3*) in *D. melanogaster*[158]. Interestingly, we found that the *Grd* gene has been duplicated in the *L. migratoria* genome, while most insect genomes sequenced to date have been reported to contain no more than one *Grd* orthologue[157,158]. Furthermore, as with *D. melanogaster* and *T. castaneum*, *L. migratoria* has two HisCl genes[159].

G-protein-coupled receptors (GPCRs) mediate physiological responses to hormones, neurotransmitters and environmental stimulants, and are thus insecticide target candidates for pest control[160]. We searched the *L. migratoria* draft genome with protein sequences corresponding to fly GPCRs[161]. The searches were performed using the AUGUSTUS gene prediction program based on protein family specific conservation[162]. Our annotation efforts resulted in the discovery of 90 GPCR genes composed of 61 rhodopsin-like receptors, 21 secretin-like receptors, 3 metabotropic glutamate receptors and 5 atypical 7 TM proteins. In the rhodopsin-like receptor family, we identified receptors for most biogenic amines, several of which are considered to be key regulators in phase transitions[29]. We found 20 GPCRs responsible for binding of biogenic amines such as dopamine, tyramine, octopamine, and serotonin (Supplementary Table S35).

Lethal insecticide candidates

Gene overexpression or silencing offers an important tool for development of alternative pest management strategies. These gene manipulation approaches enable us to protect crops by up- or down-regulating essential gene functions in pests to kill them[163]. Several essential genes in insects have been approved recently as insecticide targets; their functions are altered through chemical approaches or via uptake of dsRNA molecules[57,164,165]. However, the number of essential genes successfully utilized as insecticide targets is rather limited. Integration of genomic information with essential gene identification based on phenotypic data allows the discovery of new insecticide targets for suppressing agricultural pests. Complete genome sequences have been determined for an increasing number of insects from various orders, and these genomic resources provide a platform to further explore essential insect genes by comparative genomic analyses. Such analyses can facilitate discovery of novel insecticide targets that are unique to pests in a fair and effective manner at unprecedented selectivity. High specificity of gene manipulation approaches is necessary to guarantee safety to human health. Fine-scale, or even complete, specificity in essential-gene-based pest management depends largely on the nucleotide sequence identity between insecticide target genes in pests and similar-sequence genes of other species, including humans and transgenic plants[57]. Additionally, the specificity may be influenced by nucleotide variations of insecticide target genes in pests. Therefore, sequence similarity with other species and allelic variability should be taken into account in the identification of novel insecticide target genes. In this study, a genome-wide screening of essential genes based on comparative genomic analyses was carried out to identify candidate insecticide targets for developing selective, specific and human-safe control approaches. Firstly, all protein sequences and phenotype data for *D. melanogaster* and *C. elegans* were downloaded from Flybase (http://flybase.org/) and Wormbase (http://wormbase.org/), respectively. Following the approach used in a previous study[56], genes with mutant phenotypes of “lethal” and/or “neurophysiology defective” were considered to be essential in *D. melanogaster* while those with mutant phenotypes of “lethal”, “paralyzed”, “movement abnormal” and/or “muscle system physiology abnormal” were considered essential in *C. elegans*. Only essential genes were considered for further analysis. Secondly, protein sequences of the *L. migratoria* genes were compared with those of essential genes from *D. melanogaster* and *C. elegans* using reciprocal BLAST searches to determine orthologous relationships. The orthologues of locust essential genes were defined as those that had best–best hits in BLAST searches. Thirdly, locust essential genes with sequences similar to those of human genes were filtered to avoid harmful side effects to human health. Finally, essential gene targets from single-copy genes or lower diversity genes were given a higher priority, given that higher allelic variability is likely to contribute to increased susceptibility towards silencing resistance. Altogether, 166 *L. migratoria* essential function genes with orthologous essential functions in *C. elegans* and *D. melanogaster* were identified by this *in silico* screening approach (Supplementary Table S35). A large number (51/166, 30%) of these genes have annotated molecular function of 'enzyme or transporter or receptor activities', and comprise diverse classes of proteins that mediate critical biological process. Among the 166 essential genes, several belong to molecular classes whose representatives have been successfully utilized as chemical and RNAi targets[57,166]. For instance, kinases, ATPases, synthases, carboxylasterases and receptors have been confirmed as effective targets for pest control in several insects[57]. In conclusion, our screen revealed many essential genes that are potential insecticide targets against *L. migratoria*. Importantly, this approach can also be applied to other sequenced pests.

RNA interference

RNA interference (RNAi) mediated by short interfering double-stranded RNA molecules (dsRNA) is a conserved post-transcriptional gene silencing mechanism involving degradation of a target mRNA in a variety of eukaryotic organisms[57]. This dsRNA-mediated gene silencing can be categorized into two partially overlapping pathways: the microRNAs (miRNA) pathway and the small interfering RNA (siRNA) pathway[167]. In the miRNA pathway, endogenous genes encoding stem loop hairpin primary miRNA transcripts are cleaved into a ~70-nucleotide precursor miRNA molecules, which are processed in the nucleus by a microprocessor complex composed of Drosha and its cofactor, Pasha[168]. The resulting precursor miRNAs are then exported from the nucleus into the cytoplasm by Exportin-5, a Ran-GTP dependent nucleo–cytoplasmic transporter[169]. Dicer-1 interacts with a dsRNA binding protein partner, Loquacious (Loqs), to generate a miRNA/miRNA* duplex from precursor miRNAs[170]. In the siRNA pathway, long exogenous dsRNAs are processed into siRNAs in the cytoplasm by Dicer-2 and a dsRNA-binding domain partner protein, R2D2[171]. Both miRNAs and siRNAs bind the Argonaute (Ago) protein family in the RNA-induced silencing complex (RISC), resulting in either mRNA degradation or repression of mRNA translation[168]. As observed in the most sequenced insect genomes, the *L. migratoria* genome possesses one copy of each gene in the miRNA pathway: one Ago1, one Dicer-1, one Exportin-5, one Drosha and one Pasha, with exception of the 3 copies of Loqs (Supplementary Table S37). For siRNA biosynthesis, one copy of R2D2 was found in the *L. migratoria* genome, which is also typical of siRNA machinery in insects. However, we found duplications of Dicer-2 (2 copies) and Ago2 (2 copies) in the *L. migratoria* genome. The duplication in important proteins of siRNA machinery may reflect a functional expansion of the siRNA pathway, which requires further understanding their biological significance in locust biology.

Immune system

Locust is a notorious agricultural pest and migrate long distance after swarming. During them travel, they might encounter numerous kinds of pathogens attacking. Insect can trigger humoral and cellular immune defenses to resist infections by organizing the responses of melanization, anti-microbial peptides production and phagocytosis of hemocytes[172].

Immune genes in *L. migratoria* were identified by combining the results from both HMM profile and BLASTP based searches as previously described[173]. For the HMM method, two sets of profiles were used: one was built from manually curated protein sequences of four dipteran species, *D. melanogaster*, *A. gambiae*, *A. aegypt*， and *C. quinquefasciatus*, while the other one was built from automatically defined orthologous groups across 21 insect species. All protein sequences for each family were downloaded from ImmunoDB[174] (http://cegg.unige.ch/Insecta/immunodb). MUSCLE[175] was used to align multiple protein sequences and HMMER 3.0[176] was used to build profiles. The profiles were then searched against the *L. migratoria* proteins. For the BLASTP method, all known immune related genes in *D. melanogastor* were downloaded from ImmunoDB and were searched against the *L. migratoria* proteins. Then, all the results were integrated to produce the final list of immune related genes. For the purpose of comparison, the same method was also applied to the other three species, *A. pisum*, *P. humanus* and *D. pulex* (Supplementary Table S36).

Using the above procedures, we found that the typical immune pathways including IMD, Toll and JAK/STAT all exists in *L. migratoria*. Interestingly, we found that the humoral immune gene families of prophenoloxidases (PPOs, 8) and serine protease inhibitors (SRPNs, 23) were expanded in *L. migratoria,* as the most abundant among the 5 species. It is known that the SRPNs involved in regulation of serine proteases cascades that ultimately activate PPO during melanisation response, and these two gene classes systematically control melanisation cascades spatially and temporally[177]. Moreover, the PGRP class expands as 15 members in locust in comparison of other insect species. Thus the expansion of these humoral gene classes suggests humoral immune defences might play a crucial role in *L. migratoria* life cycle.

Environment friendly biopesticides, such as pathogenic fungus *Metarhizium*[178], are widely used to control locust outbreak. However, as in other insects, the efficiency of bio-pesticide was reduced by the immune system of locusts[172]. Based on the genomic-scale observation, the dissection of the immune system of locust in responses to the challenge with the pathogenic fungus *Metarhizium*[178] and laminarin[179] could provide the important cues in development of novel pesticides.

Cuticle metabolism

Insect cuticle is an important ecological innovation of a highly successful invertebrate phylum. It is a strong, light exoskeleton and environmental interface predominantly composed of an ordered matrix of chitin fibers and protein[180]. The biomechanical properties of cuticle and the control of its deposition during development have long been of interest to researchers. More recently, evidence has emerged that cuticular proteins are relevant to problems in applied entomology, such as insecticide resistance, immune responses, heavy metal tolerance and drought tolerance[181]. The insect-specific metabolism that occurs in the integument is vital for growth and, therefore, is a good target for development of highly selective insecticides[182]. Here, we identified several major gene families, including cuticular proteins, chitinase and yellow proteins, which are involved in insect cuticle metabolism by conducting genome-wide searches using homologue BLAST.

The cuticle consists mainly of chitin fibers embedded in a matrix of a large number of cuticular proteins (CPs)[183]. Hundreds of CPs have now been identified from various insect species[184]. The vast majority of these proteins belong to the CPR family, which is defined by a well-conserved domain termed the Rebers and Riddiford Consensus (R&R Consensus) and also recognized as pfam00379. This family has two distinct groups—RR-1 in soft cuticles, and RR-2 present in proteins from hard cuticles[185]. Putative cuticular protein genes containing the pfam00379 domain were searched using InterproScan with IPR000618. The InterproScan searches annotated 110 putative cuticular protein genes in the *L. migratoria* genome (Supplementary Table S38). R&R consensus in each putative cuticular protein gene was further identified by using a web server based on profile hidden Markov models in the cuticleDB website, which is capable of RR-1 and RR-2 consensus classification[186]. Thirty-two genes were identified as RR-1 cuticular protein genes and forty-nine were found to be RR-2 cuticular protein genes. Despite showing sequence similarity with known cuticular protein genes, nineteen other genes failed to be classified using the cuticleDB searches.

Chitin is an important component of the exoskeleton of arthropods, but it is absent in vertebrates. Therefore, it represents a useful target for drugs against insects. During insect growth and development, the cuticle must be degraded periodically and replaced to allow for growth, maturation and repair[187]. Chitinolytic enzymes (chitinase) play important roles in shedding of the old cuticle and turnover of both the PM and tracheal lining. Chitinase (EC 3.2.1.14, endochitinase) is an enzyme that catalyzes the random hydrolysis of N-acetyl-b-D-glucosamine b-1, 4 glycosidic linkages in chitin and chitodextrins in a variety of organisms. All insect chitinases belong to family 18 of glycosylhydrolases and many of them may be involved in cuticle turnover, digestion and PM degradation during molting. We identified a total of 13 chitinase and chitinase-like genes in the *L. migratoria* genome based on the presence of signature sequences of insect chitinases by using homologue searching (Supplementary Table

S39).

The *yellow* gene family is perhaps one of the most enigmatic families discovered so far. There is some evidence that one of the primary functions of insect yellow genes is related to cuticle and eggshell (chorion) formation and hardening during insect development, and that the yellow gene family is vital for insect survival[188]. The unusual phylogenetic distribution of *yellow*-like sequences suggests either multiple horizontal transfer from bacteria into eukaryotes, or extensive gene loss in eukaryote lineages. The yellow gene family contains 10 to 15 members in most insect genomes, but the *A. mellifera* yellow gene family has 26 individual *yellow*-like genes[189]. Using the *D. melanogaster* YELLOW protein sequence as query sequences for iterated PSI-BLAST searches, we found a gene family composed of 13 members, each of which contained a conserved MRJP domain. We named it the YELLOW protein family of *L. migratoria* (Supplementary Table S40).

Supplementary Methods

Genome Sequencing, Assembly and Evaluation

Samples for genome sequencing

Locust swarms devastate crops and cause major agricultural damage. They occur in many areas, especially in African, Asian, and Australian countries (Supplementary Figure S1). The migratory locust *Locusta migratoria* is one of the most famous locust species and is considered a model for the study of insect physiology. Whole genome sequencing of *L. migratoria* will enhance our ability to understand locust biology and may provide effective choices for our battle against locust plagues.

The strain used in this study for genome sequencing originated from the inbred laboratory strains of solitarious locusts at the Institute of Zoology, CAS, China[16]. Both colonies were reared under a 14:10 light/dark photo regime at 30℃ and on a diet of fresh greenhouse-grown wheat seedlings and wheat bran. To produce an even more inbred line, a sibling female adult and male adult were mated and eight generations of sib mating were then allowed to occur. DNA for genome sequencing was extracted from the whole body of one female adult except its guts.

Genome size estimation

Estimation of genome size using *k*-mer. K-mer analysis has previously been used to estimate genome size[190]. In this study, based on a *k*=17 estimation, the *L. migratoria* genome size was estimated to be 6.38 Gb (Supplementary Table S2**,** Supplementary Figure S2). However, based on *k*-mer distribution, we assumed that there was certain degree of heterozygosity in the *L. migratoria* diploid genome.

Estimation of genome size using flow cytometric analysis. The genome size of *L. migratoria* was determined with flow cytometry, using 4'-6-Diamidino-2-phenylindole (DAPI) as the stain and *Mus musculus* testis cells as internal standards. The samples from *L. migratoria* testis cells of one male and the hemolymph of one female were tested in the flow cytometric analysis. We estimated the *L. migratoria* genome size to be ~6.3 Gb per haploid genome (Supplementary Figure S3). Our estimation was close to the previous Feulgen densitometry measurement that indicated that the locust genome size ranged from 5.28 to 6.35 pg/1C or approximately 5.21 to 6.27 Gb per haploid genome[191,192].

RAD sequencing and Genetic linkage group construction

The mapping cross. A male *L. migratoria* from Hainan province was crossed with a female from the laboratory raised population, the same lineage used for the reference sequence. DNA from 106 F1 (F:55, M:51) individuals and two parents was isolated using QIAGEN DNeasy Blood&Tissue Kit (Qiagen) after getting rid of the whole gut.

RAD library preparation and sequencing. Approximate 1μg genomic DNA of each individual was digested with 20U EcoRI for 1 hour at 37. Then the digestion products were ligated to a modified Illumina P1 adapter which has a unique index. The ligation products from 24 individuals were pooled together and sheared to an average size of 500 bp. DNA samples were electrophresised on a 2% TAE gel, and DNA with length 350 bp – 500 bp was isolated with gel extraction kit (Qiagen). After end polishing and adenine adding, samples were ligated with an Illumina P2 adapter. Finally the libraries were enriched by PCR amplification and qualified by Agilent 2100 test and Q-PCR. Illumina protocols were followed for cluster generating and sequencing. One hundred and six F1 individuals and two parents were sequenced with 50 bp single end on a HiSeq 2000 platform. Parents and F1 individuals were sequenced at ~20X and ~10X, respectively.

SNP calling. The reads were aligned to the genome using BWA (version 0.6.2) and the SNPs for every individuals were called using "samtools pileup"[60]. Only the unique mapped reads were used. The SNPs were further filtered using "samtools.pl varFilter". All the SNPs sites across all F1 progenies were merged and the sites that exist or not be covered in the two F1 parents were filtered.

Genetic linkage group construction. Finally, 8,708 markers were classified into 11 linkage groups using minimum LOD 25. Each linkage map was constructed using JoinMap 3.0[61]. Assembled sequences were mapped to the linkage group based on the marker position. Totally, 7,165 scaffolds were anchored with accumulated length 2.9 Gb (44.7% of the genome).

Genome Assembly Evaluation

Strategies for resequencing-based genome assembly quality evaluation have been described previously[12]. To assess the representative of the assembly, 135 Gb (~22X) high quality reads with insert sizes of 200 bp were aligned onto the assembly using MAQ-0.7.1[59] with default parameters except -C 1. Unmapped reads were further aligned using BLAT with the following parameters: -minScore=80, -maxIntron=50, -repMatch=100. SNP calling was carried out using samtools pileup pipeline.

A total of 94.37% of the reads (90.21% by MAQ and 4.16% by BLAT) could be mapped to the assembly, suggesting that nearly the entire *L. migratoria* genome was represented in our assembly. Completeness of the assembly was assessed by the sequencing depth of each base. The proportion of a given depth was calculated and plotted, then compared to the theoretical Poisson distribution with a mean corresponding to the peak (here is 22x) in our data (Supplementary Figure S4). However, there was a minor peak at half of the peak, which suggested the presence of some redundancy in the assembly. The redundancy could have been caused by heterozygosity, which makes the regions with higher heterozygous between sister chromatids were assembled into two sequences[193], which was supported by Fig 1a track b. We found the depth distribution of the repeat regions was similar to those of the whole genome. However, the depth distributions of the gene body region of all genes and all the paralogs were similar to the theoretical distribution, which gave us confidence for further analysis. The positions with depth three times higher than 22x, comprised 1.14% of assembled sequences, indicated that repeat collapse was not a serious issue in our assembly.

To evaluate the assembly quality, 9 BACs (bacterial artificial chromosomes) were sequenced using Illumina HiSeq 2000 with 500 bp insert size and >100x coverage. The reads for each BAC were assembled with SOAPdenovo v1.05 separately to avoid the influence of repeat sequences and heterozygosity. For each BAC, different *k*-mer sizes were optimized. To validate accuracy of the assembly and to connect the BAC fragments, we also sequenced ~1.5x Sanger paired-end reads with 3-5 Kb insert sizes for 6 BACs and then mapped the Sanger reads to the assembly. Two fragments were connected if the Sanger paired-end reads were mapped with correct direction and proper distance. The statistics for accuracy of the BAC assembly by Solexa sequencing were assessed through aligning Sanger reads to the assembly (Supplementary Table S4). The sequencing error rates were estimated at 4 x 10^{-4}. The longest scaffold in each BAC assembly, ranging from 57-109 Kb, was chosen to evaluate the genome assembly (Supplementary Table S5). The alignment was carried out using LASTZ[194] with the following parameters: --match=1,5; --gap=6,1; --seed=match15; --ambiguous=n; --identity=80; --format=axt. The aligned regions were then linked using chainNet[195]. On average, 94% of regions of these BACs were covered by the assembly. The assessment results are shown in Supplementary Figure S5 and the legends there showed the methods. In BAC 107-38, the gap region in the genome assembly was annotated as repeat regions in the corresponding region of the BAC, which was a known shortcoming of the next generation sequencing assembler[196,197]. The gap length in the genome assembly was longer than the actual gap length which might also lead to the larger assembly. The depth of BAC 107-38 was also normally distributed around 20X. However, all of the gene exons were assembled well. In BAC 107-52, several regions, illustrated by light red rectangle (Supplementary Figure S5), showed extremely low depth. However, the depth of the genome assembly was normal (data not shown). Manual alignments of the two regions demonstrated that they were aligned well between the BAC and the genome assembly. However, their identity was lower than 90%, indicating heterozygosity. Since the maximum mismatch tolerance for a 32-bp seed is 2 in BWA (Burrows-Wheeler Alignment tool), the reads in these heterozygous regions could not be aligned with default parameters[198].

The gene region coverage of the assembly was also evaluated. We downloaded 41,880 EST sequences (Supplementary Table S6) > 200 bp long from LocustDB[199]. The ESTs were aligned to the assembly genome using BLAT[200] with default parameters. The cut-off for identity was set to 80%. More than 96.75% of ESTs with length > 500 bp were covered by the genome at > 90% coverage. We also aligned 71 complete *L. migratoria* CDS (Coding DNA Sequence) from GenBank to the genome assembly. On average, 95.72% region of these CDSs was covered by a single best piece (Supplementary Table S7). Additionally, among the 248 highly conserved Core Eukaryotic Genes[201], 246 (99.19%) could be covered by more than 90% using TBLASTN searches. Finally, the RNA-seq mapping ratios of the *L. migratoria* genome assembly were comparable to that of previously published genomes (Supplementary Table S20). More than 75% of the reads in all the samples were aligned to the genome. In conclusion, the genome assembly covered most of the coding genes accurately, which provided a solid base for further analysis.

Genome annotation

Gene annotation pipeline

Gene set prediction. For homology-based prediction, protein sequences of four insects were retrieved from public genome databases (of *Drosophila melanogaster* from Flybase, *Apis mellifera* from BeeBase, *Acyrthosiphon pisum* from AphidBase, and *Pediculus humanus* from VectorBase). These protein sequences were aligned to the *L. migratoria* genome using TBLASTN (E-value ≤ 1E-5) and the matches with length coverage > 20% of the homologous proteins were considered as gene model candidates. Then, to improve gene models, the corresponding homologous genome sequences were aligned against the matching proteins using Genewise[127].

For *de novo* prediction, Augustus[62], SNAP[63] and Glimmer-HMM[64] were used to determine *de novo* predicted gene structures on the repeat masked assembly sequences. RefSeq proteins from *A. pisum* and *P. humanus* were used as training data to obtain suitable parameters in the *L. migratoria* gene prediction.

For transcriptome-based prediction, ESTs and RNA-seq data were incorporated into gene prediction. The *L. migratoria* ESTs were aligned against genome sequences using BLAT (identity ≥ 95%, coverage ≥ 90%) to generate spliced alignments. Spliced EST alignments were identified using PASA to define model gene structures[202]. TopHat[203] was applied to align the RNA-seq reads of multiple libraries to the genome assembly. To obtain transcript structures, Cufflinks[204] was used to combine the junction sites from different libraries.

Finally, homology-based, *de novo* derived and transcript gene sets were merged to form a comprehensive and non-redundant reference gene set using GLEAN[66]. GLEAN genes were filtered if they satisfied any of the following criteria: 1) coverage < 50% of any evidence; 2) genes that were only supported by *de novo* evidence, with the highest expression level RPKM (reads per kilobase per million) < 5 and with RNA-seq read mapping region < 50% at all the libraries; 3) length of deduced protein sequences < 50 aa (amino acid).

Connecting split gene. Gene sets from gene annotation pipelines frequently contains split genes, which are annotated fragments on the same scaffold or across scaffolds that actually belong to the same gene[205,206]. To remove unreasonable gene models from our reference gene set, we performed large-scale manual curation. We first searched for split genes using ESPRIT[206], which was developed based on proteomes of relatively distantly related species as references. Homologous proteins from seven insect species, including *A. pisum*, *P. humanus*, *D. melanogaster*, *T. castaneum*, *B. mori*, *A. mellifera*, and *A. gambiae*, were used as evidence. In order to maximize identification of split genes, we tested several combinations of parameters and finally selected the following: MinSeqLenContig 20, MinProbContig 0.4, MaxContigOverlap 5, MinBestScore 250, DistConfLevel 5, AllowMultipleHits, StablepairTol 1.81. A total of 50 genes were refined using these parameters.

We also developed a pipeline to integrate RNA-seq data as evidence to connect split genes. Our method was inspired by Mortazavi *et al*, who have conducted transcriptome scaffolding using RNAPATH integrated within the ENRAGE package[207]. It combined the RNA-seq and homologous protein data and provided confirmation of the authenticity of the connections. The method is described below.

To obtain evidence of homologous genes, protein sequences from the seven insect species same to ESPRIT were utilized. All insect proteins were searched against the GLEAN gene set using BLASTP with parameters "-e 1e-2 -F F". The fragmental hits were then conjoined linearly by the SOLAR program[208]. Two GLEAN genes were supported by one homologous protein if: 1) two GLEAN genes with > 40% of the region were covered by the same homologous gene, and 2) no obvious conflicts occurred in hit overlap, strands and directions on the scaffold.

RNA-seq reads with unique mapping in the exon region were collected.

Split gene pairs were determined.

Based on evidence from the above two steps, two GLEAN genes were considered split from the same gene if they were hit by at least three RNA-seq read pairs or were located on the same scaffold, and were supported by at least one homologous protein. Gene pairs that were only supported by less than three RNA-seq pairs were omitted to avoid random mapping. A total of 3,953 gene pairs satisfied these criteria. The two GLEAN genes of any given split gene pair were connected in the following steps.

Split gene pairs were clustered. In one cluster, any two genes could be connected through at least one path. Any two genes from two different clusters could not be connected. A new split gene was added to the cluster if it could be connected to any member in the cluster.

Split genes that belonged to the same cluster were connected following these guidelines:

All members of a cluster must be covered by at least one homologous protein. Clusters that did not satisfy this criterion were manually split.

The GLEAN gene pairs with direction or strand conflict for any supported homologous proteins in one cluster have been manually checked.

Based on the direction of homolog alignment, the genome sequences of the genes in one cluster were connected. Gene prediction was performed using GeneWise based on the homolog protein with the highest blast score among the seven insect species. If the cluster contained more than one assembly sequence, the direction and strand were also considered. A total of 50 “N” were placed between two sequences and the coordinates were adjusted.

Based on this procedure, 2,396 GLEAN genes were refined, which covered all the genes that were discovered by the ESPRIT program.

Gene filtering based on the coverage depth of resequencing reads. To lessen the influence of assembly redundancy on gene prediction, we further filtered the GLEAN gene set based on the coverage depth of resequencing reads. The average coverage depths of genic regions were calculated based on the WGS (Whole-Genome Shotgun) reads re-mapping. Based on the depth distribution (Supplementary Figure S4) and average depth of 20x, we set the cut off to 15x as the half average depth. All the CDS sequences were self-to-self aligned using BLAT. If two CDSs had average depth < 15x, the percentage of half depth positions > 50%, the alignment identity > 90% and the overlap ratio > 70% to any sequences, one of them was considered redundant, and the longer one was retained. Finally, 210 genes were filtered.

Manual curation. Finally, we further manually improved 2,192 functionally important genes involved in detoxification, chemoreception, energy metabolism, phase changes and so on. Various information were integrated into the integrative genomics viewer[141], including homologues from the 10 insects and human genomes, genomic BLAT searches of ESTs and RNA-seq data, location of junction sites, GLEAN gene structures, isoforms predicted by cufflinks and prediction of three *de novo* methods. All of these genes were visually inspected to avoid erroneous gene models.

After filtering and manual correction, 17,307 genes were obtained (Supplementary Table S8), among which 6,837 (39.50%) were supported by three evidence, at least 9,170 (52.98%) were supported by homologous genes, 11,562 (66.81%) were supported by RNA-seq/EST, and 16,244 (93.86%) genes had RPKM > 1 in at least one sample.

To evaluate gene quality, we compared the gene parameters to other sequenced insect gene sets (Supplementary Table S8). As a consequence of large intron size, mRNA lengths of *L. migratoria* are longer than that of other insects and slightly longer than that of humans. The average CDS length is a little shorter than those of other insects, while the average exon number per gene is comparable to those of other insects. However, the average exon length is shorter than those of all insects but similar to those of humans.

Protein coding gene function assignment

Protein coding gene functions were assigned based on the best match derived from alignments to proteins annotated in SwissProt, TrEMBL[209] databases using BLASTP with E-value < 1E-5. The KEGG[210] pathway was annotated using KAAS[211] web service version 1.64a, BBH method, by searching against a representative set plus all available insect species with default parameters. We annotated motifs and domains using InterProScan[212] (version 4.7) by searching against the InterPro[213] database. Descriptions of gene products including Gene Ontology[214] were retrieved from InterPro. The statistics of annotated results are listed in Supplementary Table S9.

Repeat annotation

Both homology-based and *de novo* methods were used to perform interspersed repeat identification. We first scanned the draft genome sequence assembly of *L. migratoria* to identify putative repeat regions using the RepeatModeler package, a tool for *de novo* repeat family identification and modeling based on two de-novo repeat finding programs, RepeatScout and RECON. Unclassified repetitive elements from the RepeatModeler predictions were identified using the REPCLASS package, a program that integrates three different independent classification modules: homology, structure and target site duplication[215]. Tandem repeats were searched using the program Tandem Repeat Finder[216] with default settings. We found that most of these repeat elements showing lower similarity to known repeat elements of sequenced insects could not be classified by homology-based approaches in the previous steps. Therefore, additional approaches were conducted based on the *de novo* methods. A machine learning approach was adopted to classify unknown repeat elements in the previous steps into main functional categories using the TEclass program[217]. The total proportion of the genomic region containing interspersed repeat elements was estimated by RepeatMasker searching based on the integrated consensus library.

Since predictions made by different methods lead to redundant repeat annotations, an additional filter step was adopted to remove the redundant regions of repeats. Three priority levels were assigned to all the consensus repeats. Known TEs from homology-based annotation had the highest priority, while tandem repeats and unknown TEs received the lowest priority. If two known TEs overlapped, the latter one was split at the end of the former one, and a fragment of the latter one remained.

However, unknown TEs and tandem repeats were merged into one longer TE or repeat when they overlapped with each other. Considering that this filter step resulted in many short fragments, we removed fragments shorter than 50 bp.

Estimation of divergence time for interspersed repeats

Substitution rates in interspersed repeats can be used to estimate the time of divergence on the assumption that they are subject to decay with the same substitution rates under weak selective constraints. The time of divergence of interspersed repeats was estimated according to the molecular clock equation R = K/2T, where R is the average substitution rate, K is the average number of substitutions per site, and T is the divergence time between species. The number of substitutions per site was calculated under the one-parameter Jukes-Cantor model [-3/4 $\ln$(1-4/3P)], where *P* represents the sequence divergence rate between fragmented repeats and consensus sequences. The average nucleotide substitution rate for interspersed repeats is 1.66×10^{-8} per site per year according to substitution rates for a nuclear pseudogene in insects[218], and this rate is close to the numbers reported for substitutions in the intron region in insects[219].

Deletion rates measurements across insect genomes

Long terminal repeat (LTR) retrotransposons constitute a substantial fraction of eukaryotic genomes, and they are characterized by the presence of flanking LTR sequences. The LTR sequences are the direct sequence repeats that flank the internal protein coding domains which include genes encoding both structural and enzymatic proteins. The structural and enzymatic proteins typically are composed of open reading frames for the *GAG* and *POL* proteins. The *GAG* protein is a retroviral structural protein that is capable of assembling into virus-like particles, and the *POL* protein encodes several enzymatic functions, including a protease, a reverse transcriptase and an integrase. In addition, two structural sites critical to replication, the primer-binding site (PBS) and polypurine tract (PPT), were also includes in the LTR retrotransposon identification. The two LTR sequences of LTR retrotransposons are identical at the time of retrotransposition into the host genome, and thus the degree of divergence between the two LTRs provides an estimate of the time that has elapsed since retrotransposition[220]. Therefore, it is feasible to identify intact LTR retrotransposons based on the sequence similarity (identical or nearly identical) of LTRs sequences and internal structural signatures. Because the insertion and deletion in most of new retrotransposition copies can lead to loss-of-function, LTR retrotransposons are presumably neutral proxies and under relaxed selection pressures. The RepeatMasker program was used in the genome sequence scanning to identify the LTR retrotransposon copies using the intact LTR retrotransposons as query[221]. The repeat copies search was performed using WU-blast as sequence search engine[222]. Scanning was carried out using a cutoff value of 300 bp in length. Gaps and ambiguous sites were removed from the WU-blast alignment in order to ensure accuracy of the deletion rates measurements.

Comparative genomics analysis

Orthologous gene family assignment

Treefam[67] defines a gene family as a group of genes descending from a single gene in the last common ancestor. We constructed a pipeline to cluster individual genes into gene families and performed phylogenetic analyses:

Data preparation. We collected protein-coding sequences more than 30 aa of sequenced related species as well as those of *L. migratoria*. In total, 10 species were selected for orthologous gene assignment: *D. pulex*, *P. humanus*, *A. pisum*, *A. mellifera*, *N. vitripennis*, *T. castaneum*, *B. mori*, *A. gambiae*, *A. aegypti*, and *D. melanogaster*. The longest protein isoform was retained for each gene.

Pair-wise BLAST alignment (graph building). ALL-to-ALL alignment of all proteins were performed using BLASTP with E-value < 1E-5, and the fragmental alignments were conjoined using SOLAR[208]. A connection (edge) between two nodes (genes) was assigned if more than 1/3 of the region was aligned in both genes. H-score ranging from 0 to 100 was used to weigh the similarity of two genes (edge). For two genes G1 and G2, the H-score was defined as score (G1G2) / max (score(G1G1), score(G2G2))(score = BLAST raw score).

Gene family construction. The average distance was used in the hierarchical clustering algorithm, the minimum edge weight (H-score) was set to 10 and the minimum edge density (total number of edges/theoretical number of edges) was set to > 1/3. Having obtained gene families, we could extract special genes of one species or some relative species sharing common phylogenic node.

Phylogeny and orthology analysis. We performed multiple alignments of protein sequences for each gene family using MUSCLE[175] and converted the protein alignments to CDS alignments using an in-house Perl script.

Phylogeny, divergence estimation and gene family evolution

It has been suggested that combining data from multiple genes may potentially alleviate misleading phylogenetic signals in individual genes[223]. We conducted phylogenomic analysis based on the concatenated data set from universal single-copy genes. Gene orthologous relationships were identified with Treefam using all the protein sequences predicted by merging the GLEAN and manually curated gene sets. The predicted amino acid sequences of the 122 universal single-copy orthologues were aligned in MAFFT with its l-INS-i algorithm[142]. The resulting alignments were then manually inspected, and ambiguously aligned regions containing gaps were excluded from further analyses.

Sequences from individual gene regions were concatenated into the final set of 67,387 amino acids. The phylogenomic trees were inferred using maximum likelihood (ML) algorithms. The ML analyses were performed on the PhyML 3.0 program with the JTT substitutional matrix and discrete gamma distribution in four categories + invariant sites[131,224]. Gamma shape parameter and the fraction of invariant sites estimated from the data set were set to 1.065 and 0.148, respectively. Tree topology search by nearest-neighbour interchanges (NNIs) was used, and BioNJ tree was used to designate the starting tree. Bootstrapping was done with 100 re-sampling replicates to assess the node supports.

Estimates of divergence times for insect lineages were done using Bayesian relaxed molecular clock approaches implemented in MCMCTREE from the PAML package[225]. This method allows the use of soft age bounds and flexible probability distributions to accommodate uncertainties in fossil calibrations[226]. We considered *Daphnia* (Crustacea: Branchiopoda) to be outgroup of Insecta. The MCMC was run twice each for 100,000 generations, sampling every 2nd tree with a burn-in phase of 10,000. The simulations were repeated with different starting seed values to check for convergence of the MCMC chain. Fossil calibrations of nodes were set as soft bounds in the MCMCTREE analysis. Since a prior age for the root node (in our case the *Daphnia*–Insecta split) must be specified to effectively constrain the standard deviation of the estimated time, the minimum age of the split between Branchiopoda and Hexapoda took place ~550 MYA as suggested in a previous study[227]. This constraint is closer to the molecular divergence evidence in a recent study[228], and is also consistent with the fossil record that the oldest known fossils of hexapods are Collembolans of Rhyniella praecursor from the Lower Devonian period 400 MYA[229]. We selected the following fossil calibrations: 1) the split between Aculeata (include *Apis*) and Chalcidoidea (include *Nasonia*) dates to the middle Mesozoic period 140~180 MYA[230]; 2) the minimum data for the spilt between Lepidoptera and Diptera is around 290 MYA[230].

The rate and direction of gene family size in *L. migratoria* and its related species was inferred using CAFE[68], which is based on a stochastic birth-death model. In order to analyze gain and loss of genes with consideration for the phylogenomic tree, we built a pipeline as follows: Based on the phylogenomic tree and the gene family information gathered from the above steps, we estimated the average rate of gene turnover λ, which is the probability of both gene gain and loss per gene per unit time in the phylogeny. The significance of changes in gene family size was inferred in each branch.

Intron evolution

Intron analysis in orthologous genes. Genome sequences, gene models and coordinates were downloaded from public databases as described above. The intron length and intron number were extracted from the GFF files using customized Perl scripts to perform multiple gene comparison. The frequency distributions were built for each species and plotted using customized R scripts. To alleviate bias from multiple gene comparison, intron information of the 1:1 orthologous genes was also further retrieved based on the gene family.

Identification of U12 introns. We used the program Tophat to perform spliced alignments of the reads against the *L. migratoria* genome[203]. Tophat identifies splice junctions by mapping paired-end RNA-seq data to the genomic sequences in two steps. In the first step, all reads are aligned to the genomic sequences, and reads that do not match any location are set aside as 'initially unmapped reads'. In the following step, the program identifies putative exons and assesses whether previously unmatched reads span any of these islands. Tophat calls a splice junction if at least one read is found that spans two expressed islands (hereafter called 'spliced reads'). By default, Tophat finds any reads that span splice junctions by at least five bases on each side. Tophat also considers paired-end read information when available to support detected splice junctions. We considered a splice junction expressed in a given subspecies if it was covered by ≥5 spliced reads. The U12 introns have consensus sequences at the 5' splice site (RTATCCTTT) as well as branch site (TCCTTAACT), which are more conserved than their counterparts in U2 introns[80]. However, the 3' splice site is more variable. We considered the intron containing these two properties as the U12-type intron. The splice junctions that meet the criterion of U12 intron identification were retained for further comparison across species.

Transcriptome Analysis

Samples for RNA sequencing

Brain transcriptome during phase transition processes To reveal the molecular mechanisms underlying locust phase change, we previously used two colors cDNA array[10,11] determine the differential gene expression profiles from locust head tissues between both phases and used RNA-seq[70] determine the differential gene expression profiles from locust whole body between both phases. These studies had highlighted that the critical roles of the peripheral and central nervous systems in locust phase change. So, to further elucidate signaling pathways involved in phase change in central nervous systems, we here carried out the transcriptome sequence for brain tissues in the early process of phase change.

Gregarious and solitarious locusts were reared as previously described[10]. For isolation of gregarious *L. migratoria* (IG), the 3-day-old fourth-instar gregarious nymphs were separately reared in solitarious-rearing cages. After 0, 4, 8, 16, 32 hours, their brain tissues were dissected and immediately put into liquid nitrogen. Each treatment condition contained 20 individuals. For crowding of solitarious *L. migratoria* (CS), two solitarious fourth-instar nymphs were introduced into the gregarious-rearing cages, in which there were 20 3-day-old gregarious nymphs. After placing together with the stimulus group for 0, 4, 8, 16, 32 h, solitarous *L. migratoria* were removed from the cages for dissection of brain tissue. Each treatment condition contained 20 individuals. All samples were immediately put into liquid nitrogen and stored at -80^{o}C until further analysis. All insects were dissected at 3:00 PM.

Transcriptome of ten tissues Tissues of brain, antenna, fat body, midgut, testis, ovary, thorax flight muscle, hind leg, hemolymph, gangalia, labipalp and wing were collected from gregarious adults *L. migratoria*.

Transcriptome of mixed samples These samples were from various developmental stages, including eggs.

Transcriptome of flight Adult male locusts aging at least 8 days after the final molt were used and a computer-aided flight mill system similar to Schumacher *et al*[231] was constructed. The treated locust was fixed to the arm of the flight mill by a thin copper wire surrounding the metathorax and the wings were free to fly. For the control locust, the wings were simultaneously fastened to prevent flying. Ambient temperature was maintained at 30±2 °C. To initiate flight, a 2-second wind stimulus from an automated wind supplier above the mill was exerted when the locusts stopped flying for a period of 20 seconds. When the treated locust flied for a total of 2 hours, fat bodies were dissected from the treated and control locusts, and these tissues were each used for subsequent RNA extraction.

Alternative splicing analysis

Short paired-end reads from transcriptome sequencing datasets were aligned to genome sequence using TopHat package to identify splicing junction sites. TopHat first aligns the raw reads onto the reference and reports the “initially unmapped reads” (IUM reads) not mapped to the genome.Then, through a seed-and-extend strategy,TopHat finds reads spanning junctions from IUM reads. Based on the junction result identified by TopHat[203] and predicted gene structures, we identified alternative splicing events by comparing the position of the observed junction sites to the annotated gene models and categories them into seven categories: exonskipping (ES), intron-retention (IR), mutually exclusive exon (MXE), alternative 5’ splice site (A5SS),alternative 3’ splice site (A3SS), alternative first exon (AFE), and alternative last exon (ALE).

The current methods to detect differential splicing always require experimental replicates and well annotated reference[232,233], which is not satisfied for non model species. To simplify the question and got credible differential alternative splicing events, we used two criteria: one was the *p* value calculated based on fisher’s exact test or chi-square test, another was the ratio difference of the “percentage spliced in” (PSI)[234] between two samples.

The junction data of every sample was produced from tophat (Supplementary Figure S21). For each junction, the number of reads that support this junction *n* and the number of reads that across this junction *N*. *N* was calculated as the maximum read number across the junction region. To eliminate the bias between samples, the supporting numbers of original reads were normalized using DESeq's method[235]. The PSI was defined as *n*/*N*. For two samples, the fisher's exact test or chi-square test was performed based on the four numbers. The fisher's exact test was selected when there is any theory number smaller than 5. *P* values of multiple test were adjusted using Benjamini's FDR[65,236]. The differential junctions were detected as adjusted *p* value < 0.1 and the PSI difference > 20%. BEDTools[237] was used to extract the junctions that overlapped with annotated genes. Finally, 45 differentially spliced genes (DSG) were found between gregarious and solitarious brain samples (Supplementary Table S23).

Enrichment analysis

Enrichment analysis for the supplied gene list was carried out based on an algorithm presented by GOstat[238], with the whole annotated gene set as the background. The *p*-value was approximated using the Chi-square test. Fisher's exact test was used when any expected value of count was below 5. This program was implemented as a pipeline[70]. For the GO and IPR enrichment analyses, in order to obtain succinct results, if one item was ancestor of another and the enriched gene list of these two items were the same, the ancestor item was deleted from the results. To adjust for multiple testing, we calculated the False Discovery Rate using the Benjamini-Hochberg method[236] for each class.

Reduced Representation Bisulfite Sequencing data analysis

Bioinformatic processing of the data

Short reads generated by Illumina sequencing were first processed by Trimmomatic-0.22[239] with parameters "SLIDINGWINDOW:4:15 MINLEN:40" for filtering low quality, adaptor contaminated reads. After filtering, the remain reads were aligned to *L. migratoria* genome sequence using Bismark v0.7.12[240] with default parameters. Bismark aligned the converted reads to the converted reference genome using bowtie[241] (version 2 was used in our analysis), and the unique best alignment was used to determine the methylation states of cytosine position by comparing the reads with their corresponding genomic sequences. The unique mapped reads were 39~50% for the four RRBS and one whole genome libraries (Supplementary Table S16). After mapping the reads to the reference genome, BAM files were generated. Based on these BAM files, insert size distribution were plotted using picard (http://picard.sourceforge.net/). The insert size was ideally centered at 60 bp for short libraries and 130 bp for large libraries, which were consistent with expect (Supplementary Figure S15).

The methylation state of cytosine of every reads was extracted using bismark_methylation_extractor. The extractor outputted the overall methylation level of three kinds cytosine for all reads, which was defined as the ratio of the number of methylated C sites to the total number of C sites on the reads (Supplementary Table S17). Based on the methylation state of cytosine of every reads, the CG methylation level for the regions of gene body, exon, intron, intergenic sequence, promoter were calculated (Supplementary Figure S17). In total, 7,568,981 and 7,996,483 CpG sites were covered by more than 10X for G and S samples respectively. The methylation levels across all CpGs was also plotted (Supplementary Figure S16) and followed bimodal distribution. Among these CpG sites, 954,031 (12.6%) and 959,172 (12.0%) were found in the gene body. In total, 11,447 and 11,337 genes were covered at least 4 CpG sites (Supplementary Table S18).

Differentially methylated genes

To identify differentially methylated (DM) gene (DMG), we first identified DM CG sites using methylKit version 0.5.7[242]. 4,345,168 CpG sites were covered at minimum 10X in both samples. The *P*-value of Fisher's exact test of CG site was calculated using the number of sequenced methylated and non-methylated cytosines in gregarious and solitarious brain samples. The *P*-value was adjusted by FDR[236]. The DM CG site was defined as FDR < 0.01 and the difference of methylation level between two samples > 0.25. Because the reads of RRBS were singled-end in 50 bp length, the covered regions were not continuous as those whole genome bisulfite sequencing. So we defined the DMG as those with at least 4 DM CG sites (Supplementary Table S19). 89 DMGs were identified between two phases in the genome.

Supplementary References

71. Hemming, C.F. *The Locust Menace*, (Centre for Overseas Pest Research, 1974).
72. Ye, J. *et al.* WEGO: a web tool for plotting GO annotations. *Nucleic Acids Res* **34**, W293-7 (2006).
73. Mackenzie, P.I. *et al.* The UDP glycosyltransferase gene superfamily: recommended nomenclature update based on evolutionary divergence. *Pharmacogenetics* **7**, 255-69 (1997).
74. Johnson, G. & Moore, S.W. The carboxylesterase/cholinesterase gene family in invertebrate deuterostomes. *Comp Biochem Physiol Part D Genomics Proteomics* **7**, 83-93 (2012).
75. Oakeshott, J.G. *et al.* Metabolic enzymes associated with xenobiotic and chemosensory responses in Nasonia vitripennis. *Insect Mol Biol* **19 Suppl 1**, 147-63 (2010).
76. Bactrian Camels Genome, S. *et al.* Genome sequences of wild and domestic bactrian camels. *Nat Commun* **3**, 1202 (2012).
77. McLysaght, A., Enright, A.J., Skrabanek, L. & Wolfe, K.H. Estimation of synteny conservation and genome compaction between pufferfish (Fugu) and human. *Yeast* **17**, 22-36 (2000).
78. Vinogradov, A.E. Intron-genome size relationship on a large evolutionary scale. *J Mol Evol* **49**, 376-84 (1999).
79. Tarn, W.Y. & Steitz, J.A. A novel spliceosome containing U11, U12, and U5 snRNPs excises a minor class (AT-AC) intron in vitro. *Cell* **84**, 801-11 (1996).
80. Burge, C.B., Padgett, R.A. & Sharp, P.A. Evolutionary fates and origins of U12-type introns. *Mol Cell* **2**, 773-85 (1998).
81. Frilander, M.J. & Steitz, J.A. Initial recognition of U12-dependent introns requires both U11/5′ splice-site and U12/branchpoint interactions. *Genes Dev* **13**, 851-863 (1999).
82. Russell, A.G., Charette, J.M., Spencer, D.F. & Gray, M.W. An early evolutionary origin for the minor spliceosome. *Nature* **443**, 863-6 (2006).
83. Lin, C.F., Mount, S.M., Jarmolowski, A. & Makalowski, W. Evolutionary dynamics of U12-type spliceosomal introns. *BMC Evol Biol* **10**, 47 (2010).
84. Bartschat, S. & Samuelsson, T. U12 type introns were lost at multiple occasions during evolution. *BMC Genomics* **11**, 106 (2010).
85. Burnette, J.M., Miyamoto-Sato, E., Schaub, M.A., Conklin, J. & Lopez, A.J. Subdivision of large introns in Drosophila by recursive splicing at nonexonic elements. *Genetics* **170**, 661 (2005).
86. Hatton, A.R., Subramaniam, V. & Lopez, A.J. Generation of alternative Ultrabithorax isoforms and stepwise removal of a large intron by resplicing at exon-exon junctions. *Mol Cell* **2**, 787-796 (1998).
87. Law, J.A. & Jacobsen, S.E. Establishing, maintaining and modifying DNA methylation patterns in plants and animals. *Nat Rev Genet* **11**, 204-20 (2010).

88. Lyko, F. & Maleszka, R. Insects as innovative models for functional studies of DNA methylation. *Trends Genet* **27**, 127-31 (2011).
89. Peckham, M., Cripps, R., White, D. & Bullard, B. Mechanics and Protein-Content of Insect Flight Muscles. *J Exp Biol* **168**, 57-76 (1992).
90. Syme, D.A. & Josephson, R.K. How to build fast muscles: synchronous and asynchronous designs. *Integr Comp Biol* **42**, 762-70 (2002).
91. Rome, L.C. & Lindstedt, S.L. The Quest for Speed: Muscles Built for High-Frequency Contractions. *Physiology* **13**, 261-268 (1998).
92. Mizisin, A.P. & Josephson, R.K. Mechanical power output of locust flight muscle. *J Comp Physiol A Neuroethol Sens Neural Behav Physiol* **160**, 413-419 (1987).
93. Dirks, J.-H. & Taylor, D. Veins Improve Fracture Toughness of Insect Wings. *PLoS ONE* **7**, e43411 (2012).
94. Wootton, R.J. Functional Morphology of Insect Wings. *Annu Rev Entomol* **37**, 113-140 (1992).
95. De Celis, J.F. & Diaz-Benjumea, F.J. Developmental basis for vein pattern variations in insect wings. *Int J Dev Biol* **47**, 653-63 (2003).
96. Marcus, J.M. The development and evolution of crossveins in insect wings. *J Anat* **199**, 211-6 (2001).
97. Tobe, S.S. & Pratt, G.E. The influence of substrate concentrations on the rate of insect juvenile hormone biosynthesis by corpora allata of the desert locust in vitro. *Biochem J* **144**, 107-13 (1974).
98. Min, K.J., Jones, N., Borst, D.W. & Rankin, M.A. Increased juvenile hormone levels after long-duration flight in the grasshopper, Melanoplus sanguinipes. *J Insect Physiol* **50**, 531-7 (2004).
99. de Oliveira Tozetto, S., Rachinsky, A. & Engels, W. Juvenile hormone promotes flight activity in drones (Apis mellifera carnica). *Apidologie* **28**, 77-84 (1997).
100. Mayoral, J.G., Nouzova, M., Navare, A. & Noriega, F.G. NADP+-dependent farnesol dehydrogenase, a corpora allata enzyme involved in juvenile hormone synthesis. *Proc Natl Acad Sci U S A* **106**, 21091-6 (2009).
101. Liu, S. *et al.* Molecular cloning and characterization of a juvenile hormone esterase gene from brown planthopper, Nilaparvata lugens. *J Insect Physiol* **54**, 1495-502 (2008).
102. Nilsen, K.A. *et al.* Insulin-like peptide genes in honey bee fat body respond differently to manipulation of social behavioral physiology. *J Exp Biol* **214**, 1488-97 (2011).
103. Barbieri, M., Bonafe, M., Franceschi, C. & Paolisso, G. Insulin/IGF-I-signaling pathway: an evolutionarily conserved mechanism of longevity from yeast to humans. *Am J Physiol Endocrinol Metab* **285**, E1064-71 (2003).
104. Sajid, W. *et al.* Structural and Biological Properties of the Drosophila Insulin-like Peptide 5 Show Evolutionary Conservation. *J Biol Chem* **286**, 661-673 (2011).
105. Gronke, S., Clarke, D.F., Broughton, S., Andrews, T.D. & Partridge, L.

Molecular evolution and functional characterization of Drosophila insulin-like peptides. *PLoS Genet* **6**, e1000857 (2010).

106. Zhan, S., Merlin, C., Boore, Jeffrey L. & Reppert, Steven M. The Monarch Butterfly Genome Yields Insights into Long-Distance Migration. *Cell* **147**, 1171-1185 (2011).
107. Brogiolo, W. *et al.* An evolutionarily conserved function of the Drosophila insulin receptor and insulin-like peptides in growth control. *Curr Biol* **11**, 213-21 (2001).
108. Pierce, S.B. *et al.* Regulation of DAF-2 receptor signaling by human insulin and ins-1, a member of the unusually large and diverse C. elegans insulin gene family. *Genes Dev* **15**, 672-86 (2001).
109. Van der Horst, D.J. & Rodenburg, K.W. Locust flight activity as a model for hormonal regulation of lipid mobilization and transport. *J Insect Physiol* **56**, 844-53 (2010).
110. Bickel, P.E., Tansey, J.T. & Welte, M.A. PAT proteins, an ancient family of lipid droplet proteins that regulate cellular lipid stores. *Biochim Biophys Acta* **1791**, 419-40 (2009).
111. Kimmel, A.R., Brasaemle, D.L., McAndrews-Hill, M., Sztalryd, C. & Londos, C. Adoption of PERILIPIN as a unifying nomenclature for the mammalian PAT-family of intracellular lipid storage droplet proteins. *J Lipid Res* **51**, 468-71 (2010).
112. Beller, M. *et al.* PERILIPIN-dependent control of lipid droplet structure and fat storage in Drosophila. *Cell Metab* **12**, 521-32 (2010).
113. Miura, S. *et al.* Functional conservation for lipid storage droplet association among Perilipin, ADRP, and TIP47 (PAT)-related proteins in mammals, Drosophila, and Dictyostelium. *J Biol Chem* **277**, 32253-7 (2002).
114. Marchler-Bauer, A. *et al.* CDD: a Conserved Domain Database for the functional annotation of proteins. *Nucleic Acids Res* **39**, D225-9 (2011).
115. Teixeira, L., Rabouille, C., Rorth, P., Ephrussi, A. & Vanzo, N.F. Drosophila Perilipin/ADRP homologue Lsd2 regulates lipid metabolism. *Mech Dev* **120**, 1071-81 (2003).
116. Chmurzynska, A. The multigene family of fatty acid-binding proteins (FABPs): function, structure and polymorphism. *J Appl Genet* **47**, 39-48 (2006).
117. Barbieri, E. & Sestili, P. Reactive oxygen species in skeletal muscle signaling. *J Signal Transduct* **2012**, 982794 (2012).
118. Yan, L.J. & Sohal, R.S. Prevention of flight activity prolongs the life span of the housefly, Musca domestica, and attenuates the age-associated oxidative damamge to specific mitochondrial proteins. *Free Radic Biol Med* **29**, 1143-50 (2000).
119. Felton, G.W. & Summers, C.B. Antioxidant systems in insects. *Arch Insect Biochem Physiol* **29**, 187-97 (1995).
120. Corona, M. & Robinson, G.E. Genes of the antioxidant system of the honey bee: annotation and phylogeny. *Insect Mol Biol* **15**, 687-701 (2006).
121. Koua, D. *et al.* PeroxiBase: a database with new tools for peroxidase family

classification. *Nucleic Acids Res* **37**, D261-6 (2009).

122. Manevich, Y. *et al.* 1-Cys peroxiredoxin overexpression protects cells against phospholipid peroxidation-mediated membrane damage. *Proc Natl Acad Sci U S A* **99**, 11599-604 (2002).
123. Manevich, Y. & Fisher, A.B. Peroxiredoxin 6, a 1-Cys peroxiredoxin, functions in antioxidant defense and lung phospholipid metabolism. *Free Radic Biol Med* **38**, 1422-32 (2005).
124. Chen, J.W., Dodia, C., Feinstein, S.I., Jain, M.K. & Fisher, A.B. 1-Cys peroxiredoxin, a bifunctional enzyme with glutathione peroxidase and phospholipase A2 activities. *J Biol Chem* **275**, 28421-7 (2000).
125. Gardiner, A., Barker, D., Butlin, R.K., Jordan, W.C. & Ritchie, M.G. Drosophila chemoreceptor gene evolution: selection, specialization and genome size. *Mol Ecol* **17**, 1648-57 (2008).
126. Croset, V. *et al.* Ancient protostome origin of chemosensory ionotropic glutamate receptors and the evolution of insect taste and olfaction. *PLoS Genet* **6**, e1001064 (2010).
127. Birney, E., Clamp, M. & Durbin, R. GeneWise and Genomewise. *Genome Res* **14**, 988-95 (2004).
128. Altschul, S.F. *et al.* Gapped BLAST and PSI-BLAST: a new generation of protein database search programs. *Nucleic Acids Res* **25**, 3389-402 (1997).
129. Keller, O., Kollmar, M., Stanke, M. & Waack, S. A novel hybrid gene prediction method employing protein multiple sequence alignments. *Bioinformatics* **27**, 757-63 (2011).
130. Smadja, C., Shi, P., Butlin, R.K. & Robertson, H.M. Large gene family expansions and adaptive evolution for odorant and gustatory receptors in the pea aphid, Acyrthosiphon pisum. *Mol Biol Evol* **26**, 2073-86 (2009).
131. Guindon, S. *et al.* New algorithms and methods to estimate maximum-likelihood phylogenies: assessing the performance of PhyML 3.0. *Syst Biol* **59**, 307-21 (2010).
132. Wanner, K.W. & Robertson, H.M. The gustatory receptor family in the silkworm moth Bombyx mori is characterized by a large expansion of a single lineage of putative bitter receptors. *Insect Mol Biol* **17**, 621-629 (2008).
133. Jin, X. *et al.* Expression and immunolocalisation of odorant-binding and chemosensory proteins in locusts. *Cell Mol Life Sci* **62**, 1156-66 (2005).
134. Vieira, F.G. & Rozas, J. Comparative genomics of the odorant-binding and chemosensory protein gene families across the Arthropoda: origin and evolutionary history of the chemosensory system. *Genome Biol Evol* **3**, 476-90 (2011).
135. McGuffin, L.J., Bryson, K. & Jones, D.T. The PSIPRED protein structure prediction server. *Bioinformatics* **16**, 404-5 (2000).
136. Mackenzie, P.I. *et al.* Nomenclature update for the mammalian UDP glycosyltransferase (UGT) gene superfamily. *Pharmacogenet Genomics* **15**, 677-85 (2005).
137. Ahn, S.J. *et al.* Metabolic detoxification of capsaicin by

UDP-glycosyltransferase in three Helicoverpa species. *Arch Insect Biochem Physiol* **78**, 104-18 (2011).

138. Ahn, S.J., Vogel, H. & Heckel, D.G. Comparative analysis of the UDP-glycosyltransferase multigene family in insects. *Insect Biochem Mol Biol* **42**, 133-47 (2012).
139. Hughes, J. & Hughes, M.A. Multiple secondary plant product UDP-glucose glucosyltransferase genes expressed in cassava (Manihot esculenta Crantz) cotyledons. *Mitochondrial DNA* **5**, 41-49 (1994).
140. Friedman, R. Genomic organization of the glutathione S-transferase family in insects. *Mol Phylogenet Evol* **61**, 924-32 (2011).
141. Robinson, J.T. *et al.* Integrative genomics viewer. *Nat Biotechnol* **29**, 24-6 (2011).
142. Katoh, K., Asimenos, G. & Toh, H. Multiple alignment of DNA sequences with MAFFT. *Methods Mol Biol* **537**, 39-64 (2009).
143. Darriba, D., Taboada, G.L., Doallo, R. & Posada, D. ProtTest 3: fast selection of best-fit models of protein evolution. *Bioinformatics* **27**, 1164-5 (2011).
144. Stamatakis, A. RAxML-VI-HPC: maximum likelihood-based phylogenetic analyses with thousands of taxa and mixed models. *Bioinformatics* **22**, 2688-90 (2006).
145. Singh, S.P., Coronella, J.A., Beneš, H., Cochrane, B.J. & Zimniak, P. Catalytic function of Drosophila melanogaster glutathione S‐transferase DmGSTS1‐1 (GST‐2) in conjugation of lipid peroxidation end products. *Eur J Biochem* **268**, 2912-2923 (2001).
146. Ishida, Y. & Leal, W.S. Rapid inactivation of a moth pheromone. *Proc Natl Acad Sci U S A* **102**, 14075-9 (2005).
147. Robin, C., Bardsley, L.M., Coppin, C. & Oakeshott, J.G. Birth and death of genes and functions in the beta-esterase cluster of Drosophila. *J Mol Evol* **69**, 10-21 (2009).
148. Charpentier, A., Menozzi, P., Marcel, V., Villatte, F. & Fournier, D. A method to estimate acetylcholinesterase-active sites and turnover in insects. *Anal Biochem* **285**, 76-81 (2000).
149. Sturm, A., Cunningham, P. & Dean, M. The ABC transporter gene family of Daphnia pulex. *BMC Genomics* **10**, 170 (2009).
150. Zdobnov, E.M. & Apweiler, R. InterProScan–an integration platform for the signature-recognition methods in InterPro. *Bioinformatics* **17**, 847-848 (2001).
151. Marchler-Bauer, A. & Bryant, S.H. CD-Search: protein domain annotations on the fly. *Nucleic Acids Res* **32**, W327-31 (2004).
152. Labbe, R., Caveney, S. & Donly, C. Genetic analysis of the xenobiotic resistance-associated ABC gene subfamilies of the Lepidoptera. *Insect Mol Biol* **20**, 243-56 (2011).
153. Feyereisen, R. Evolution of insect P450. *Biochem Soc Trans* **34**, 1252-5 (2006).
154. Millar, N.S. & Denholm, I. Nicotinic acetylcholine receptors: targets for commercially important insecticides. *Invert Neurosci* **7**, 53-66 (2007).
155. Janssen, D., Derst, C., Rigo, J.M. & Van Kerkhove, E. Cys-loop ligand-gated

chloride channels in dorsal unpaired median neurons of Locusta migratoria. *J Neurophysiol* **103**, 2587-98 (2010).

156. Jones, A.K., Bera, A.N., Lees, K. & Sattelle, D.B. The cys-loop ligand-gated ion channel gene superfamily of the parasitoid wasp, Nasonia vitripennis. *Heredity (Edinb)* **104**, 247-59 (2010).
157. Dermauw, W. *et al.* The cys-loop ligand-gated ion channel gene family of *Tetranychus urticae*: implications for acaricide toxicology and a novel mutation associated with abamectin resistance. *Insect Biochem Mol Biol* **42**, 455-65 (2012).
158. Dale, R.P. *et al.* Identification of ion channel genes in the Acyrthosiphon pisum genome. *Insect Mol Biol* **19 Suppl 2**, 141-53 (2010).
159. Jones, A.K. & Sattelle, D.B. The cys-loop ligand-gated ion channel gene superfamily of the red flour beetle, Tribolium castaneum. *BMC Genomics* **8**, 327 (2007).
160. Bai, H. & Palli, S.R. G Protein-Coupled Receptors as Target Sites for Insecticide Discovery. in *Advanced Technologies for Managing Insect Pests* (eds. Ishaaya, I., Palli, S.R. & Horowitz, A.R.) 57-82 (2012).
161. Brody, T. & Cravchik, A. Drosophila melanogasterG Protein–Coupled Receptors. *J Cell Biol* **150**, F83-F88 (2000).
162. Stanke, M. & Morgenstern, B. AUGUSTUS: a web server for gene prediction in eukaryotes that allows user-defined constraints. *Nucleic Acids Res* **33**, W465-W467 (2005).
163. Price, D.R. & Gatehouse, J.A. RNAi-mediated crop protection against insects. *Trends Biotechnol* **26**, 393-400 (2008).
164. Casida, J.E. & Quistad, G.B. Golden age of insecticide research: past, present, or future? *Annu Rev Entomol* **43**, 1-16 (1998).
165. Zlotkin, E. The insect voltage-gated sodium channel as target of insecticides. *Annu Rev Entomol* **44**, 429-455 (1999).
166. Xue, X.-Y., Mao, Y.-B., Tao, X.-Y., Huang, Y.-P. & Chen, X.-Y. Chapter 3 - New Approaches to Agricultural Insect Pest Control Based on RNA Interference. in *Advances in Insect Physiology*, Vol. Volume 42 (ed. Elizabeth, L.J.) 73-117 (Academic Press, 2012).
167. Okamura, K., Robine, N., Liu, Y., Liu, Q. & Lai, E.C. R2D2 organizes small regulatory RNA pathways in Drosophila. *Mol Cell Biol* **31**, 884-96 (2011).
168. Jaubert-Possamai, S. *et al.* Expansion of the miRNA pathway in the hemipteran insect Acyrthosiphon pisum. *Mol Biol Evol* **27**, 979-87 (2010).
169. Lund, E., Guttinger, S., Calado, A., Dahlberg, J.E. & Kutay, U. Nuclear export of microRNA precursors. *Science* **303**, 95-8 (2004).
170. Tomoyasu, Y. *et al.* Exploring systemic RNA interference in insects: a genome-wide survey for RNAi genes in Tribolium. *Genome Biol* **9**, R10 (2008).
171. Okamura, K. & Lai, E.C. Endogenous small interfering RNAs in animals. *Nat Rev Mol Cell Biol* **9**, 673-8 (2008).
172. Hoffmann, J.A. The immune response of Drosophila. *Nature* **426**, 33-8 (2003).
173. Bartholomay, L.C. *et al.* Pathogenomics of Culex quinquefasciatus and

meta-analysis of infection responses to diverse pathogens. *Science* **330**, 88-90 (2010).

174. Waterhouse, R.M. *et al.* Evolutionary dynamics of immune-related genes and pathways in disease-vector mosquitoes. *Science* **316**, 1738-43 (2007).
175. Edgar, R.C. MUSCLE: multiple sequence alignment with high accuracy and high throughput. *Nucleic Acids Res* **32**, 1792-7 (2004).
176. Eddy, S.R. Profile hidden Markov models. *Bioinformatics* **14**, 755-63 (1998).
177. Cerenius, L., Lee, B.L. & Soderhall, K. The proPO-system: pros and cons for its role in invertebrate immunity. *Trends Immunol* **29**, 263-71 (2008).
178. Mullen, L.M. & Goldsworthy, G.J. Immune responses of locusts to challenge with the pathogenic fungus Metarhizium or high doses of laminarin. *J Insect Physiol* **52**, 389-98 (2006).
179. Wells, K.L. The effects of immune challenge on phenoloxidase activity in locust salivary glands in vitro. *Bioscience Horizons* **1**, 122-127 (2008).
180. Neville, A.C. *Biology of the arthropod cuticle*, (Springer-verlag New York:, 1975).
181. Willis, J.H. & Muthukrishnan, S. Insect Cuticle. Foreword. *Insect Biochem Mol Biol* **40**, 165 (2010).
182. Kramer Karl, J., Hopkins Theodore, L. & Schaefer, J. Insect Cuticle Structure and Metabolism. in *Biotechnology for Crop Protection*, Vol. 379 160-185 (American Chemical Society, 1988).
183. Andersen, S.O., Hojrup, P. & Roepstorff, P. Insect cuticular proteins. *Insect Biochem Mol Biol* **25**, 153-76 (1995).
184. Cornman, R.S. *et al.* Annotation and analysis of a large cuticular protein family with the R&R Consensus in Anopheles gambiae. *BMC Genomics* **9**, 22 (2008).
185. Andersen, S.O. Studies on proteins in post-ecdysial nymphal cuticle of locust, Locusta migratoria, and cockroach, Blaberus craniifer. *Insect Biochem Mol Biol* **30**, 569-77 (2000).
186. Karouzou, M.V. *et al.* Drosophila cuticular proteins with the R&R Consensus: annotation and classification with a new tool for discriminating RR-1 and RR-2 sequences. *Insect Biochem Mol Biol* **37**, 754-60 (2007).
187. Merzendorfer, H. & Zimoch, L. Chitin metabolism in insects: structure, function and regulation of chitin synthases and chitinases. *J Exp Biol* **206**, 4393-412 (2003).
188. Li, J. & Christensen, B. Biological Function of Insect Yellow Gene Family. in *Recent Advances in Entomological Research* (eds. Liu, T. & Kang, L.) 121-131 (Springer Berlin Heidelberg, 2012).
189. Ferguson, L.C., Green, J., Surridge, A. & Jiggins, C.D. Evolution of the insect yellow gene family. *Mol Biol Evol* **28**, 257-72 (2011).
190. Li, Z. *et al.* Comparison of the two major classes of assembly algorithms: overlap-layout-consensus and de-bruijn-graph. *Brief Funct Genomics* **11**, 25-37 (2012).
191. Wilmore, P.J. & Brown, A.K. Molecular properties of orthopteran DNA. *Chromosoma* **51**, 337-45 (1975).

192. Rees, H., Shaw, D.D. & Wilkinson, P. Nuclear DNA Variation among Acridid Grasshoppers. *Proc R Soc Lond B Biol Sci* **202**, 517-525 (1978).

193. Baker, M. De novo genome assembly: what every biologist should know. *Nat Methods* **9**, 333-7 (2012).

194. Harris, R.S. Ph.D, The Pennsylvania State University (2007).

195. Kent, W.J., Baertsch, R., Hinrichs, A., Miller, W. & Haussler, D. Evolution's cauldron: duplication, deletion, and rearrangement in the mouse and human genomes. *Proc Natl Acad Sci U S A* **100**, 11484-9 (2003).

196. Treangen, T.J. & Salzberg, S.L. Repetitive DNA and next-generation sequencing: computational challenges and solutions. *Nat Rev Genet* **13**, 36-46 (2012).

197. Mak, H.C. Genome interpretation and assembly-recent progress and next steps. *Nat Biotechnol* **30**, 1081-3 (2012).

198. Li, H. & Durbin, R. Fast and accurate short read alignment with Burrows-Wheeler transform. *Bioinformatics* **25**, 1754-60 (2009).

199. Ma, Z., Yu, J. & Kang, L. LocustDB: a relational database for the transcriptome and biology of the migratory locust (Locusta migratoria). *BMC Genomics* **7**, 11 (2006).

200. Kent, W.J. BLAT--the BLAST-like alignment tool. *Genome Res* **12**, 656-64 (2002).

201. Parra, G., Bradnam, K. & Korf, I. CEGMA: a pipeline to accurately annotate core genes in eukaryotic genomes. *Bioinformatics* **23**, 1061-7 (2007).

202. Tuskan, G.A. *et al.* The genome of black cottonwood, Populus trichocarpa (Torr. & Gray). *Science* **313**, 1596-604 (2006).

203. Trapnell, C., Pachter, L. & Salzberg, S.L. TopHat: discovering splice junctions with RNA-Seq. *Bioinformatics* **25**, 1105-11 (2009).

204. Trapnell, C. *et al.* Transcript assembly and quantification by RNA-Seq reveals unannotated transcripts and isoform switching during cell differentiation. *Nat Biotechnol* **28**, 511-5 (2010).

205. Hubbard, T.J. *et al.* Ensembl 2009. *Nucleic Acids Res* **37**, D690-7 (2009).

206. Dessimoz, C. *et al.* Comparative genomics approach to detecting split-coding regions in a low-coverage genome: lessons from the chimaera Callorhinchus milii (Holocephali, Chondrichthyes). *Brief Bioinform* **12**, 474-84 (2011).

207. Mortazavi, A. *et al.* Scaffolding a Caenorhabditis nematode genome with RNA-seq. *Genome Res* **20**, 1740-7 (2010).

208. Yu, X.J., Zheng, H.K., Wang, J., Wang, W. & Su, B. Detecting lineage-specific adaptive evolution of brain-expressed genes in human using rhesus macaque as outgroup. *Genomics* **88**, 745-51 (2006).

209. UniProt, C. The Universal Protein Resource (UniProt) in 2010. *Nucleic Acids Res* **38**, D142-8 (2010).

210. Kanehisa, M. *et al.* KEGG for linking genomes to life and the environment. *Nucleic Acids Res* **36**, D480-4 (2008).

211. Moriya, Y., Itoh, M., Okuda, S., Yoshizawa, A.C. & Kanehisa, M. KAAS: an automatic genome annotation and pathway reconstruction server. *Nucleic Acids*

Res **35**, W182-5 (2007).

212. Quevillon, E. *et al.* InterProScan: protein domains identifier. *Nucleic Acids Res* **33**, W116-20 (2005).
213. Hunter, S. *et al.* InterPro: the integrative protein signature database. *Nucleic Acids Res* **37**, D211-5 (2009).
214. Ashburner, M. *et al.* Gene ontology: tool for the unification of biology. The Gene Ontology Consortium. *Nat Genet* **25**, 25-9 (2000).
215. Feschotte, C., Keswani, U., Ranganathan, N., Guibotsy, M.L. & Levine, D. Exploring repetitive DNA landscapes using REPCLASS, a tool that automates the classification of transposable elements in eukaryotic genomes. *Genome Biol Evol* **1**, 205-20 (2009).
216. Benson, G. Tandem repeats finder: a program to analyze DNA sequences. *Nucleic Acids Res* **27**, 573-80 (1999).
217. Abrusan, G., Grundmann, N., DeMester, L. & Makalowski, W. TEclass--a tool for automated classification of unknown eukaryotic transposable elements. *Bioinformatics* **25**, 1329-30 (2009).
218. Pons, J. & Vogler, A.P. Complex pattern of coalescence and fast evolution of a mitochondrial rRNA pseudogene in a recent radiation of tiger beetles. *Mol Biol Evol* **22**, 991-1000 (2005).
219. Papadopoulou, A., Anastasiou, I. & Vogler, A.P. Revisiting the insect mitochondrial molecular clock: the mid-Aegean trench calibration. *Mol Biol Evol* **27**, 1659-72 (2010).
220. Baucom, R.S., Estill, J.C., Leebens-Mack, J. & Bennetzen, J.L. Natural selection on gene function drives the evolution of LTR retrotransposon families in the rice genome. *Genome Res* **19**, 243-54 (2009).
221. Smit, A., Hubley, R. & Green, P. RepeatMasker Open-3.0. (1996).
222. Lopez, R., Silventoinen, V., Robinson, S., Kibria, A. & Gish, W. WU-Blast2 server at the European bioinformatics institute. *Nucleic Acids Res* **31**, 3795-3798 (2003).
223. Delsuc, F., Brinkmann, H. & Philippe, H. Phylogenomics and the reconstruction of the tree of life. *Nat Rev Genet* **6**, 361-75 (2005).
224. Jones, D.T., Taylor, W.R. & Thornton, J.M. The rapid generation of mutation data matrices from protein sequences. *Comput Appl Biosci* **8**, 275-82 (1992).
225. Yang, Z. PAML 4: phylogenetic analysis by maximum likelihood. *Mol Biol Evol* **24**, 1586-91 (2007).
226. Yang, Z. & Rannala, B. Molecular phylogenetics: principles and practice. *Nat Rev Genet* **13**, 303-14 (2012).
227. Regier, J.C., Shultz, J.W. & Kambic, R.E. Phylogeny of basal hexapod lineages and estimates of divergence times. *Ann Entomol Soc Am* **97**, 411-419 (2004).
228. Rehm, P. *et al.* Dating the arthropod tree based on large-scale transcriptome data. *Mol Phylogenet Evol* **61**, 880-7 (2011).
229. Whalley, P. Unfair to ancient fossil springtails. *Antenna* **19**, 2-3 (1995).
230. Grimaldi, D.A. & Engel, M.S. *Evolution of the Insects*, (Cambridge Univ Press, 2005).

231. Schumacher, P., WeyEneth, A., Weber, D.C. & Dorn, S. Long flights in Cydia pomonella L. (Lepidoptera: Tortricidae) measured by a flight mill: influence of sex, mated status and age. *Physiol Entomol* **22**, 149-160 (1997).
232. Anders, S., Reyes, A. & Huber, W. Detecting differential usage of exons from RNA-seq data. *Genome Res* **22**, 2008-17 (2012).
233. Trapnell, C. *et al.* Differential analysis of gene regulation at transcript resolution with RNA-seq. *Nat Biotechnol* **31**, 46-53 (2012).
234. Katz, Y., Wang, E.T., Airoldi, E.M. & Burge, C.B. Analysis and design of RNA sequencing experiments for identifying isoform regulation. *Nat Methods* (2010).
235. Anders, S. & Huber, W. Differential expression analysis for sequence count data. *Genome Biol* **11**, R106 (2010).
236. Benjamini, Y. & Hochberg, Y. Controlling the False Discovery Rate: a Practical and Powerful Approach to Multiple Testing. *J Roy Stat Soc B Met* **57**, 289-300 (1995).
237. Quinlan, A.R. & Hall, I.M. BEDTools: a flexible suite of utilities for comparing genomic features. *Bioinformatics* **26**, 841-2 (2010).
238. Beissbarth, T. & Speed, T.P. GOstat: find statistically overrepresented Gene Ontologies within a group of genes. *Bioinformatics* **20**, 1464-5 (2004).
239. Lohse, M. *et al.* RobiNA: a user-friendly, integrated software solution for RNA-Seq-based transcriptomics. *Nucleic Acids Res* **40**, W622-7 (2012).
240. Krueger, F. & Andrews, S.R. Bismark: a flexible aligner and methylation caller for Bisulfite-Seq applications. *Bioinformatics* **27**, 1571-2 (2011).
241. Langmead, B., Trapnell, C., Pop, M. & Salzberg, S.L. Ultrafast and memory-efficient alignment of short DNA sequences to the human genome. *Genome Biol* **10**, R25 (2009).
242. Akalin, A. *et al.* methylKit: a comprehensive R package for the analysis of genome-wide DNA methylation profiles. *Genome Biol* **13**, R87 (2012).